Friedrich-Alexander-Universität
Naturwissenschaftliche Fakultät

MAX PLANCK INSTITUTE
FOR PHYSICS

Master's Thesis
in Physics

Entanglement studies with Belle $\Upsilon(5S)$ Monte Carlo data

---

Vanessa Geier

Supervisor (FAU): Prof. Dr. Christopher van Eldik

Produced at Max Planck Institute for Physics (MPP)

Supervisor (MPP): Dr. Hans-Günther Moser

Submission date: 17.11.2025

Abstract

In this work, we study the entanglement of the B mesons produced in Υ(5S) decays into the final states each with $C = \pm 1$ eigenvalue

$$\Upsilon(5\mathrm{S}) \to B^0\bar{B}^0 \ (C=-1), \quad \Upsilon(5\mathrm{S}) \to B^0\bar{B}^{0*} + \text{c.c.} \ (C=+1), \quad \Upsilon(5\mathrm{S}) \to B^{0*}\bar{B}^{0*} \ (C=-1).$$

For this purpose, we use Belle Monte Carlo data. The B mesons are reconstructed from hadronic decays:

$$\begin{aligned}
&B^0 \to D^-\pi^+, \text{ with } D^- \to K^+\pi^-\pi^- \\
&B^0 \to D^{*-}\pi^+, \text{ with } D^{*-} \to \bar{D}^0\pi_s^- \text{ and } \bar{D}^0 \to K^+\pi^- \\
&B^0 \to D^{*-}\pi^+, \text{ with } D^{*-} \to \bar{D}^0\pi_s^- \text{ and } \bar{D}^0 \to K^+\pi^-\pi^+\pi^- .
\end{aligned}$$

We then determine the decay–time difference of the B meson pairs to investigate the time dependence of their quantum entanglement. Since an entanglement analysis has never been performed for Υ(5S) decays, this thesis establishes the foundation for such a study. This includes deriving the theoretical framework of entanglement at the Υ(5S), performing the necessary kinematic considerations for the decaytime calculation, and developing new time and flavor variables for the analysis, since the Belle II software framework is only partially applicable to the Υ(5S)) case. In addition, we generate Signal Monte Carlo samples of $1 \cdot 10^6$ $B^{0(*)}\bar{B}^{0(*)}$ events to increase statistical precision. In the Υ(5S) system, it is possible to obtain two different types of entanglement. When these two types are mixed, one obtains a disentangled state, with the degree of disentanglement being equal to the mixing ratio of the two entangled states. By applying the model of partial spontaneous disentanglement (PSD), which introduces a fraction ζ, we can measure this disentanglement fraction when mixing the states and thereby validate the theoretical prediction. To achieve this, we implemented the PSD framework for the Υ(5S) case. We verified that, when mixing the two entangled states in equal proportions, the expected disentanglement fraction of 100% is successfully reproduced.

Kurzfassung

In dieser Arbeit untersuchen wir die Verschränkung der B Mesonen, die aus $\Upsilon(5S)$-Zerfällen mit zugehörigem $C = \pm 1$ Eigenzustand entstehen: $\Upsilon(5S)$ decays into the final states each with $C = \pm 1$ value

$$\Upsilon(5\mathrm{S}) \to B^0\bar{B}^0 \ (C = -1), \quad \Upsilon(5\mathrm{S}) \to B^0\bar{B}^{0*} + \text{c.c.} \ (C = +1), \quad \Upsilon(5\mathrm{S}) \to B^{0*}\bar{B}^{0*} \ (C = -1).$$

Dafür benutzen wir Belle Monte-Carlo (MC) Daten. Die B Mesonen werden aus hadronischen Zerfällen rekonstruiert

$$B^0 \to D^-\pi^+, \text{ with } D^- \to K^+\pi^-\pi^-$$

$$B^0 \to D^{*-}\pi^+, \text{ with } D^{*-} \to \bar{D}^0\pi_s^- \text{ and } \bar{D}^0 \to K^+\pi^-$$

$$B^0 \to D^{*-}\pi^+, \text{ with } D^{*-} \to \bar{D}^0\pi_s^- \text{ and } \bar{D}^0 \to K^+\pi^-\pi^+\pi^- .$$

Anschließend bestimmen wir die Zerfallszeitdifferenz der B Mesonenpaare, um die zeitabhängige Quantenverschränkung zu untersuchen. Da bisher keine Verschränkungsanalyse für $\Upsilon(5S)$ Zerfälle durchgeführt wurde, bildet diese Arbeit die Grundlage für eine solche Untersuchung. Das beinhaltet die Herleitung der Theorie der Verschränkung des $\Upsilon(5S) \to B^{0(*)}\bar{B}^{0(*)}$ Systems, die kinematischen Betrachtungen zur Berechnung der Zerfallszeiten sowie die Entwicklung neuer Zeit- und Flavorvariablen für die Analyse, da die BelleII Software nur eingeschränkt auf den $\Upsilon(5S)$ Fall anwendbar ist. Darüber hinaus erzeugen wir Signal Monte Carlo Date mit $1 \cdot 10^6$ $B^{0(*)}\bar{B}^{0(*)}$ Ereignissen, um die statistische Präzision zu erhöhen. Im $\Upsilon(5S)$ System können zwei verschiedene Arten von Verschränkung auftreten. Werden diese beiden Arten miteinander gemischt, erhält man einen unverschränkten Zustand. Der Anteil an nicht verschränkten B mesonen ist dann abhängig vom Mischungsverhältnis der beiden verschränkten Zustände. Ziel dieser Arbeit ist es, diesen Anteil unverschränkter B-Mesonen, beschrieben durch den Parameter ζ, experimentell zu bestimmen und damit die theoretische Vorhersage zu überprüfen. Hierzu verwenden wir das Modell des Partial Spontaneous Disentanglement (PSD), das den Grad des Verschränkungsverlustes ebenfalls über den Parameter ζ beschreibt. Hierfür haben wir das PSD-Framework auf den $\Upsilon(5S)$-Fall übertragen. Wir konnten bestätigen, dass bei einer gleichmäßigen Mischung der beiden verschränkten Zustände der erwartete Entverschränkungsanteil von 100% korrekt reproduziert wird.

Contents

1 Introduction

Belle and its successor, Belle II, are detectros at so-called B-Factories. The Belle experiment was a high-precision particle physics detector located in Tsukuba, Japan. Its goals were, on the one hand, to observe rare decays in the search for physics beyond what the Standard Model can currently predict and more importantly to measure CP violation in the B-sector and confirm the Kobayashi–Maskawa mechanism, which is a theory that describes charge parity (CP) violation. The collider accelerated electrons and positrons to the exact center-of-mass energy required to produce a Υ(4S) resonance. The reason for this is that the mass of the Υ(4S) lies just above the threshold for producing two B mesons, causing it to decay predominantly into $B\bar{B}$ pairs. At energies corresponding to the Υ(4S), no B mesons containing a strange quark are produced.

One of the most important results of the B Factories, including the Belle and Belle II experiments, is the observation that CP violation in quark flavor-changing processes is described by the Kobayashi–Maskawa (KM) mechanism [1]. CP stands for two quantum numbers: charge conjugation (C) and parity (P), which are used in quantum mechanics to describe states and the operations that can be applied to them. Charge conjugation C exchanges a particle with its antiparticle, while parity P inverts the spatial coordinates, effectively mirroring a process $x \to -x$. Assuming CP symmetry, one would expect that the laws of physics remain unchanged if all particles are replaced by their antiparticles and the process is spatially mirrored. However, in weak interaction, e.g. quark flavor-changing processes, where a quark can change into another quark, which can be observed in mesons such as Kaons and B mesons, this symmetry is violated, meaning that CP-mirrored interactions are possible. The Cabibbo–Kobayashi–Maskawa (CKM) matrix describes how quarks of different flavors mix under the weak interaction, meaning how they change their flavor. The KM mechanism describes why this mixing process behaves differently when examining CP mirrored processes. It can be described as one fundamental weak phase in the CKM matrix (the Kobayashi-Maskawa phase δ). CP violation is essential to explain why our universe is dominated by matter. This is why B Factories such as Belle are particularly interested in studying the properties of B mesons, where one can observe $B\bar{B}$ mixing — the oscillation between a B meson and its antiparticle $\bar{B}$.

For the analysis of CP violation in B systems, it is crucial to determine the characteristics of the B mesons, in particular their flavor the flavor, i.e. whether the particle is a B or $\bar{B}$ meson. In the Belle experiment, we exploit the fact that both B mesons originate from the same resonance, the Υ(4S), and therefore share a common wave function that describes the entire $B\bar{B}$ system. We assume that the flavors of the produced B mesons are 100% entangled, meaning that there are correlations, that can not be classically described, between the flavor measurements of the two mesons.

For example, if one measures the flavor of one meson to be B, it is immediately known that the flavor of the other meson must be $\bar{B}$, even if the two mesons are spatially separated. However, previous Belle studies have shown derivations from a perfect (100%) entanglement, since a 10% fraction of disentanglement cannot be excluded [2], leading to systematic uncertainties in the analysis.

Because of this, and because quantum entanglement is an interesting topic in its own, several studies have been initiated to investigate the entangled nature of B mesons, including the one presented in this Master's thesis. So far, such entanglement studies have only been performed using Υ(4S) data. In this thesis, we aim to investigate B mesons produced from the Υ(5S) resonance. The Υ(5S) is heavier than the Υ(4S), which allows the production of excited B-meson states such as B^{0*}, which decay into a ground-state B meson and a photon(see Table 1.1). There are several advantages for entanglement studies when using B mesons produced from Υ(5S) decays such as

Resonance	**Decay product(s)**	**Branching fraction [%]**
Υ(4S)	$B\bar{B}$	> 96
	$B\bar{B}$	(5.5 ± 1.0)
Υ(5S)	$B\bar{B}^* +$ c.c.	(38.1 ± 3.4)
	$B^*\bar{B}^*$	(13.7 ± 1.6)

Table 1.1: Decay products and corresponding branching fractions for the Υ(4S) and Υ(5S) resonances [3].

1. Possibility to investigate and measure the decay times of the individual B mesons produced in the Υ(5S) system. Due to the higher momentum of the B mesons, their spatial separation is larger, which enables time-dependent measurements (see Section 2.3.1). At the Υ(4S) only the decay time difference of the B mesons can be measured.

2. Possibility to study different quantum states by separating each decay channel, e.g. $\Upsilon(5S) \to B^0\bar{B}^0$, $\Upsilon(5S) \to B^0\bar{B}^{0*} +$ c.c., and $\Upsilon(5S) \to B^{0*}\bar{B}^{0*}$. Due to the emission of a photon from the excited B meson, one gains access to additional quantum configurations, allowing each B system and its entanglement properties to be investigated separately (see Section 2.2.2).

3. Because it is possible to separate the different quantum states and study the entanglement properties of each, we can also construct disentangled states by mixing two distinct, fully entangled quantum states. This allows us to control the level of disentanglement and the entanglement properties of a given data sample, and to create a cross-check channel for the $\Upsilon(4S) \rightarrow B^0\bar{B}^0$ system, where a small degree of disentanglement would be possible (see Section 2.3.4 for further details).

The goal of this analysis is to prepare the measurement of the entanglement of those quantum states. To this end methods to reconstruct and measure the time evolution of these $B^{0(*)}\bar{B}^{0(*)}$ states are studies with Monte Carlo (MC) data including effects of detector resolution.

2 Theory

2.1 Quantum mechanics and entanglement

In 1927, almost 100 years ago, the physicists Heisenberg, Born and Bohr introduced the "Copenhagen interpretation" as an interpretation of quantum mechanics. More than a century after the inception of quantum mechanics, the Copenhagen interpretation remains popular among physicists, as the UN also declared the year 2025 as the quantum year, due to the prelude of quantum mechanics 100 years ago. Several modern interpretations of quantum mechanics take inspiration from the Copenhagen interpretation. The important principles of the interpretation are the following:
In quantum mechanics, physical quantities do not have definite values, as long as they are not measured. Only the act of measurement determines the result. That is, the outcome of a measurement can only be described in terms of probability, but the result cannot be determined precisely in advance. Moreover, a measurement results in the collapse of the wavefunction. The information about the possible outcomes of the state before a measure disappears, and the system ends up in the state corresponding to the observed result. The physicists propose that the description of quantum mechanics is a complete theory to describe the physical truth, even though it is not deterministic [4].
But there was also a lot of criticism towards this new description of the world. In particular, Einstein, Podolsky, and Rosen [5] had a problem with the idea of wavefunction collapse and with the fact that the outcome of a physical state is dependent on the measurement. In their view, quantum mechanics did not mirror the common and intuitive understanding of classical physics because it is a non-realistic and non-local theory as explained in the following. To demonstrate that quantum mechanics is an incomplete theory, Einstein, Podolsky, and Rosen introduced a Gedankenexperiment.
They refereed to the Heisenberg uncertainty relation, which states that in quantum mechanics it is impossible to measure the momentum and the position of a system with arbitrary precision, since measuring the momentum influences the position measurement and vice versa. They also relied on the concept of entanglement, which is a quantum mechanical property of particles. Entanglement

can be illustrated with an example: Alice and Bob each receive a particle whose spin can be either up or down. The two particles are entangled, meaning that if one particle is measured to have spin up, the other must have spin down, and vice versa. The state of one particle is correlated with the state of the other particle. This correlation is stronger than what one can classically observe and is called entanglement. To describe entanglement more precise, the two particles must be treated as one combined system consisting of two subsystems (e.g. the particles). While the overall state of the combined system is fully determined, no definite statements can be made about the individual subsystem states prior to measurement. In the Alice and Bob example, each particle can be either up (u) or down (d), but they cannot be in the same state at the same time. Thus, the total system can be in one of the two possible combinations, ud or du, before measurement, but it is impossible to know which particle has which spin until a measurement is performed [6].

In the EPR paradox, the uncertainty principle and the property of entanglement are combined. In their Gedankenexperiment, Einstein, Podolsky, and Rosen considered two entangled subsystems A and B. This time, the entanglement concerns momentum and position rather than spin. The two systems are spatially separated. When the momentum of A is measured, the momentum of B is immediately determined due to the entanglement. Since A and B are far apart, measuring the momentum of A cannot disturb the position of B. According to the uncertainty relation, the position of A can no longer be known precisely after the momentum measurement. However, the position of B can still be measured precisely, and because of the entanglement, this indirectly determines the position of A as well. Thus, if one measures the momentum of system A, one can still measure the position of system B and thereby obtain the position of system A. However, determining both momentum and position of the same system seems to violate Heisenberg's uncertainty principle. This was what troubled Einstein, Podolsky and Rosen. In their view, a physical theory is complete only if it accounts for every element of physical reality, such as momentum and position in this Gedankenexperiment. According to the uncertainty principle, momentum and position cannot simultaneously belong to physical reality because they cannot both be measured with arbitrary precision—yet the EPR Gedankenexperiment appears to allow exactly that. This contradiction constitutes the EPR paradox [5] [7].

Quantum mechanics was nonlocal to them because of the entanglement property, which can be found in quantum mechanical systems, and was first introduced by Schrödinger in 1935. He even stated that entanglement is a characteristic feature of quantum mechanics. Here, it seems that information can be transmitted faster than the speed of light, which is in complete contrast to the theory of relativity.

Because of this, Einstein, Podolsky, and Rosen suggested that quantum mechanics describes the physical truth correctly but is not complete and so-called "hidden parameters" exist, which would resolve the problem of nonlocality and nonrealism [5]. Paradoxically, entanglement, which is one of the most nonclassical features of quantum mechanics, was used by Einstein, Podolsky, and Rosen in their attempt to assign definite values to physical quantities prior to measurement. Bell later demonstrated the opposite: it is entanglement that fundamentally excludes such a possibility [8]. To answer the question of whether quantum mechanics constitutes a complete theory or whether additional hidden parameters are required, he derived an inequality that must be satisfied under the assumption of hidden parameters, that is, under the assumption of a local and realist theory [9].

Bell's inequaltity was extended to realizable systems by Clauser, Horne, Shimony, and Holt (CHSH, whose generalization of Bell's inequality can be tested experimentally,thus testing all local hidden-variable theories see [10]. Since the 1960s, numerous experiments testing the CHSH inequality, for instances those performed by Aspect, Freedmann, Causer, Zeillinger [10], have provided evidence against the existence of the hidden variables postulated by Einstein, Podolsky, and Rosen.

As one can see, entanglement is a fundamental quantum mechanical property that still lacks a universally accepted definition. Numerous interpretations and descriptions of quantum entanglement exist, as it was related to the notion of "knowledge" in quantum context as in [4], . Only in the second half of the 90's it was formalized in terms of entropic inequalities based on Von Neumann entropy [11]. Entanglement is from thereon most often studied in the field of quantum computing (see [12] and [13]), where one also speaks of qbits when an entire system is composed of two subsystems, as it was the case in the Alice and Bob Gedankenexperiment from above. In this thesis we will focus on the interpretation employed by [14], which is based on von Neumann entropy.

But first we describe an entangled state as follows: In classical physics a state of a composite system is given in the phasespace. In quantum mechanics this phasespace is replaced by the Hilbertspace. We consider a composite system consisting of n subsystems each with Hilbertspace H_i, $i \in \{1, ..., n\}$. The Hilbertspace for the whole system is given by $H = \otimes_{i=1}^{n} H_i$. Applying the principle of superposition, one can write the total state of the system as

$$|\psi\rangle = \sum_{\mathbf{i_n}} c_{\mathbf{i_n}} |\mathbf{i_n}\rangle \ , \tag{2.1}$$

where $\mathbf{i_n} = i_1, i_2, ..., i_n$ is a multiindex and $|\mathbf{i_n}\rangle = |i_i\rangle \otimes \ |i_2\rangle \otimes ... \otimes |i_n\rangle$. That means that eq. 2.1 cannot be described as a general state of individual subsystems $|\psi\rangle \neq |\psi_1\rangle \otimes \ |\psi_2\rangle \otimes ... \otimes |\psi_n\rangle$, which means that it is not possible to assign a single state vector to any of the n subsystems. As a result, the state is not separable and we call it entangled [8].

2.1.1 Quantifying entanglement: Entanglement of formation

We want to quantify the amount of entanglement in a system based on the von Neumann entropy, which extends the concept of Gibbs entropy to quantum systems as it is based entirely on density matrices for the description of quantum ensembles [11]. For that we consider two subsystems A and B with Hilbert spaces H_A and H_B with the orthonormal basis vectors $\{|u_i\rangle_A\} \in H_A$ and $\{|v_i\rangle_B\} \in H_B$ the pure state $\psi \in H_A \otimes H_B$ is given as

$$\psi = \Sigma_{i=1}^{r} \lambda_i \, |u_i\rangle_A \otimes |v_i\rangle_B \ , \tag{2.2}$$

with λ_i being the Schmidt coefficient and r being the Schmidt rank, where $r > 1$ indicates entanglement, since the state isn't separable anymore. A maximally entangled state has equal Schmidt coefficients $\lambda_i = 1/\sqrt{r}$ [12].
To obtain a measure for entanglement, e.g. the von Neumann entropy, we have to distinguish between pure and mixed states, since correlations in pure states are purely non-classical, while mixed states can contain both: quantum correlation and classical correlations. We define the von Neumann entropy as follows.

$$S(\rho) = -\mathrm{Tr}\rho \ln(\rho) \, , \tag{2.3}$$

with $\rho = |\psi\rangle \langle\psi|$ being the pure state density matrix. We consider the pure state ψ in Schmidt decomposition from eq. 2.2 and obtain the following for the density matrix for subsystem A:

$$\rho_A = \Sigma_{i=1}^{r} \lambda_i^2 \, |u_i\rangle_A \langle u_i|_A \tag{2.4}$$

and with eq. 2.3 the von Neumann entropy for subsystem A is given by

$$S(\rho_A) = -\mathrm{Tr}(\rho_A \ln(\rho_A)) = -\Sigma_{i=1}^{r} \lambda_i^2 \ln \lambda_i^2 = S(\rho_B) \, , \tag{2.5}$$

since the Schmidt coefficients for ρ_A and ρ_B are the same. For a separable state, e.g. a not entangled state, the Schmidt coefficient is one, leading to a entropy of zero:

$$S(\rho_A) = -1 \ln(1) = 0 \, , \tag{2.6}$$

whereas for a fully entangled state, e.g. $\lambda_i = 1/\sqrt{r}$, the entropy reaches the maximum value of

$$S(\rho_A) = \ln r \, . \tag{2.7}$$

As a result, one can say that the higher the entropys, the higher the degree of entanglement of the subsystems.
For a mixed state we have to consider another quantity to get a measure of entanglement. We want to derive a similar form for the measure of entanglement for mixed states so that we can obtain a direct computation between entanglement and the density matrix of a state. For simplicity, we consider only a bipartite system, in particular a two-qbit system, since this approach will also be required later in the thesis. In general, the idea is that when given a mixed state ρ of two quantum

states A and B, one considers all possible ways of expressing ρ as an ensemble of pure states $|\psi_i\rangle$ with associated possibilities p_i:

$$\rho = \Sigma_i p_i |\psi_i\rangle \langle\psi_i| \ . \tag{2.8}$$

The entanglement of the formation of ρ, $E(\rho)$ is defined as the minimum, over all ensembles, of the average entanglement of the pure states. The resulting ensemble is then given by

$$E = \min \Sigma_i p_i E(\psi_i) \, . \tag{2.9}$$

The starting point for the discussion of the two-qubit system is the so-called "magic basis", consisting of the following four states [14].

$$|e_1\rangle = \frac{1}{\sqrt{2}} (|\downarrow\downarrow\rangle + |\uparrow\uparrow\rangle) \, , \tag{2.10}$$

$$|e_2\rangle = \frac{i}{\sqrt{2}} (|\downarrow\downarrow\rangle - |\uparrow\uparrow\rangle) \, , \tag{2.11}$$

$$|e_3\rangle = \frac{i}{\sqrt{2}} (|\downarrow\uparrow\rangle + |\uparrow\downarrow\rangle) \, , \tag{2.12}$$

$$|e_4\rangle = \frac{1}{\sqrt{2}} (|\downarrow\uparrow\rangle - |\uparrow\downarrow\rangle) \, . \tag{2.13}$$

Then each pure state can be written as $|\psi\rangle = \Sigma_i \alpha_i |e_i\rangle$ and its entanglement can be expressed in terms of the coefficients α_i

$$\varepsilon(x) = H(\frac{1}{2} + \frac{1}{2}\sqrt{1-x^2}) \quad \text{for} \quad 0 \leq x \leq 1 \, , \tag{2.14}$$

with H being the binary entropy function $H(x) = -[x \log_2(x) + (1-x)\log_2(1-x)]$. The entanglement of formation for $|\psi\rangle$ is then given by

$$E(\psi) = \varepsilon(C(\psi)) \tag{2.15}$$

with C being the concurrence, given by the coefficients α_i:

$$C(\psi) = \left| \sum_i \alpha_i^2 \right| \, . \tag{2.16}$$

Like the entanglement of formation E, the concurrence C also reaches zero to one and is monotonically related to E, which means that the concurrence is also a measure of entanglement. As derived in eq. 2.8, The entanglement of a mixed state is defined as the minimum of the average entanglement over all pure states that decompose the mixed state ρ. To obtain this minimum, we look for a set of pure states with the same concurrence, i.e., the same amount of entanglement.

We want to express E in terms of a Hermitian matrix R as a function of ρ and its conjugate of compelx ρ^* in the magic basis of which it is $\rho^* = \sum_{i,j} |e_i\rangle\langle e_j| \, \rho \, |e_i\rangle\langle e_j|$:

$$R(\rho) = \sqrt{\sqrt{\rho}\rho^*\sqrt{\rho}}\,. \tag{2.17}$$

The eigenvalues of this operator R are of interest, since we can write the concurrence as a function of those eigenvalues. As a result, we obtain a measure for entanglement directly computable from the density matrix of a mixed state: Let $\lambda_{\max}$ be the largest eigenvalue of $R(\rho)$, then the entanglement of formation of ρ is given by

$$E(\rho) = \varepsilon(C)\,; \quad C = \max(0, 2\lambda_{\max} - \mathrm{Tr}R)\,. \tag{2.18}$$

The concurrence C and with that the formation of entanglement E is zero if the state is fully disentangled and one if it is fully entangled. We not only obtained the minimum average of entanglement that is needed to create a mixed state by deriving $E(\rho)$, but also a direct computation from the density matrix ρ to a quantitative measure of entanglement in mixed states. Concurrence has become a standard tool for quantifying entanglement in two-qubit systems and will be particularly useful for the analysis of Υ(5S) decay [14].

2.2 Entanglement in B physics

B meson pairs produced from the decay of the Υ(5S) are entangled. The resulting B mesons are always prodces in flavor and anti-flavor pairs e.g. $\Upsilon(5\mathrm{S}) \to B^0\bar{B}^0$, $\Upsilon(5\mathrm{S}) \to B^{0*}\bar{B}^0$+ c.c. and $\Upsilon(5\mathrm{S}) \to B^{0*}\bar{B}^{0*}$. The flavors of the B mesons are entangled, meaning that by measuring the flavor of the first be meson, at time t_1, we instantly know that the other B meson has to have the opposite flavor also at time t_1[1] The B mesons operate as subsystems which of which the entire system (the B meson pair) is built of, when we compare it with the Alice and Bob example from 2.1, Alice and Bob each get an B meson, but this time they don't measure the spin, but the flavor. Now the interesting part is, that the B mesons have the ability of mixing, meaning that a B^0 can oscillate in its antiparticle $\bar{B}^0$ in time (see sec. 2.2.1). Now the question arises how the entanglement and the mixing of the B mesons affect each other. For that we again consider a Gedankenexperiment:

We imagine the two B mesons as two coins. The coins are entangled, which means that if one coin shows heads, the other must show tails. Now we place each coin into a box. One box contains a coin with heads facing up, the other with tails facing up. Then we swap the boxes so that we no longer know which box contains heads and which contains tails. Additionally, we shake both boxes, allowing the coins inside to rotate, so we also lose track of whether the boxes now contain

[1]This is valid for the $C = -1$ case, which will be discussed in sec. 2.2.2.

heads–tails, tails–heads, heads–heads or tails–tails. This reflects the mixing of B mesons, i.e., the transformation between particle and antiparticle see sec. 2.2.1. Only when we open a box, which corresponds to a measurement, we find out whether the coin inside shows heads or tails.
In the case of entanglement, we know that until we open the first box (that is, until the first measurement at time t_1), the two coins must show opposite sides. We do not know where heads or tails is located, but we do know that one must be heads and the other must be tails. If we open one box at time t_1 and observe that the coin shows heads, we immediately know that the coin in the other box must show tails. From the moment of this measurement, i.e., after t_1, the coins are no longer entangled, and the coin in the second box begins to flip between heads and tails, since the box is shaken. When we measure at time t_2, we again determine the coin to show heads or tails, because the entanglement has been removed. Thus, at times t_1 and t_2, we know what each coin showed. For the B meson, this means that we know its flavor at times t_1 (indirectly, due to entanglement) and t_2.
If there is no entanglement, then both boxes are being shaken already from $t = 0$, corresponding to the decay time of the $\Upsilon(5\mathrm{S})$. In this case, we no longer know that the coins must always show opposite sides. If we open a box at time t_1 and see that it shows heads, this gives us no information about the coin in the other box, because the coins are not entangled and have been shaken, i.e., they have oscillated, since the beginning. Only when we open the second box can we determine what it shows. The same applies to the B mesons: without entanglement, both mesons oscillate independently immediately after being produced, so no flavor relation can be deduced from the decay of the first B meson. Entanglement is therefore crucial for determining the flavor of a B meson at times t_1 and t_2. More about oscillation and the mathematical description of B-meson entanglement will be explained in the following.

2.2.1 $\mathrm{B}^0\bar{\mathrm{B}}^0$ mixing

Neutral B mesons are particles composed of an anti-bottom quark and either a strange or down quark. In this thesis we will only focus on the B^0_d mesons, meaning neutral mesons composed of anti-bottom and down quark. From now on, they are denoted as B^0
As predicted by Gell-Mann and Pais, neutral mesons can oscillate between their particle and antiparticle states [15]. This phenomenon can also be observed in neutral B mesons. The Feynman diagrams in Figure 2.1 illustrate the two leading-order processes through which neutral B mesons oscillations can occur.

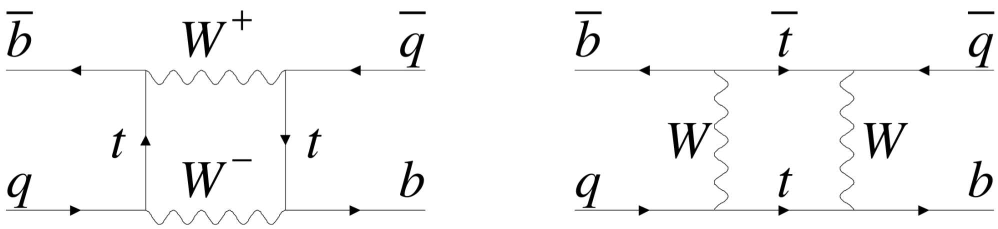

Figure 2.1: Leading order box diagrams for $B_q^0 \to \overline{B}_q^0$ transitions, with $q = d, s$. As the Yukawa coupling is proportional to quark mass, the dominant contribution in virtual particles comes from the top quark. [3]

The mixing phenomenon is due to the fact that the mass eigenstates $|\mathrm{B_H}\rangle$ and $|\mathrm{B_L}\rangle$ (H stands for heavy and L for light), which are used to describe the decay and propagate of the B mesons, are linear combinations of the weak eigenstates, which are responsible for the mixing:

$$|B_L\rangle = p\,|B^0\rangle + q\,|\bar{B}^0\rangle\,, \tag{2.19}$$
$$|B_H\rangle = p\,|B^0\rangle - q\,|\bar{B}^0\rangle\,, \tag{2.20}$$

with complex coefficients that satisfy $|p|^2 + |q|^2 = 1$. We now want to derive the time evolution of the B mesons in the weak eigenbasis which will serve as the mathematical foundation for our further studies. For that we consider the time-dependent Schrödinger equation with the effective Hamiltonian $\hat{H}_{\text{eff}} \in \mathbb{C}^2$ that describes the propagation and decay of the particles. For our purposes, we only consider the $2x2$ effective Hamiltonian operator.

$$i\hbar\partial_t\,|\psi(t)\rangle = \hat{H}_{\text{eff}}\,|\psi(t)\rangle \tag{2.21}$$
$$\hat{H}_{\text{eff}} = \hat{M} - \frac{i}{2}\hat{\Gamma}\,, \tag{2.22}$$

$\hat{M}$ and $\hat{\Gamma}$ are $2x2$ Hermitian matrices. Due to CPT conservation, the off-diagonal matrix elements can be written as $M_{12} = M_{21}^*$ and $\Gamma_{12} = \Gamma_{21}^*$ and the diagonal elements as $M_{11} = M_{22}$ and $\Gamma_{11} = \Gamma_{22}$. The time dependent Schrödinger equation takes now the form of

$$i\hbar\frac{\partial}{\partial t}\begin{pmatrix}|B_L(t)\rangle\\|B_H(t)\rangle\end{pmatrix} = \begin{pmatrix}M_{11} - \frac{i}{2}\Gamma_{11} & M_{12} - \frac{i}{2}\Gamma_{12}\\ M_{12}^* - \frac{i}{2}\Gamma_{12}^* & M_{22} - \frac{i}{2}\Gamma_{22}\end{pmatrix}\begin{pmatrix}|B_L(t)\rangle\\|B_H(t)\rangle\end{pmatrix}. \tag{2.23}$$

To obtain the time evolution of the B mesons, which is given by the eigenvalues of the effective Hamiltonian $\hat{H}_{\text{eff}}$, we have to solve the eigenvalue problem from equation 2.23, by diagonalizing the Hamiltonian. The eigenvalues $\lambda_{\mathrm{L,H}}$ are given by

$$\lambda_{\mathrm{L,H}} = (M_{11} - i\Gamma_{11}) \pm \sqrt{(M_{12} - i\Gamma_{12})(M_{12}^* - i\Gamma_{12}^*)} \tag{2.24}$$

Due to diagonalization, we obtain the condition

$$\frac{q}{p} = \sqrt{\frac{M_{12}^* - \mathrm{i}/2\Gamma_{12}^*}{M_{12} - \mathrm{i}/2\Gamma_{12}}}\,. \tag{2.25}$$

For simplifying the terms, we also define

$$m_{\mathrm{L,H}} = Re(\lambda_{\mathrm{L,H}}) \tag{2.26}$$

$$-\frac{\mathrm{i}}{2}\Gamma_{\mathrm{L,H}} = Im(\lambda_{\mathrm{L,H}})\,. \tag{2.27}$$

Now one can solve eq. 2.23 as the solution and with that the time evolution of the mass eigenstates is given by an exponential function:

$$|B_H(t)\rangle = e^{-i(m_H - \frac{i}{2}\Gamma_H)t}\,|B_H\rangle = e^{-i(m_H - \frac{i}{2}\Gamma_H)t}\left(p\,|B^0\rangle + q\,|\bar{B}^0\rangle\right) \tag{2.28}$$

$$|B_L(t)\rangle = e^{-i(m_L - \frac{i}{2}\Gamma_L)t}\,|B_L\rangle = e^{-i(m_L - \frac{i}{2}\Gamma_L)t}\left(p\,|B^0\rangle - q\,|\bar{B}^0\rangle\right)\,. \tag{2.29}$$

A linear combination of eq. 2.28 and 2.29 yield the time evolution of the B meson which includes the mixing of flavor states and decay:

$$|\bar{B}^0(t)\rangle = g_+(t)\,|\bar{B}^0\rangle + \frac{p}{q}\,g_-(t)\,|B^0\rangle \tag{2.30}$$

$$|B^0(t)\rangle = g_+(t)\,|B^0\rangle + \frac{q}{p}\,g_-(t)\,|\bar{B}^0\rangle \tag{2.31}$$

with the notations

$$g_+(t) = e^{-i\bar{m}t}\,e^{-\frac{1}{2}\bar{\Gamma}t}\left[\cosh\left(\frac{\Delta\Gamma\,t}{4}\right)\cos\left(\frac{\Delta m\,t}{2}\right) - i\sinh\left(\frac{\Delta\Gamma\,t}{4}\right)\sin\left(\frac{\Delta m\,t}{2}\right)\right], \tag{2.32}$$

$$g_-(t) = e^{-i\bar{m}t}\,e^{-\frac{1}{2}\bar{\Gamma}t}\left[-\sinh\left(\frac{\Delta\Gamma\,t}{4}\right)\cos\left(\frac{\Delta m\,t}{2}\right) + i\cosh\left(\frac{\Delta\Gamma\,t}{4}\right)\sin\left(\frac{\Delta m\,t}{2}\right)\right], \tag{2.33}$$

with $\bar{m} = \frac{m_{\mathrm{L}}+m_{\mathrm{H}}}{2}$, $\Delta m = m_{\mathrm{H}} - m_{\mathrm{L}}$ and $\Delta\Gamma = \Gamma_{\mathrm{H}} - \Gamma_{\mathrm{L}}$. Experimental limits for these values are [16] $\Delta m_d = (0.5069 \pm 0.0019)\ \mathrm{ps}^{-1}$, $\Delta\Gamma_d = (0.0007 \pm 0.0066)\ \mathrm{ps}^{-1}$ and $\bar{\Gamma}_d = (0.659 \pm 0.002)\ \mathrm{ps}^{-1}$. In this thesis, we approximate $\Delta\Gamma_d = 0$ and neglect CP violation, so $p/q = 1$.

2.2.2 Entanglement in the Υ(5S) to $B^{0(*)}\bar{B}^{0(*)}$ system

We now understand how the B mesons propagate. Next, we will examine how B mesons are produced in the decay of the Υ(5S) and how this decay influences the physics of the B mesons. There are several possible decay channels through which the Υ(5S) resonance can produce entangled neutral B meson pairs. Because of its higher mass, the Υ(5S) can decay, in contrast to the Υ(4S) resonance, into excited B mesons, denoted as B^* mesons, as well as into B_s. The latter, however, are not of interest in this thesis. The Υ(5S) resonance lies at a higher energy of $(10885.24^{+2.6}_{-1.6}$ MeV/c^2 than the the Υ(4S) resonance (10579.4 ± 1.2 MeV/c^2 [3]. The additional decay modes involving excited B mesons are of physical interest, as they allow the study of different quantum systems and, consequently, different forms of entanglement. This will be discussed in the following section. The detailed decay modes of the Υ(5S) and their branching fractions are listed in table 2.2.

The exited B mesons decay electromagnetically into a B meson through the emission of a photon, which has an energy of 45 MeV in the B^* meson's rest frame [3]. One may then ask wether this photon emission leads to the breaking of the entanglement of the B meson pairs originated from the Υ(5S), resulting in a transition from entangled pair in which at least one meson was excited. This idea arises from the analogy that the decay of an excited B meson could act similar to a measurement process such as a flavor measurement on one of the B mesons, which destroys the entanglement. But it seems unlikely, because the electromagnetic decay doesn't reveal any flavor information of the B mesons. Additionally we then would also see an bigger effect in the disentanglement studies in this analysis. But in general this question could not be answered in the course of this analysis, however, the effect of the photon emission on the entanglement was investigated and interesting results were obtained. We begin by examining the different quantum numbers and, consequently, the wavefunctions of the possible systems resulting from the Υ(5S) decay. We expect two different wavefunctions representing the entanglement of the pairs of B mesons after the Υ(5S) decay. These wavefunctions differ according to the quantum number of the charge conjugation C, which is the eigenvalue of the charge conjugation operator applied to the flavor wavefunctions. It can take the values -1 and $+1$. The value of C is determined by the production mechanism of the B mesons (see table 2.1). The two possible wavefunctions are:

$$|\psi_{C=-1}\rangle = \frac{1}{\sqrt{2}}[|B^0\rangle_1 \otimes |\bar{B}^0\rangle_2 - |\bar{B}^0\rangle_1 \otimes |B^0\rangle_2] \tag{2.34}$$

$$|\psi_{C=+1}\rangle = \frac{1}{\sqrt{2}}[|B^0\rangle_1 \otimes |\bar{B}^0\rangle_2 + |\bar{B}^0\rangle_1 \otimes |B^0\rangle_2] \tag{2.35}$$

We characterize the type of entanglement in terms of the cases given by eq. 2.34 and 2.35, corresponding to an antisymmetric wavefunction (eq. 2.34) with charge conjugation $C = -1$ and a symmetric wavefunction (eq. 2.35) with $C = +1$.

To determine the value of the charge conjugation, we examine the different decay modes from perspective of their quantum numbers, see table 2.1. Due to conservation laws, the quantum numbers of the Υ(5S) resonance must be conserved. Therefore, every system resulting from its decay, for instance $\mathrm{B^0\bar{B}^0}$, $\mathrm{B^{0*}\bar{B}^0}$ + c.c. and $\mathrm{B^{0*}\bar{B}^{0*}}$, must share the same total quantum numbers (see table 2.1).
The two decay channels $\Upsilon(5S) \rightarrow B^0\bar{B}^0$ and $\Upsilon(5S) \rightarrow B^{0*}\bar{B}^{0*}$ both result in an antisymmetric wavefunction. Taking into account the decay of $\Upsilon(5S) \rightarrow \mathrm{B^0\bar{B}^0}$, the total angular momentum of Υ(5S) is $J = 1$ and must be conserved. The total angular momentum is given by the sum of the Spin S and the orbital angular momentum L of the system. Since both the B and anti-B mesons have spin zero ($S = 0$), the orbital angular momentum of the system must be $L = 1$ to conserve $J = 1$. The $\mathrm{B^{0*}\bar{B}^{0*}}$ case is more complex, as two transitions have to be considered. First, we examine the transition $\Upsilon(5S) \rightarrow \mathrm{B^{0*}\bar{B}^{0*}}$. The excited B meson and anti-B meson each have spin quantum number $S = 1$ and $S = -1$ due to the additional internal photon coupling, which results in an orbital angular momentum of $L = 1$ in order to conserve the total angular momentum $J = 1$ of the Υ(5S). Subsequently, the excited (anti-)B mesons decay electromagnetically into the ground state (anti-)B mesons via photon emission. In this process, the spin of the system is transferred to the emitted photon, and the resulting (anti-)B meson have spin quantum number $S = 0$.
In both cases ($\mathrm{B^0\bar{B}^0}$ and $\mathrm{B^{0*}\bar{B}^{0*}}$) the charge conjugation is given by $C = (-1)^L$ which results in $C = -1$, corresponding to a p-wave configuration and thus an antisymmetric spatial wavefunction. Consequently, the flavor wavefunction must be antisymmetric under the charge conjugation operator.
On the other hand, in the $\Upsilon(5S) \rightarrow \mathrm{B^{0*}\bar{B}^0}$+ c.c. decay, only one of the B mesons is excited. This results in a total spin of $S = 1$ for the $\mathrm{B^{0*}\bar{B}^0}$+ c.c. system. To conserve the total angular momentum, $J = 1$ of the Υ(5S), the orbital angular momentum must therefor be $L = 0$. After the subsequent electromagnetic decay of the excited (anti-)B meson, a photon is emitted, and the spin quantum number of the system reduces to $S = 0$. For this configuration, the charge conjugation is $C = +1$, implying that the flavor wavefunction must be symmetric under charge conjugation. Consequently, the resulting $\mathrm{B^0\bar{B}^0}$ system is describes by a s-wave.
It is important to note that the photon emission occurs before the B meson mixing, since the electromagnetic interaction is much faster than the weak interaction responsible for the mixing. Therefor, we assume that the mixing occurs not between the excited and ground state B mesons, but rather between the ground state B mesons produces in the Υ(5S) decay and the B meson resulting from the electromagnetic decay.
As already mentioned, it is not known whether the photon emission acts as a measurement that breaks the entanglement of the B meson pair. However, in this thesis we assume that this is not the case, and that the entanglement remains preserved as explained above.
Next we discuss the case in which the B meson pairs are, for whatever reason, not entangle and

don't share a wavefunction as the two in eq. 2.34 and 2.35, since they oscillate independently from each other. We then describe the B mesons by these two functions:

$$|\psi\rangle = |B^0\rangle_1 \otimes |\bar{B}^0\rangle_2 \; or \tag{2.36}$$

$$|\psi\rangle = |\bar{B}^0\rangle_1 \otimes |B^0\rangle_2 \; . \tag{2.37}$$

each wavefunctions occurs with probability 1/2. There are three models describing the disentanglement behavior. We intoduce them, since we need a measure of the amount of disentanglement in a system, when we create it out of a mixture of fully entangled $C = -1$ and $C = +1$ states. For that we introduce: Spontaneous Disentanglement (SD), Partial Spontaneous Disentanglement (PSD) and the Time Dependent Disentanglement (TDD) Model. However, a variety of TDD models have been proposed to describe possible mechanisms for the loss of entanglement in the B meson system (see [17], [18], [19]). Since a different approach is used in this thesis, one that focuses primarily on the time difference between the decay times of the B mesons to describe disentanglement effects, the discussion becomes model-independent, as absolute decay time dependent effects are integrated out. Therefor we will not describe each of the proposed disentanglement models in detail. Moreover, in the Υ(5(S)) analysis we have the possibility to model disentanglement effects by mixing the two different entanglement forms corresponding to $C = +1$ and $C = -1$ wavefunctions. This allows us to create an disentangled state that can serve as a control channel for a disentanglement model in the Υ(4S) analysis. The details of this approach will be discussed in the following sections.

In the SD model the two B meson resulting from the Υ(5S) decay disentangle instantly after the production and oscillate independently.

In the model of PSD the amount of spontaneous disentangled B meson pairs is reduced to a fraction given by a factor denoted as $\zeta \in [0, 1]$, where $\zeta = 1$ corresponds to all pairs being disentangled and $\zeta = 0$ corresponds to all pairs remaining fully entangled. This model will be later used in this analysis (see sec 5.1.2).

The TDD model, on the other hand, assumes full entanglement at the production time of the B meson pairs. Afterward, they lose their entanglement, which is modeled by an exponential damping. To apply this model, both decay times of the B mesons have to be reconstructed. This is challenging in the Υ(4S) analysis, since the decay time of the B mesons are derived from kinematics, and consequently, from their vertex positions, (see section 2.3.1). Because the B mesons are not spatially separated enough to resolve the individual decay times, more sophisticated reconstruction techniques are required. These methods are used at the Belle groups of the University Hawai'i INDFN Trieste and DESY ([20]), but here we don't need these methods since the Υ(5S) provides enough kinematic energy to the B mesons to allow a big enough spatial separation and by that reconstructing the decay times.

Table 2.1: Detailed quantum numbers of the different particles and decay modes and their respective flavor wave functions (Source: [21]).

Particle/System	S	L	J^{PC}	**Flavor Wave Function**
$\Upsilon(5S)$	1	0	1^{--}	$\lvert b\bar{b}\rangle$
B^0	0	0	0^-	$\lvert d\bar{b}\rangle$
$\bar{B}^0$	0	0	0^-	$\lvert \bar{d}b\rangle$
B^{0*}	1	0	1^-	$\lvert d\bar{b}\rangle$ with aligned spins
$\Upsilon(5S) \to B^0\bar{B}^0$	0	1	1^{--}	$\frac{1}{\sqrt{2}}\left(\lvert B^0\rangle_1 \lvert \bar{B}^0\rangle_2 - \lvert \bar{B}^0\rangle_1 \lvert B^0\rangle_2\right)$
$\Upsilon(5S) \to B^{0*}\bar{B}^{0*} \to B^0\bar{B}^0$	0	1	1^{--}	$\frac{1}{\sqrt{2}}\left(\lvert B^0\rangle_1 \lvert \bar{B}^0\rangle_2 - \lvert \bar{B}^0\rangle_1 \lvert B^0\rangle_2\right)$
$\Upsilon(5S) \to B^{0*}\bar{B}^0 + \text{c.c.} \to B^0\bar{B}^0$	0	0	0^{++}	$\frac{1}{\sqrt{2}}\left(\lvert B^0\rangle_1 \lvert \bar{B}^0\rangle_2 + \lvert \bar{B}^0\rangle_1 \lvert B^0\rangle_2\right)$

Decay mode	**Branching fraction [%]**
$B\bar{B}$	(5.5 ± 1.0)
$B\bar{B}^* + \text{c.c.}$	(13.7 ± 1.6)
$B^*\bar{B}^*$	(38.1 ± 3.4)
$B\bar{B}^{(*)}\pi$	< 19.7
$B\bar{B}\pi\pi$	< 8.9
$B_s^{(*)}\bar{B}_s^{(*)}$	(20.1 ± 3.1)

Table 2.2: Main decay modes of the Υ(5S) resonance into B mesons and their branching fractions [22]. $B^{\pm}$ and B^0) are not distinguished here and are assumed to be produced in equal amounts. Expect for the B_s^0, since they are only neutral.

2.3 Υ(5S) to $\mathrm{B}^{0(*)}\bar{\mathrm{B}}^{0(*)}$ decay

We look at the Υ(5S) system, because it allows to study B meson pairs under different conditions. It allows us to study both the $C = +1$ and $C = -1$ states due to the electromagnetic transition of the excited B meson. This is interesting for the discussion of entanglement since the mixture of both states may cause disentanglement (see section 2.3.4). Another advantage is that producing the Υ(5S) requires a higher beam energy, resulting in a higher momentum of the B mesons in both the Υ(5S) rest frame and the laboratory frame. This, in turn, leads to a greater spatial separation of the two B mesons, allowing the measurement of both decay times (see section 2.3.1).

2.3.1 Kinematics

We aim to study the entanglement of B mesons by measuring their decay times after the process $\Upsilon(5S) \rightarrow B^{0(*)}\bar{B}^{0(*)}$ using Monte Carlo data from the Belle experiment. The Υ(5S) resonance is produced in e^-e^+ collisions. At Belle, the beam energies are 8 GeV for the electron beam and 3.5 GeV for the positron beam, which results in a boost of the Υ(5S) center-of-mass system along the z-axis of $\beta\gamma = 0.425$ into the laboratory frame. The center-of-mass energy of the Υ(5S) is 10.885 GeV. This leads to a boost of the produced B mesons of $\beta\gamma = 0.243$.
For the time dependent analysis, it is essential to understand the kinematics of the B meson system in order to determine the decay times of the B mesons. Since the production vertex of the B meson cannot be reconstructed, because the neutral B mesons don't leave a trace in the vertex detector, only their decay vertices are known. Consequently, the absolute decay times of the B mesons from a $B\bar{B}$ pair cannot be measured directly.
Instead the time difference Δt is determined from the spatial separation of the decay vertices, measured in the x-, y-, and z-directions. It is therefore important that the two B mesons are spatially well separated, so that the difference in their vertex positions can still be resolved.
In the Υ(4S) analysis, the B mesons are separated only by the boost of the e^-e^+ collision of the accelerator into the laboratory frame. As a result, they are mainly separated along the z-direction but not significantly in the x-y-plane, since they experience only a small boost in the Υ(4S) rest frame and are thus not well separated in space. The higher beam energy required to produce the Υ(5S) leads to a higher momenta of the B mesons in the Υ(5S) system (see tab. 4.3 for momentum values). As the Υ(5S) decay is isotropic, a larger spatial separation is observed in both longitudinal and transverse direction in both the Υ(5S) system and the laboratory system.
Our goal is to determine the decay times of both B mesons, for a more precise entanglement analysis, since the additional time information allows a more precises differentiation between disentangled and entangled state, as will be discussed in more detail in 2.2.2. To achieve this, we first study the kinematics. In general three transformations are required:

1. We begin in the Υ(5S) rest frame to understand the underlying physics.

2. The decay times are then transformed into the B meson rest frame using the Lorentz boost $\beta_B\gamma_B$.

3. Finally , the system is transformed into the laboratory frame, where the vertex positions are measured, using the Lorentz boost $\beta\gamma$.

Since the boost is not aligned with the z-axis (the electron and positron beams collide at an angle of 22 mrad), the laboratory frame must be rotated into the z-axis. Table 2.3 summarizes all Lorentz factors used in this analysis. In calculating β_B and γ_B the photon energy of 45 MeV from the

excited B mesons is neglected, since it is small compared to the B meson mass of 5.4 GeV.
In the Υ(5S) rest frame the four momenta of the particles are given as

$$P_{B_1}^{\Upsilon(5S)} = \begin{pmatrix} E_B \\ \vec{p} \end{pmatrix} , P_{B_2}^{\Upsilon(5S)} = \begin{pmatrix} E_B \\ -\vec{p} \end{pmatrix} , P_{B}^{\Upsilon(5S)} = \begin{pmatrix} m_{\Upsilon(5S)} \\ \vec{0} \end{pmatrix} . \tag{2.38}$$

In Fig. **??**, a sketch of the $B\bar{B}$ system in the Υ(5S) rest frame is shown. The B mesons have the same mass and are emitted in opposite directions with equal momentum magnitude. The angle θ denotes the angle between the z-axis and the direction in which the B mesons are emitted. The velocity of the B mesons in the Υ(5S) rest frame is given by:

$$\beta_{B_1,i}^{\Upsilon} = \frac{p_i}{E_B} , \beta_{B_2,i}^{\Upsilon} = \frac{-p_i}{E_B} \tag{2.39}$$

with $E_B = \sqrt{|\vec{p}|^2 + m_B^2}$ being the energy of each B meson in the Υ(5S) rest frame. The velocity of the B mesons in z-direction in the Υ(5S) rest frame is given as

$$\beta_{B_1,z}^{\Upsilon} = \frac{|\vec{p}| \cos(\theta_{\text{CMS}})}{E_B} = -\beta_{B_2,z}^{\Upsilon} , \tag{2.40}$$

with θ_{CMS} being the polar angle in the CMS. It is given by the

$$\theta_{\text{CMS}} = \arccos\left(\frac{p_{z,\text{CMS}}}{p_{\text{CMS}}}\right) \tag{2.41}$$

with $p_{z,\text{CMS}}$ being the z-direction of the momentum of the B_1 meson in the CMS and p_{CMS} being the absolute value of its momentum in the CMS. In Fig. **??** one can see a sketch for the perpendicular x-y-direction. In this case, the velocities are given by

$$\beta_{B_1,xy} = \frac{|\vec{p}| \sin(\theta_{\text{CMS}})}{E_B} = -\beta_{B_2,xy}^{\Upsilon} . \tag{2.42}$$

We now define β_{B_1} as β_B The decay lengths in the z-direction in the Υ(5S) rest frame are given as

$$z_1^{\Upsilon} = \beta_{B,z}^{\Upsilon} c t_1^{\Upsilon} , z_2^{\Upsilon} = -\beta_{B,z}^{\Upsilon} c t_2^{\Upsilon} . \tag{2.43}$$

The decay times are now given in the Υ(5S) rest frame, but we want them to be expressed in the B meson rest frame. To achieve this, we transform the times into the B meson rest frame. The decay lengths in z-direction are:

$$z_1^{\Upsilon} = \beta_{B,z}^{\Upsilon} \gamma_B c t_1 , z_2^{\Upsilon} = -\beta_{B,z}^{\Upsilon} \gamma_B c t_2 \tag{2.44}$$

with $\gamma_B = E_B/m_B$. We apply the same procedure in the x-y direction and obtain:

$$xy_1^{\Upsilon} = \beta_{B,xy}^{\Upsilon} \gamma_B c t_1 , xy_2^{\Upsilon} = -\beta_{B,xy}^{\Upsilon} \gamma_B c t_2 \tag{2.45}$$

The distances between the B mesons in the $\Upsilon(5S)$ rest frame are given as

$$\Delta z^{\Upsilon} = \beta_B \cos(\theta_{\mathrm{CMS}})\gamma_B(t_1 + t_2) \tag{2.46}$$

$$\Delta xy^{\Upsilon} = \beta_B \sin(\theta_{\mathrm{CMS}})\gamma_B(t_1 + t_2)\,. \tag{2.47}$$

We now have to transform the length differences into the laboratory frame. To do this, we apply a Lorentz boost and rotate the system around the z-axis by an angle of 22 mrad. In the z-direction, the expressions for z_1 and z_2 are given by the following

$$z_1 = \gamma(-c\beta_B\gamma_B t_1 \cos(\theta_{\mathrm{CMS}}) + \beta c\gamma_B t_1) \tag{2.48}$$

$$z_2 = \gamma(c\beta_B\gamma_B t_1 \cos(\theta_{\mathrm{CMS}}) + \beta c\gamma_B t_1) \tag{2.49}$$

$$\Delta z = \gamma\gamma_B\beta_B c(t_2 + t_1)\cos(\theta_{\mathrm{CMS}}) + \gamma_B\gamma c(t_2 - t_1) \tag{2.50}$$

with γ and β being the Lorentz boost parameters in the Laboratory frame. For the x-y-direction we obtain

$$xy_1 = -\beta c t_1 sin(\theta_{\mathrm{CMS}}) \tag{2.51}$$

$$xy_2 = \beta c t_1 sin(\theta_{\mathrm{CMS}}) \tag{2.52}$$

$$\Delta xy = c\beta_B\gamma_B(t_2 + t_1)\sin(\theta_{\mathrm{CMS}})\,. \tag{2.53}$$

Note that $\Delta xy = \sqrt{\Delta x^2 + \Delta y^2}$. Since we had to rotate the laboratory frame in x-z plane by an angle of $\alpha = 22$ mrad in order to apply the Lorentz transformation only in the z-direction, Δx and Δy are given as

$$\Delta x = (x_{B_1} - x_{B_2})\cos(\alpha) + (z_{B_1} - z_{B_2})\sin(\alpha) \tag{2.54}$$

$$\Delta z = (z_{B_1} - z_{B_2})\cos(\alpha) - (x_{B_1} - x_{B_2})\sin(\alpha)\,, \tag{2.55}$$

where x_{B_i} and z_{B_i} are the vertex positions measured in the laboratory frame in the x- and z-directions.

As can be seen in eq. 2.51 and eq. 2.48 the vertex measurement in x-y-direction depends only on the sum of the absolute decay times Σt, whereas the vertex measurement in z-direction depends on both the time difference Δt as well as Σt.

Thus, by measuring all vertex positions, one can obtain information about each absolute decay time by constructing a linear combination of Σt and Δt. Σt and Δt are given as

$$\Sigma t = \frac{\Delta xy}{\beta_B \sin(\theta_{\mathrm{CMS}})\gamma_B} \tag{2.56}$$

$$\Delta t = \frac{\Delta z}{\gamma_B\gamma\beta} - \frac{\Delta xy \cot(\theta_{\mathrm{CMS}})}{\beta_B\beta}\,. \tag{2.57}$$

The main difference between the $\Upsilon(5S)$ and the $\Upsilon(4S)$ system is that, in the $\Upsilon(4S)$ rest frame the B mesons don't have sufficient momentum in perpendicular direction and are therefore not spatially separated enough for the detector to resolve the distance in the x-y-direction. Consequently, it is not possible to extract the individual Σt information, as can be done in the $\Upsilon(5S)$ system by measuring Δxy.
Thus only the $\Upsilon(5S)$ system allows to determine the two absolute decay times, more precisely the liner combinations of Δt and Σt.

Particle	γ	β	$\langle\Delta z\rangle$ (μm)	$\langle\Delta xy\rangle$ (μm)
$\Upsilon(5S)$ in laboratory frame	1.086	0.39	–	–
B meson in $\Upsilon(5S)$ restframe	1.031	0.236	194	70

Table 2.3: Lorentz factors and average spatial separations for the $\Upsilon(5S) \to B^0\bar{B}^0$ system [21].

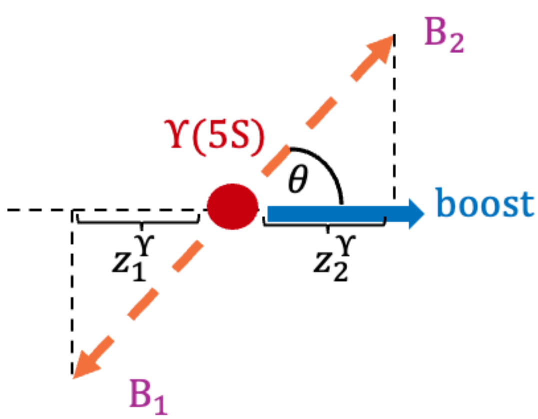

(a) B meson z coordinates in the $\Upsilon(5S)$ rest frame.

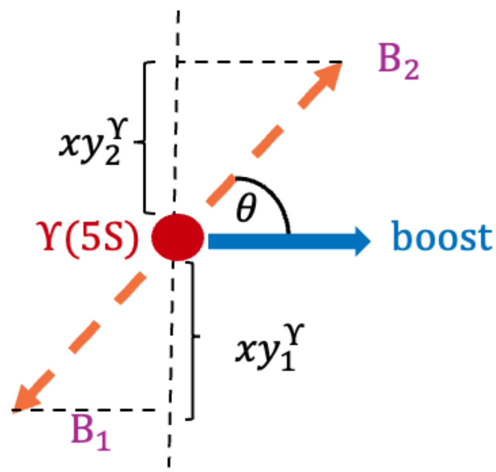

(b) B meson xy coordinates in the $\Upsilon(5S)$ rest frame.

Figure 2.2: Sketch of the decay of the $\Upsilon(5S \to B^0\bar{B}^0)$ system in the $\Upsilon(5S)$ rest frame.

2.3.2 Time dependence of the different wavefunctions

In sections 2.1.1 and 2.2.2 we discussed the different possible B meson configurations in each wavefunction and the corresponding entanglement properties. Now we want to derive the proper probability density function in dependency of the absolute decay times of each B mesons as well as their difference Δt and their sum Σt, which can later be used for entanglement measurements in the Υ(5S) system.
The probability density function (PDF) P to measure a system ϕ in a certain state ψ in quantum mechanics is given as the squared absolute value of the wavefunctions:

$$P = |\langle\phi|\,|\psi\rangle\,|^2\,. \tag{2.58}$$

We can apply this to our B meson system after the decay. The resulting state ψ corresponds to one of the wavefunctions discussed above: the antisymmetric entangled wavefunction from eq. 2.34, the symmetric entangled wavefunction from eq. 2.35 or the disentangled wavefunctions given by eq. 2.36 and eq. 2.37. The state ϕ represents one of the possible B meson configurations, e.g.

$$|\mathrm{B}^{0(*)}\rangle_1 \otimes |\bar{\mathrm{B}}^{0(*)}\rangle_2 \;\text{ and }\; |\bar{B}^{0(*)}\rangle_1 \otimes |\mathrm{B}^{0(*)}\rangle_2\,, \tag{2.59}$$

which are referred to as opposite flavor events and

$$|\mathrm{B}^{0(*)}\rangle_1 \otimes |\mathrm{B}^{0(*)}\rangle_2 \;\text{ and }\; |\bar{\mathrm{B}}^{0(*)}\rangle_1 \otimes |\bar{\mathrm{B}}^{0(*)}\rangle_2\,, \tag{2.60}$$

which are referred to as same flavor events.

Entangled case

Antisymmetric wavefunction $C = -1$ We will start with the PDF for the antisymmetric case, so $C = -1$. As a reminder, the antisymmetric wavefunction is given by

$$|\Psi_{C=-1}\rangle\,(t_1,t_2) = \frac{1}{\sqrt{2}}\left(|B^0(t1)\rangle \otimes |\bar{B}^0(t_2)\rangle - |\bar{B}^0(t_1)\rangle_1 \otimes |B^0(t_2)\rangle\right) \tag{2.61}$$

the time dependencies for $|B^0(t)\rangle$ and $|\bar{B}^0(t)\rangle$ are given in section 2.2.1 in eq. 2.31 and eq. 2.30. Resulting in the wavefunction:

$$|\Psi_{C=-1}(t_1,t_2)\rangle = \frac{1}{\sqrt{2}}\Big[\frac{p}{q}\big(g_+(t_1)g_-(t_2) - g_-(t_1)g_+(t_2)\big)\,|B^0B^0\rangle \tag{2.62}$$

$$+\big(g_+(t_1)g_+(t_2) - g_-(t_1)g_-(t_2)\big)\,|B^0\bar{B}^0\rangle \tag{2.63}$$

$$+\big(g_-(t_1)g_-(t_2) - g_+(t_1)g_+(t_2)\big)\,|\bar{B}^0B^0\rangle \tag{2.64}$$

$$+\frac{q}{p}\big(g_-(t_1)g_+(t_2) - g_+(t_1)g_-(t_2)\big)\,|\bar{B}^0\bar{B}^0\rangle\,\Big] \tag{2.65}$$

g_+ is given by eq. 2.32 and g_- is given by eq. 2.33. We neglect CP Violation, so $p/q = 1$ and $\Delta\Gamma = 0$. Then we obtain the probability density functions:

$$P_{C=-1}(B^0B^0) = \frac{\Gamma^2}{4}e^{-\Gamma(t_1+t_2)}\left[1-\cos(\Delta m(t_1-t_2))\right] = P_{C=-1}(\bar{B}^0\bar{B}^0), \tag{2.66}$$

$$P_{C=-1}(\bar{B}^0B^0) = \frac{\Gamma^2}{4}e^{-\Gamma(t_1+t_2)}\left[1+\cos(\Delta m(t_1-t_2))\right] = P_{C=-1}(B^0\bar{B}^0)\,. \tag{2.67}$$

The exponential terms are the damping factors for the oscillation, reflecting the decay of the particles, while the trigonometric functions are due to the mixing property of the particles. The entire function depends on the two individual decay times t_1 and t_2.
These two times cannot be resolved in the Υ(4S) system as discussed in section 2.3.1, but they can be resolved in the Υ(5S) analysis. Since we will later perform a one-dimensional fit of the PDF to the data, we will not go into detail regarding the resolution of the individual decay times. Therefore, we focus on the dependence of the PDF on Δt and Σt.
We obtain the Δt distribution by integrating over t_1 and fixing the difference $t_1 - t_2 = \text{const}$. Moreover, we define $t_1 + t_2 = 2t_1 - \Delta t$. As a result, the over t_1 integrated PDFs as a function of Δt are given by [21]:

$$\int_0^\infty dt_1\, P_{C=-1}(B^0B^0) = \frac{1}{8\Gamma}\, e^{-\Gamma|\Delta t|}\left[1-\cos(\Delta m\,\Delta t)\right] = \int_0^\infty dt_1\, P_{C=-1}(\bar{B}^0\bar{B}^0), \tag{2.68}$$

$$\int_0^\infty dt_1\, P_{C=-1}(\bar{B}^0B^0) = \frac{1}{8\Gamma}\, e^{-\Gamma|\Delta t|}\left[1+\cos(\Delta m\,\Delta t)\right] = \int_0^\infty dt_1\, P_{C=-1}(B^0\bar{B}^0)\,. \tag{2.69}$$

(2.70)

The theoretical PDFs integrated over t_1 for same flavor (SF) and opposite flavor (OF) events are shown in the upper plot in figure 2.3. The dotted curve shows the OF events, which peak at $\Delta t = 0$. The full curve represents the SF events, which vanish at $\Delta t = 0$, since the B mesons are described by a p-wave function. Consequently, at the exact same decay time, it is not possible to produce two B mesons with the same flavor, which is a consequence of Bose Einstein statistics for Bosons in an antisymmetric state [23].
This behavior is consistent with the interpretation of entanglement in the $\Upsilon(5S)$ decay: measuring one particle immediately determines the flavor state of the other to be opposite. This does not necessarily hold for all cases, as we will see later when discussing the symmetric wavefunction.
We can also examine the dependence of the PDFs on Σt dependency of the PDFs. For this, we integrate again over t_1, while keeping $t_1 + t_2$ fixed. The new integration limits are from 0 to T, since the sum of both decay times cannot exceed $t_1 + t_2 = \Sigma t = T$. The resulting PDFs are given

by:

$$\int_0^{\Sigma t} dt_1\, P_{C=-1}(B^0 B^0) = \frac{1}{4}\, e^{-\Gamma \Sigma t} \left[\Sigma t - \frac{\sin(\Delta m\, \Sigma t)}{\Delta m} \right] = \int_0^{\Sigma t} dt_1\, P_{C=-1}(\bar{B}^0 \bar{B}^0), \tag{2.71}$$

$$\int_0^{\Sigma t} dt_1\, P_{C=-1}(\bar{B}^0 B^0) = \frac{1}{4}\, e^{-\Gamma \Sigma t} \left[\Sigma t + \frac{\sin(\Delta m\, \Sigma t)}{\Delta m} \right] = \int_0^{\Sigma t} dt_1\, P_{C=-1}(B^0 \bar{B}^0)\,. \tag{2.72}$$

$$\tag{2.73}$$

The dependency of Σt are shown in fig. 2.4.

Symmetric wavefunction $C = +1$ We use the same procedure as in $C = +1$ case. The only difference is that our wavefunction is now symmetric, meaning that the B meson configurations are connected by a plus sign. Physically, this implies that it is now possible to observe same-flavor (SF) events even at $\Delta t = 0$, since the system is describe by a s-wavefunction. The general wavefunction is given by

$$|\Psi_{C=-1}\rangle\,(t_1, t_2) = \frac{1}{\sqrt{2}} \big(|B^0(t_1)\rangle \otimes |\bar{B}^0(t_2)\rangle + |\bar{B}^0(t_1)\rangle \otimes |B^0(t_2)\rangle \big) \tag{2.74}$$

again we use the time dependencies for the flavor eigenfunctions $|\mathrm{B}^0(t)\rangle$ and $|\bar{\mathrm{B}}^0(t)\rangle$ from eq. 2.31 and 2.30

$$|\Psi_{C=-1}(t_1, t_2)\rangle = \frac{1}{\sqrt{2}} \Big[\frac{p}{q} \big(g_+(t_1) g_-(t_2) + g_-(t_1) g_+(t_2) \big)\, |B^0 B^0\rangle \tag{2.75}$$

$$+ \big(g_+(t_1) g_+(t_2) + g_-(t_1) g_(t_2) \big)\, |B^0 \bar{B}^0\rangle \tag{2.76}$$

$$+ \big(g_-(t_1) g_-(t_2) + g_+(t_1) g_+(t_2) \big)\, |\bar{B}^0 B^0\rangle \tag{2.77}$$

$$+ \frac{q}{p} \big(g_-(t_1) g_+(t_2) + g_+(t_1) g_-(t_2) \big)\, |\bar{B}^0 \bar{B}^0\rangle \Big] \tag{2.78}$$

We use the notations from eq. 2.33 and eq. 2.32 and neglect CP-violation so $p/q = 1$ and approximate $\Delta\Gamma = 0$. Then we obtain the PDFs for the symmetrical wavefunction:

$$P_{C=+1}(B^0 B^0) = \frac{1}{4} e^{-\Gamma(t_1+t_2)} \left[1 - \cos(\Delta m (t_1 + t_2)) \right] = P_{C=+1}(\bar{B}^0 \bar{B}^0), \tag{2.79}$$

$$P_{C=+1}(\bar{B}^0 B^0) = \frac{1}{4} e^{-\Gamma(t_1+t_2)} \left[1 + \cos(\Delta m (t_1 + t_2)) \right] = P_{C=+1}(B^0 \bar{B}^0)\,. \tag{2.80}$$

Both PDFs differ from the antisymmetric case only in the time dependence of the trigonometric function. Here, the PDF depends on the sum of the absolute decay times. However, the overall form of the equation remains the same, since the exponential function still describes the decay of the particles, and the trigonometric function describes the oscillation of the B mesons. We also want to obtain the PDFs integrated over t_1 so that we can study the PDFs as function of both

Δt and $\sum t$ for the analysis. We start with the Δt dependence. For this ww fix Δt and rewrite $t_2 = \Delta t + t_1$ [21]

$$\int_0^\infty dt_1\, P_{C=+1}(B^0 B^0) = \frac{1}{4\Gamma}\, e^{-\Gamma|\Delta t|}\left[\frac{1}{2\Gamma} - \frac{\Gamma\cos(\Delta m\,\Delta t)}{2\Gamma^2 + 2\Delta m^2} + \frac{\Delta m \sin(\Delta m\,\Delta t)}{2\Gamma^2 + 2\Delta m^2}\right] \tag{2.81}$$

$$= \int_0^\infty dt_1\, P_{C=+1}(\bar{B}^0 \bar{B}^0), \tag{2.82}$$

$$\int_0^\infty dt_1\, P_{C=+1}(\bar{B}^0 B^0) = \frac{1}{4\Gamma}\, e^{-\Gamma|\Delta t|}\left[\frac{1}{2\Gamma} + \frac{\Gamma\cos(\Delta m\,\Delta t)}{2\Gamma^2 + 2\Delta m^2} - \frac{\Delta m \sin(\Delta m\,\Delta t)}{2\Gamma^2 + 2\Delta m^2}\right] \tag{2.83}$$

$$= \int_0^\infty dt_1\, P_{C=+1}(B^0 \bar{B}^0)\,. \tag{2.84}$$

$$\tag{2.85}$$

Compared to the $C = -1$ case from eq. 2.69 and eq.2.68, an additional sine term appears, which leads to a phase shift of the function as well as an additional damping factor is obtained (see fig. 2.3). As already noted at $\Delta t = 0$, the probability of observing SF events is not zero anymore. This behavior is not intuitive from the entanglement perspective discussed earlier, since at the decay time of one B meson, the other meson can now be in the same flavor state.
We now proceed to derive the Σt dependence:

$$\int_0^{\Sigma t} dt_1\, P_{C=+1}(B^0 B^0) = \frac{\Gamma^2}{4}\, e^{-\Gamma\Sigma t}\left[1 - \cos(\Delta m\,\Sigma t)\right]\cdot \Sigma t = \int_0^{\Sigma t} dt_1\, P_{C=+1}(\bar{B}^0 \bar{B}^0), \tag{2.86}$$

$$\int_0^{\Sigma t} dt_1\, P_{C=+1}(\bar{B}^0 B^0) = \frac{\Gamma^2}{4}\, e^{-\Gamma\Sigma t}\left[1 + \cos(\Delta m\,\Sigma t)\right]\cdot \Sigma t = \int_0^{\Sigma t} dt_1\, P_{C=+1}(B^0 \bar{B}^0)\,. \tag{2.87}$$

$$\tag{2.88}$$

The dependencies are shown in fig. 2.4.

Disentangled case

We also aim to derive the PDF for the disentangled case, for comparing it with the entangled case. It is also required to describe the model of partial spontaneous disentanglement and to obtain a measure of the fraction of disentanglement in the measured system. We begin with the two wavefunctions given in eq. 2.36 and eq. 2.37.

$$|\Psi_{\mathrm{SD}}(t_1, t_2)\rangle_1 = |B^0(t_1)\rangle \otimes |\bar{B}^0(t_2)\rangle\ , \tag{2.89}$$

$$|\Psi_{\mathrm{SD}}(t_1, t_2)\rangle_2 = |\bar{B}^0(t_1)\rangle \otimes |B^0(t_2)\rangle\ . \tag{2.90}$$

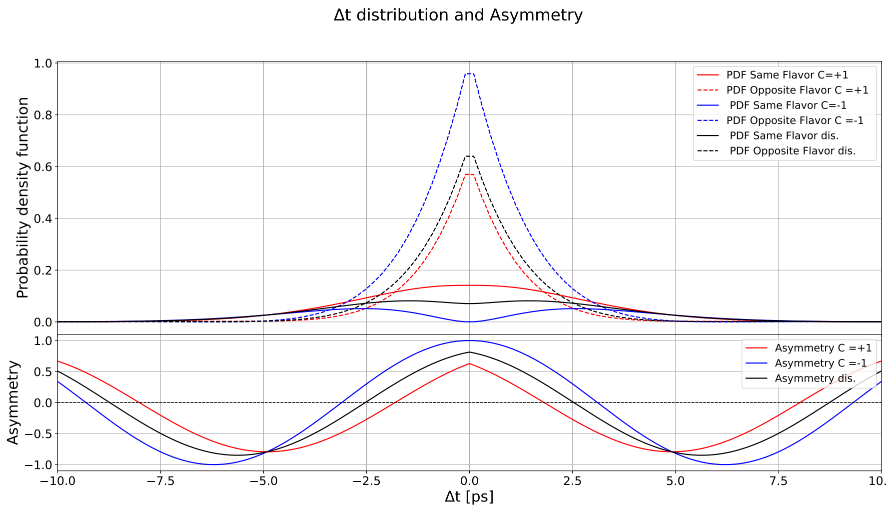

Figure 2.3: Δt t distribution and time-dependent asymmetry in dependency of Δt for the case of charge conjugation C = −1 (blue), C = +1 (red) and full disentanglement (black).

Our disentangled system is described by a mixture of the two states, each with a probability of 1/2, resulting in a mixed state. To calculate the probability of observing the system in a particular state $|\psi\rangle$, we need to define the density matrix of this state. In our case, the density matrix is given by

$$\rho(t_1,t_2) = \frac{1}{2}\Big(|\Psi(t_1,t_2)\rangle_1 \langle\Psi_1(t_1,t_2)|_1 + |\Psi_2(t_1,t_2)\rangle_2 \langle\Psi_2(t_1,t_2)|_2 \Big) \tag{2.91}$$

with the wavefunctions $|\psi(t_1,t_2)\rangle_1$ and $|\psi(t_1,t_2)\rangle_2$:

$$|\Psi_{\mathrm{SD}}(t_1,t_2)\rangle_1 = g_-(t_1)g_+(t_2)\,|B^0B^0\rangle + g_-(t_1)g_-(t_2)\,|B^0\bar{B}^0\rangle \tag{2.92}$$

$$+ g_+(t_1)g_+(t_2)\,|\bar{B}^0B^0\rangle + g_+(t_1)g_-(t_2)\,|\bar{B}^0\bar{B}^0\rangle\,, \tag{2.93}$$

$$|\Psi_{\mathrm{SD}}(t_1,t_2)\rangle_2 = g_+(t_1)g_-(t_2)\,|B^0B^0\rangle + g_+(t_1)g_+(t_2)\,|B^0\bar{B}^0\rangle \tag{2.94}$$

$$+ g_-(t_1)g_-(t_2)\,|\bar{B}^0B^0\rangle + g_-(t_1)g_+(t_2)\,|\bar{B}^0\bar{B}^0\rangle\;, \tag{2.95}$$

where we again use the notation from eq. 2.33 and eq. 2.32 for g_- and g_+ and we neglect CP violation, so $p/q = 1$. The probability density function can now be calculated by

$$P_{\mathrm{SD}}(\phi_1\phi_2) = \langle\phi_1\phi_2|\,\rho(t_1,t_2)\,|\phi_2\phi_2\rangle = \frac{1}{2}\left[|\langle\phi_1\phi_2|\Psi_{\mathrm{SD}}(t_1,t_2)\rangle_1|^2 + |\langle\phi_1\phi_2|\Psi_{\mathrm{SD}}(t_1,t_2)\rangle_2|^2\right]\,, \tag{2.96}$$

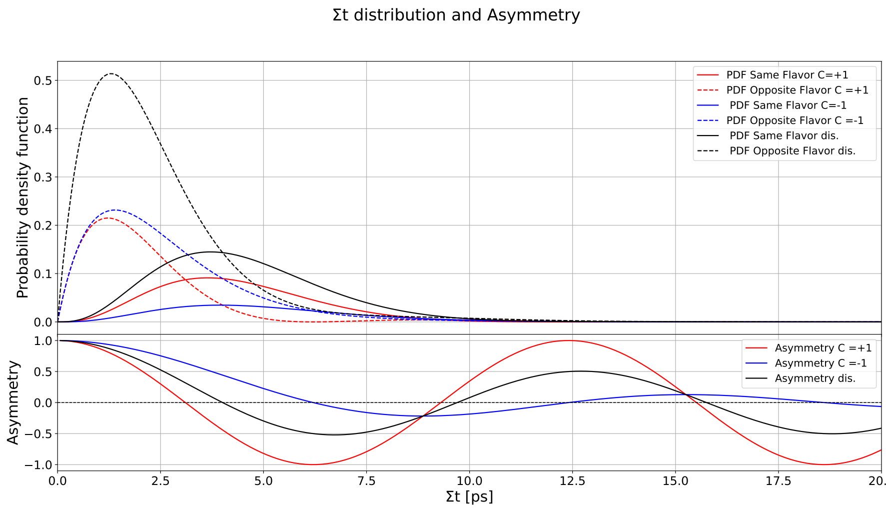

Figure 2.4: Σt t distribution and time-dependent asymmetry in dependency of Δt for the case of C = −1 (blue), C = +1 (red) and full disentanglement (black).

where $\phi_1\phi_2$ denotes the B anti-B meson configurations (for example, $B^0\bar{B}^0$). The probability functions now for each configurations are:

$$P_{\text{SD}}(B^0B^0) = \frac{1}{4}e^{-\Gamma(t_1+t_2)}\left[1-\cos(\Delta m\, t_1)\cos(\Delta m\, t_2)\right] = P_{\text{SD}}(\bar{B}^0\bar{B}^0)\,, \tag{2.97}$$

$$P_{\text{SD}}(\bar{B}^0B^0) = \frac{1}{4}e^{-\bar{\Gamma}(t_1+t_2)}\left[1+\cos(\Delta m\, t_1)\cos(\Delta m\, t_2)\right] = P_{\text{PSD}}(B^0\bar{B}^0)\,, \tag{2.98}$$

Now, the trigonometric function depends on the individual decay times, representing the oscillation of the particles independently of each other. We again aim to derive the time integrated PDF over t_1 [21]:

$$\int_0^\infty dt_1\, P_{\text{SD}}(B^0B^0) = \frac{1}{16\Gamma(\Gamma^2+\Delta m^2)}\, e^{-\Gamma|\Delta t|} \tag{2.99}$$

$$\left[2(\Gamma^2+\Delta m^2) - (2\Gamma^2+\Delta m^2)\cos(\Delta m\,\Delta t) + \Gamma\Delta m\sin(\Delta m|\Delta t|)\right] \tag{2.100}$$

$$= \int_0^\infty dt_1\, P_{\text{SD}}(\bar{B}^0\bar{B}^0), \tag{2.101}$$

$$\int_0^\infty dt_1\, P_{\text{SD}}(\bar{B}^0B^0) = \frac{1}{16\Gamma(\Gamma^2+\Delta m^2)}\, e^{-\Gamma|\Delta t|} \tag{2.102}$$

$$\left[2(\Gamma^2+\Delta m^2) + (2\Gamma^2+\Delta m^2)\cos(\Delta m\,\Delta t) - \Gamma\Delta m\sin(\Delta m|\Delta t|)\right] \tag{2.103}$$

$$= \int_0^\infty dt_1\, P_{\text{SD}}(B^0\bar{B}^0)\,. \tag{2.104}$$

Compared to the entangled asymmetric case as a function of Δt, the disentangled function as a function of Δt is damped by the prefactor of the cosine term and phase-shifted by the sine term. This is how disentanglement and entanglement can be distinguished. The functions, compared to the entangled cases, are plotted in 2.3. Since we can also resolve Σt, we now calculate the time-integrated PDF as a function of Σt to analyze the system in more detail. We obtain:

$$\int_0^{\Sigma t} dt_1\, P_{\mathrm{SD}}(B^0 B^0) = \frac{1}{4\Delta m}\, e^{-\Gamma\Sigma t}\, [2\Sigma t\Delta m - \sin(\Delta m\, \Sigma t) - \Sigma t\Delta m \cos(\Delta m\, \Sigma t)] \tag{2.105}$$

$$= \int_0^{\Sigma t} dt_1\, P_{\mathrm{SD}}(\bar{B}^0 \bar{B}^0), \tag{2.106}$$

$$\int_0^{\Sigma t} dt_1\, P_{\mathrm{SD}}(\bar{B}^0 B^0) = \frac{1}{4\Delta m}\, e^{-\Gamma\Sigma t}\, [2\Sigma t\Delta m + \sin(\Delta m\, \Sigma t) + \Sigma t\Delta m \cos(\Delta m\, \Sigma t)] \tag{2.107}$$

$$= \int_0^{\Sigma t} dt_1\, P_{\mathrm{SD}}(B^0 \bar{B}^0)\,. \tag{2.108}$$

$$\tag{2.109}$$

Compared to the entangled case with the symmetric wavefunction, we again obtain a damping prefactor in front of the cosine term, as well as a phase shift resulting from the sine term. In Fig.2.4, all cases are shown as functions of Σt for comparison.

Partial Spontaneous Disentanglement We introduce the Partial Spontaneous Disentanglement (PSD) model again, since we aim to fit this model to the Δt distributions of the the B mesons and with that obtain a value for the disentanglement fraction ζ in the B meson system after the $\Upsilon(5S)$ system. The fraction is defined as $\zeta \in [0,1]$, 1 meaning complete disentanglement and 0 meaning complete entanglement. The model is constructed out of the time integrated PDF of one of the entangled cases, denoted as P_{QM} as well as the time integrated PDF of the disentangled case, denoted as P_{SD}:

$$P_{\text{PSD}}(\Delta t, \zeta) = (1-\zeta)P_{\text{QM}}(\Delta t) + \zeta P_{\text{SD}(\Delta t)} \tag{2.110}$$

In this model we want to combine the disentangled and entangled PDFs that are integrated over time, so that the resulting PSD PDF is only dependent on the difference of the individual decay times. As already mentioned in the PSD model, the fraction of spontaneously disentangles $B^0\bar{B}^0$ pairs are reduces to a fraction $\zeta \in [0,1]$, 1 meaning complete disentanglement and 0 meaning complete entanglement. The model is constructed out of the time integrated PDF of one of the entangled cases, denoted as P_{QM} as well as the time integrated PDF of the disentangled case, denoted as P_{SD}:

$$P_{\text{PSD}}(\Delta t, \zeta) = (1-\zeta)P_{\text{QM}}(\Delta t) + \zeta P_{\text{SD}(\Delta t)} \tag{2.111}$$

or now, we will focus only on the Δt dependence, so that we can build on the existing entanglement analysis using the PSD model for the $\Upsilon(4S)$ by Belle et al. [24]. In their study, they investigated the disentanglement fraction ζ by measuring the time-dependent asymmetry (which is described in the nect section 2.3.3) of 152 million $B\bar{B}$ pairs produced after the $\Upsilon(4S)$ resonance.
For the measurement of the asymmetry, they deconvoluted detector effects. and corrected experimental effects. Moreover, they used semi-leptonic decay channels for the reconstruction of the B mesons such as $B^0 \to D^* l^+ \nu$ with $D^{*-} \to \bar{D}^0[K^+\pi^-(\pi^0)]\pi_s^-$ and $D^{*-} \to K^+\pi^-\pi^+\pi^-$. Using semileptonic decay channels provides more precise flavor information than the hadronic channels used in this analysis (the flavor tagger algorithm that provides the vertex information of the reconstructed B mesons is described in [25]). n this $\Upsilon(5S)$ analysis it is not possible to study semileptonic decays because the neutrino in the final state carries away energy. Due to its continuous energy distribution, the different decay channels ($\Upsilon(5S) \to B^{0(*)}\bar{B}^{0(*)}$) can no longer be separated, and therefore the corresponding $C = \pm 1$ states cannot be distinguished.

In total, they determined the fraction of disentanglement ζ in the $B^0\bar{B}^0$ system to be

$$\zeta = 0.029 \pm 0.057\,, \tag{2.112}$$

by fitting the time dependent asymmetry with a free ζ parameter.

2.3.3 Asymmetry

As already mentioned, a measure used to distinguish between entangled and disentangled B meson pairs is the time-dependent asymmetry A. It is defined as the ratio of the difference between opposite-flavor (OF) and same-flavor (SF) events to their sum:

$$A = \frac{P(OF) - P(SF)}{P(OF) + P(SF)} \tag{2.113}$$

Depending on the case — e.g., $C = 1$ entangled, $C = +1$ entangled, or disentangled, we obtain three different asymmetry formulas. We can then derive each asymmetry as a function of Δt, Σt or t_1 and t_2 separately. This is particularly useful, as the cases can be distinguished more clearly when considering two variables simultaneously, as illustrated in Figs. 2.5. The asymmetrys as a function of Δt and Σt are shown in the lower panels of fig 2.3 for Δt and fig 2.4 for Σt .
We start by examining the $C = -1$ entangled case: the PDF are given by eq. 2.66 for SF events and eq. 2.67. We then insert these two formulas into the general asymmetry formula 2.113 and obtain

$$A_{\mathrm{C=-1}}(t_1, t_2) = \cos(\Delta m(t_1 - t_2)) \tag{2.114}$$

For $\Delta t = 0$, the asymmetry is equal to one, since no SF events occur and only OF events are present. This means that the number of OF events divided by the total number of events equals one, resulting in an asymmetry of one. Now we want to derive the asymmetry for the $C = +1$ case, also as a function of Δt. For this we use the PDFs from eq. 2.81 for SF and eq. 2.83 for OF events. The asymmetry for the $C = +1$ case as a function of Δt is given by

$$A_{\mathrm{C=+1}}(\Delta t) = \frac{\Gamma[\Gamma\cos(\Delta m|\Delta t|) - \Delta m \sin(\Delta m(|\Delta t|))]}{\Gamma^2 + \Delta m^2} \,. \tag{2.115}$$

The asymmetry as a function of Δt for the $C = +1$ case is damped by the prefactor of the cosine term and phase-shifted due to the sine term, as is the case for the PDFs. These two forms of entanglement can be distinguished by examining either the asymmetry or the time dependence of the PDFs.
In general the PDF for the entangled symmetrical $C = +1$ case is calculated by looking at eq. 2.80 for OF events and eq. 2.79 for SF events. We obtain the asymmetry as a function of t_1 and t_2:

$$A_{\mathrm{C=+1}} = \cos(\Delta m(t_1 + t_2)) \,. \tag{2.116}$$

It is the same as in the case of the asymmetry in dependency of Σt. When looking at the asymmetry in dependency of Σt for the entangled $C = -1$ case we get

$$A_{C=-1}(\Sigma t) = \frac{\sin(\Delta m \Sigma t)}{\Sigma t \Delta m} \tag{2.117}$$

The asymmetry as a function of Σt is shown in fig. 2.4 (bottom panel). As can be seen, the $C = -1$ asymmetry is damped by a factor and phase-shifted. Thus, the two entanglement cases can be distinguished by examining either the asymmetry or the PDFs.

We also investigate the behavior of the disentangled case. For this, we again use the time-dependent PDFs, this time for the SD function from eq. 2.98 for OF events and eq. 2.97 for SF events. The corresponding asymmetry is then given by

$$A_{\mathrm{SD}} = \cos(\Delta m t_1)\cos(\Delta m t_2)\,, \tag{2.118}$$

This again represents the independent oscillation of each particle, since each cosine term is a function of the separate decay times. The asymmetry as a function of Δt is shown in fig. 2.3, where one can clearly see how the three cases can be distinguished from each other. The function is given by:

$$A_{\mathrm{SD}} = \frac{(2\Gamma^2 + \Delta m^2)\cos(\Delta m(|\Delta t|) - \Gamma\Delta m \sin(\Delta m|\Delta t)|)}{2(\Gamma^2 + \Delta m^2)} \tag{2.119}$$

And in dependence of Σt

$$A_{\mathrm{C=+1}}(\Sigma t) = \frac{\sin(\Delta m \Sigma t) + \Sigma t \Delta m \cos(\Delta m \Sigma t))}{\Sigma t \Delta m} \tag{2.120}$$

The asymmetries of the disentangled case are also shown in Fig. REF for the Δt dependence and Fig. REF for the Σt dependence. One can clearly see that, in theory, it is possible to distinguish each case by integrating out the absolute decay times and considering only Σt and Δt. This is due to the different damping factors and phase shifts.

Since we can measure both t_1 and t_2, it is also possible to investigate the asymmetry and PDFs as functions of both variables. This provides a more detailed separation of the three different cases because we gain an additional dimension in which to study the effects (one could also choose Δt and Σt for this purpose). In Fig. 2.5a and 2.5b, the two entangled cases are shown in a three-dimensional plot, with axes representing the absolute decay times t_1 and t_2 in picoseconds. In Fig. 2.5c, the disentangled case is shown. Examining the two-dimensional distributions allows better differentiation of each case.

In particular, for the entangled case, the two distributions are perpendicular to each other, whereas in one dimension one could only distinguish them by looking at the damping and phase shift. This effect can be smeared when including detector effects and background. For the disentangled case, the distribution exhibits more maxima and minima and appears more oscillatory compared to the entangled cases.

It is interesting to separate the three cases because we can manipulate the entanglement by mixing the $C = +1$ and $C = -1$ states, thereby creating states that are (partially) disentangled. This will be described in the next section 2.3.4.

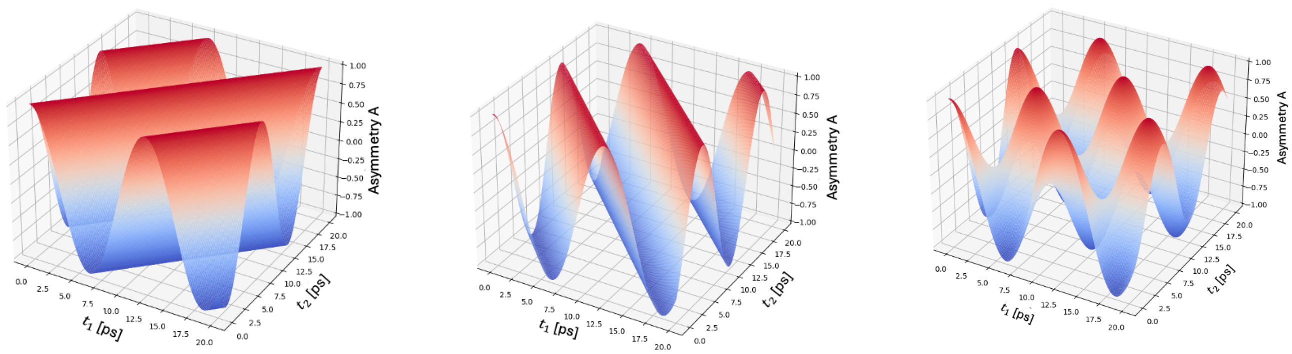

(a) $C = -1$ entangled case (b) $C = +1$ entangled case (c) Disentangled case

Figure 2.5: Time dependent asymmetry as a function of t_1 and t_2 for the three cases: (a) $C = -1$ entangled, (b) $C = +1$ entangled, and (c) disentangled [21].

2.3.4 Entanglment of formation in the $B^0\bar{B}^0$ system

As discussed in Section 2.1.1, the entanglement of a system can be quantified using the entanglement of formation. For a two-qubit system, as in the $B^0\bar{B}^0$ system, one transforms to the "magic basis" and expresses the wavefunctions in this basis. In the $B^0\bar{B}^0$ system, the two possible wavefunctions, the antisymmetric $C = -1$ and the symmetric $C = +1$ states, can be represented in the magic basis as:

$$|e_3\rangle = \frac{1}{\sqrt{2}}[|B_1^0\rangle \otimes |\bar{B}^0\rangle + |\bar{B}_1^0\rangle \otimes |B_2^0\rangle] = |\psi_{C=+1}\rangle \tag{2.121}$$

$$|e_4\rangle = \frac{1}{\sqrt{2}}[|B_1^0\rangle \otimes |\bar{B}^0\rangle - |\bar{B}_1^0\rangle \otimes |B_2^0\rangle] = |\psi_{C=-1}\rangle \tag{2.122}$$

When mixing both entangled states $C = -1$ and $C = +1$, by a mixing parameter p, we obtain the density matrix ρ for this mixed state:

$$\rho = p\,|e_3\rangle\,\langle e_3| + (1-p)\,|e_4\rangle\,\langle e_4|\,, \tag{2.123}$$

the concurrence is then given by the Eigenvalues of the hermitian operator R, which depends on ρ see eq. 2.16:

$$C = \max\{0, \max(p, 1-p) - \min(p, 1-p)\} = |2p-1|\,. \tag{2.124}$$

We can then calculate the entanglement of formation for this mixed state as

$$E(\rho) = H\left(\frac{1}{2} + \frac{1}{2}\sqrt{1-|2p-1|}\right)\,. \tag{2.125}$$

Depending on the mixing parameter p, we can create different entangled states, since $E(\rho)$ can take any value in $[0,1]$. As an example, we consider $p = 0$, representing the fully entangled $C = -1$

case, $p = 1$ representing the fully entangled $C = +1$ case; and $p = 0.5$ representing the disentangled state. When we calculate the concurrence and entanglement of formation, we obtain $E(p) = 1$ and $C(p) = 1$ for $p = 0$ and $p = 1$, indicating that these states are fully entangled, as expected. It becomes more interesting for the $p = 0.5$ mixture. Calculating the entanglement of formation and concurrence for this case yields $E(p) = 0$ and $C(p) = 0$, showing that this mixed state is completely disentangled. This can also be observed by comparing the asymmetry of the disentangled case with the asymmetry of the equally mixed state: the two distributions are indistinguishable (see Fig.2.6 for the mixed case and Fig. 2.5c for the disentangled case). The same behavior can also be seen mathematically. When calculating the asymmetry of this mixed state, we obtain:

$$A_{\text{mixed}} = 0.5 \cdot \cos(\Delta m(t_1 + t_2)) + 0.5 \cdot \cos(\Delta m(t_1 - t_2)) = \cos(\Delta m t_1)\cos(\Delta m t_2)\,, \tag{2.126}$$

This is the same formula as for the disentangled case. As we can see, it is possible to create a truly disentangled state by selecting a mixture of $C = +1$ and $C = -1$ states, which are indistinguishable from genuinely independent states.

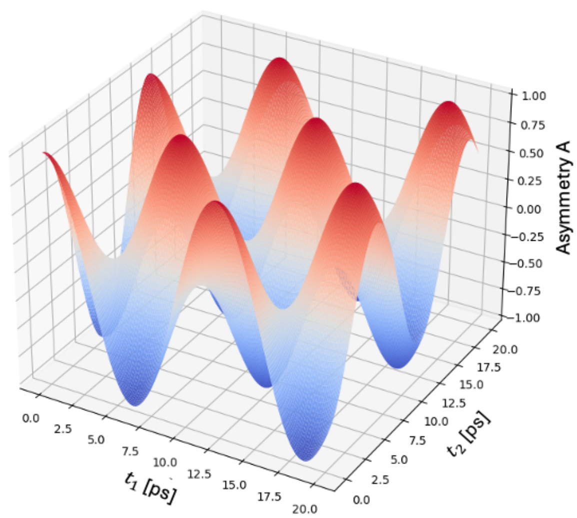

Figure 2.6: Time dependent asymmetry as a function of t_1 and t_2 for a 50/50 mixture of $C = -1$ and $C = +1$ entnagled states.

3 Belle Experiment

The Belle experiment, which operated at the KEKB asymmetric-energy e^+e^- collider in Tsukuba, Japan, between 1999 and 2010, was a high-precision particle physics experiment primarily designed to measure CP violation in the decay of B mesons. It consisted of the KEKB collider and the Belle detector. In 2001, large CP asymmetries in B decays were observed by Belle and BaBar, consistent with the theoretical prediction by Kobayashi and Maskawa [26].

The investigation of entanglement was not a specific goal of the Belle experiment [27]. The entanglement properties of the B mesons was primarily used for the measurement of CP violation. This was possible because the entanglement allowed for the precise determination of the flavor of the still undecayed B meson at the decay time of its paired B meson. It was initially assumed that the B meson pairs were 100% entangled. However, during the course of various analyses, it became evident that this assumption might not be entirely accurate. As a result, potential systematic uncertainties in the CP violation measurements could arise from wrong entanglement assumptions. Consequently, the entanglement properties of the B meson pairs were studied in more detail, leading to analyses such as those performed at the $\Upsilon(4S)$ resonance [2].

3.1 KEKB Accelerator

KEKB is an asymmetric double-ring collider, consisting of two side by side 3 km rings, namely the high energy electron ring (HER) and the low energy positron ring (LER). Before entering the rings, the electrons and positrons are accelerated by a Linear accelerator (Linac). Inside the Linac, electrons are accelerated to an energy of 3.7 GeV, and then directed onto a water-cooled tungsten target to produce positrons. Subsequently, both electrons and positrons are further accelerated and separated into their respective storage rings — electrons into the HER and positrons into the LER [28] [29].

The electrons are accelerated to an energy of 8 GeV, while the positrons reach about 3.5 GeV, corresponding to a center of mass energy of about 10.58 GeV, which is sufficient to create either the $\Upsilon(4S)$ or $\Upsilon(5S)$ resonance. The beams cross at the interaction point, exactly where the Belle detector is located, where electrons and positrons collide with a small angle of 22 mrad. [28]. In

Fig. 3.1 a sketch of the KEKB Accelerator is shown. More about the accelerator can be read in [28] and [30].

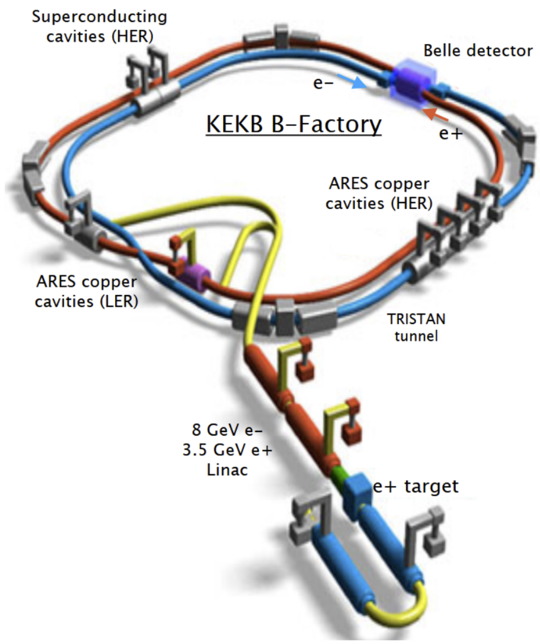

Figure 3.1: Schematic layout of the KEKB accelerator complex [31]

.

3.2 Belle Detector

The Belle detector precisely measures the decay products of interest while dealing with large instantaneous luminosity conditions of the KEKB accelerator. To achieve that it consists of several subsystems allowing to measure tracks, energy and momenta of the particles. In Fig. 3.2 the Belle detector is shown.

The detector is configured around a 1.5 T superconducting solenoid and an iron structure surrounding the KEKB beams at the interaction region. The B meson decay vertices are measured by a silicon vertex detector (SVD) situated just outside of a cylindrical beam pipe. Charged particle tracking is provided by a wire drift chamber (CDC). Particle identification is provided by $\mathrm{d}E/\mathrm{d}x$ measurements in CDC, aerogel Cherenkov counters (ACC) and time-of-flight counters (TOF) situated radially outside the CDC [30]. In the following only the most important sub-detector of the Belle detector are explained. Further details on the detector system can be found in [30] and [1].

Silicon vertex detector (SVD) The goal of the SVD is to measure the precise decay vertex positions, in particular the difference in z-vertex positions between the two B mesons, with a

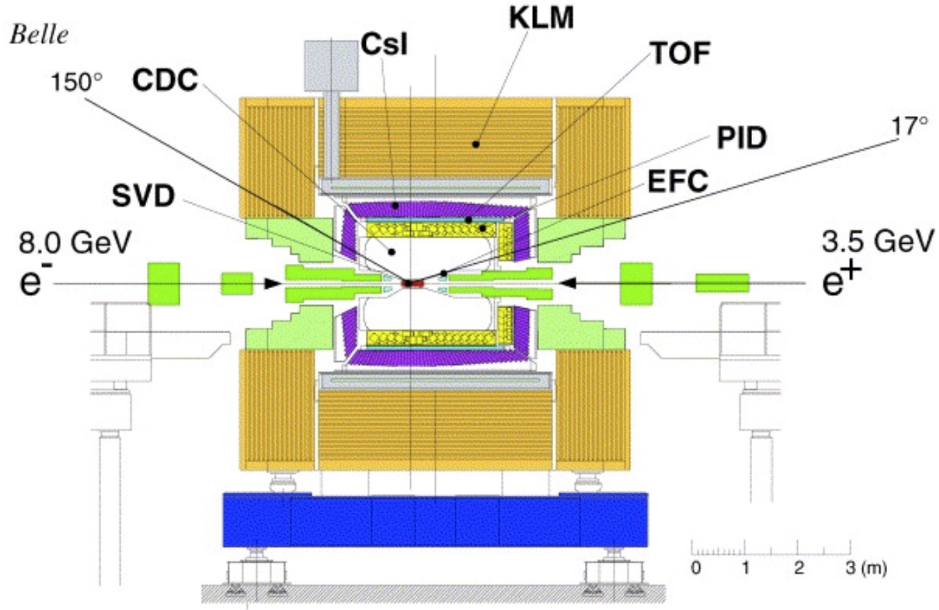

Figure 3.2: Sketch of the Belle detector with its of the different detector subsystems [30]

.

resolution of about 100 μm to reconstruct the decay times of the B mesons and with that observing time-dependent CP asymmetries in the decays of B mesons [30]. The second and final version of the Silicon Vertex Detector (SVD2) consists of four layers of double-sided silicon strip detectors (DSSDs) and covers the full angular acceptance of the detector ($17° < \theta < 150°$) [1]. In this analysis a precise measurement of the decay vertices is crucial since we obtain the time variables that are investigated here trough the vertex information as explained in 2.3.1.

Central Drift Chamber (CDC) The CDC is responsible for detecting charged particles and is located around the SVD. In addition to the SVD, it also reconstructs tracks of the charged particles, measures their hit coordinates precisely, enables to reconstruct their momenta and additionally provides particle identification information using measurements of $\mathrm{d}E/\mathrm{d}x$ within its gas volume. Since low momentum tracks don't reach the particle identification system, they can be identified using the CDC alone. The CDC is asymmetric in the z direction with an angular coverage of $17° < \theta < 150°$ and has a maximum wire length of 2400 mm. The inner radius of the CDC lies at 80 mm. The outer radius is 880 mm [1]. It is important to know the exact momentum of the particles since we separate the different decay channels of the $\Upsilon(5S)$ via the momentum of the B mesons as explained in sec 4.1.2. Also we reconstruct the B mesons from the charged decay product particles, so it is important to correctly identify them for rebuilding the B mesons (see chapter 4).

Electromagnetic Calorimeter (ECL) To detect photons that originate from different B meson decays, such as $B^0 \to \gamma\gamma$, or photons from a π^0, which decays almost exclusively to two photons, the Electromagnetic Calorimeter (ECL) is needed. The ECL consists of a barrel section and a forward and backward end-cap. Each section is equipped with a highly segmented array of 8736 thallium-doped caesium iodide crystals. The scintillation light produced inside the crystals is then detected by silicon photodiodes [1]. The ECL is not only crucial for measurements of photon energies but also for angular coordinates as well as for detection of clusters made by neutral pions with high momenta. Together with the KLM, the calorimeter generates signals for trigger processes [32].

Time of Flight Detector (TOF) and Cherenkov counter (ACC) Particle Identification in Belle, particularity for kaons and pions, is performed by combining the information of the $\mathrm{d}E/\mathrm{d}x$ measurement of the CDC detector and in addition the information of the the time-of-flight detector (TOF) and aerogel Cherenkov counter (ACC).
The ACC uses the angle of the emitted Cerenkov light produced by charged particles to differentiate them. Since pions and kaons differ in mass, the emission angle of the Cherenkov light differs. The emitted photons can be registered in a photon detector.
The TOF system consists of 64 modules, each containing two TOF counters and one thin trigger scintillation (TSC) counter. Photomultiplier are mounted at the end of the TOF [31]. The TOF system allows to distinguish between kaons and pions for tracks with momenta in the range of 0.24 GeV which corresponds to the minimum momentum that is needed to reach the TOF counters and 1.2 GeV. The system measures the flight time of charged tracks reconstructed by the CDC. [30].

$\mathrm{K_L}$ **and Muon Detection System** The aim of the K_L and Muon detection (KLM) system is to identify K_L's and muons with momenta over 600 MeV. The KLM is divided into a barrel section and two end-cap regions, covering an angular range of $20° < \theta < 155°$ [30]. The detector contains alternating layers of charged particle detectors and 4.7 cm thick iron plates. There are 15 detector and 14 iron layers in the barrel region and 14 layers of each in the end-caps. The several layers of materials is needed to make the K_L's interact within the detector, producing showers of ionizing particles that can be measured. These ionizing particles are detected by glass-electrode resistive plate counters (RPCs). When charged particles pass through, they ionize the gas, initiating an avalanche or streamer discharge, which induces a local signal on the electrodes. From these signals, both the position and timing of the ionization event can be reconstructed. Charged hadrons and muons are separated by their range and transverse scattering, with muons traveling further with smaller deflections than hadrons [30].

3.3 Available Υ(5S) Data

The Belle experiment collected different samples at the Υ(5S) resonance energy in various experiments and runs.
Generic Monte Carlo (MC) is available for the experiments exp 43, 53, 67, 69, 71. Four kind of events are prepared:

1. charm ($e^+e^- \to c\bar{c}$)
2. uds ($e^+e^- \to u\bar{u}, d\bar{d}, s\bar{s}$)
3. bsbs ($e^+e^- \to \Upsilon(5S) \to B_s^{(*)}\bar{B}_s^{(*)}$)
4. nonbsbs ($e^+e^- \to \Upsilon(5S) \to B^{(*)}\bar{B}^{(*)}(\pi), \Upsilon(4S)\gamma$) .

We only investigated the new/enhanced reprocessing, which includes improvements in tracking [33].
The most important dataset for this analysis is the Υ(5S) on-resonance data. This corresponds to a number of $\approx 23,651 \cdot 10^6$ B^0 mesons (see sec. 5.1 for the amount of B mesons in each reconstructed decay). It was collected with the goal of producing as many Υ(5S) mesons as possible. The e^+e^- center-of-mass energy was set to (10.8656 ± 0.0020) GeV to enable this [34]. In total data of an integrated luminosity of 121.4 fb^{-1} was taken on the Υ(5S) resonance. In addition to the on-resonance data, 1.73 fb^{-1} of off-resonance data was collected at a center-of-mass energy slightly below the production threshold of the Υ(5S) resonance. This data can be used to study the background, which occurs in the on-resonance data, without Υ(5S) events [34]. In total we have six times the amount of generic MC data then real data.

3.4 Simulation and Analysis Software at Belle II

A variety of software is used for event and detector simulations, reconstruction and data analysis. The software that is used in this analysis is the Belle II Software Framework basf2 [35]. Since we are working with Belle data, we need to convert the data by using a module in the basf2 software that is called b2bii. After the conversion one can use the given Software framework, only some changes need to be applied see sec. 4.4.1. In the following the Event Simulation process including the simulation of signal and non-signal events and radiation using EvtGen, PYTHIA 8.2 and PHOTOS and the simulation of the detector response using Geant3 will be explained. Also tools used in the analysis such as Track and Vertex Reconstruction and the process of Flavor Tagging are presented.

3.4.1 Event Simulation

Signal Monte Carlo (MC) data generation is essential for the study of the B decays at Belle, since the amount of provided signal B mesons in the generic MC data is too little and the reconstruction of the B mesons would take a lot of time when always using the generic data. More on the simulation of signal MC data can be read in sec. 4.4.1.
To simulate data one uses the event generator EvtGen, which is a tool designed for simulating particle decays. The generation of Signal MC data involves several steps, such as implementing decay models, compiling the necessary C++ code, generating the simulated events, and validating the output against known standards (see sec. 4.4.1). The information about EvtGen is taken from Ref. [36] if not stated otherwise. More on the simulation of signal MC data can be read in sec. 4.4.1. EvtGen operates within the framework of the Belle II Analysis Software, allowing a seamless simulation workflow, because of already integrated software packages. The physical processes originating from e^+e^- collisions at the $\Upsilon(5S)$ resonance followed by the decay into B meson pairs which are recreated using MC samples. Also the final states of interest as well as other background processes are simulated using MC data. For these complex particle interactions and detector behavior, multiple software tools are used:

1. Modeling the decay chain of B mesons into exclusive final states is done using the generator `EvtGen`. In so called decay file (dec file), the specific decay chain as well as the branching fraction for each decay step is determinate. EvtGen simulates according to the dec file the production of $B^0\bar{B}^0$-meson pairs and proceeds through their subsequent decays. For neutral B mesons, the oscillation is modeled according to specific EvtGen decay models, which is described in more detail in sec. 4.4.1. More on EvtGen can be read in [37].

2. `PYTHIA 8.2`: To simulate hadronic events from the e^+e^- collision through the decay of the Upsilon resonances and the direct production of $u\bar{u}$, $s\bar{s}$, $d\bar{d}$ and $c\bar{c}$ pairs, PYTHIA 8.2 is used. PYTHIA 8.2 complements the decays into exclusive final states given by the dec file and specific EvtGen model, by considering hadronization, for any final states not explicitly covered in the dec file. Ensuring a more realistic outcome of the simulated data since the simulated events account for all possible outcomes.

3. Final state radiation (FSR) is employed by PHOTOS. It impacts on the final state kinematics, because it imitates photons during particle decays.

4. The interaction of the particles with the Belle detector are modeled using Geant3. This toolkit mimics the detector geometry and the interaction of the particles with the single sub detectors as well as additional hits from real background events to mimic the the background

activity. All in all it allows a realistic simulation of particle tracking, energy deposition, and detector responses.

3.4.2 Track Reconstruction

Charged particles from primary and secondary vertices are reconstructed by track reconstruction. This information is needed to obtain the precise vertex position of the B mesons to properly reconstruct their decay times and investigate their propagation in time.
Track reconstruction includes track finding and track fitting. Track finding involves recognizing clusters and pattern in the CDC and SVD wire hits to assign them to one charged particle. Then the track fitting takes this information as an input and reconstructs trajectories of each particle from the hit positions [38]. The track reconstruction in basf2 is based on the GENFIT tracking framework, an optimized Kalman filter and novel multivariate methods. A detailed description can be found in [36].
The trajectory of a charged particle in a constant homogeneous magnetic field, as given in the Belle detector, follows a helix described by five parameters at a point of the trajectory. This point is chosen to be the point of closest approach to the interaction point (IP), determined by extrapolating the track to the z axis [38]. The five track parameters are:

1. d_0: The signed transverse distance from the IP to the point of closest approach. The sign convention is defined such that, when moving along the track in the direction of the particle's momentum, the sign is positive (negative) if the IP is to the right (left) of the track at the point of closest approach.

2. z_0: The longitudinal distance from the IP to the point of closest approach.

3. ϕ_0: The azimuthal angle ϕ of the track at the point of closest approach.

4. $\tan\lambda$: The tangent of the angle between the momentum at the point of closest approach and the transversal plane.

5. ω: The track curvature. The sign corresponds to the charge of the particle.

These track parameters are fundamental to reconstructing particle trajectories and obtaining precise measurements of decay vertices [38]. d_0 and z_0 are shown in Fig 3.3. These track parameters are fundamental to reconstructing particle trajectories and obtaining precise measurements of decay vertices [38]. Impact parameters d_0 and z_0 are collected in bins of the pseudo-momentum. To characterize the precision of track reconstruction impact parameter resolutions σ^{d_0} and σ^{z_0} can be defined as:

$$\sigma^{d_0} = \sqrt{a^2 + \frac{b^2}{p\beta \sin^{3/2}\theta}}, \quad \sigma^{z_0} = \sqrt{a^2 + \frac{b^2}{p\beta \sin^{5/2}\theta}}, \tag{3.1}$$

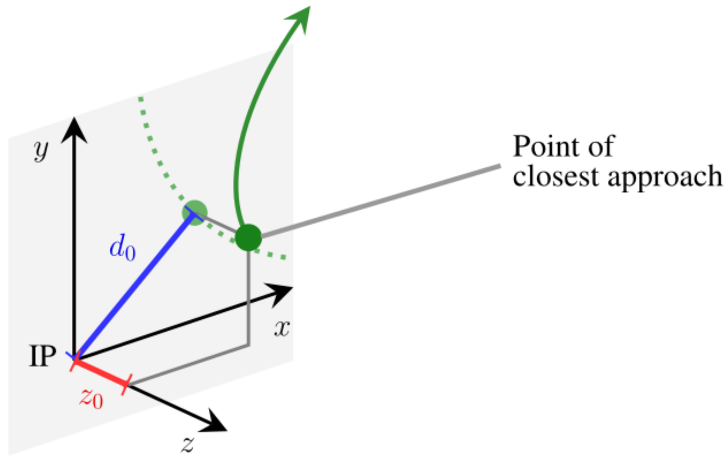

Figure 3.3: Schematic view of track reconstruction parameters. Solid green line shows the particle's track with the dashed green line showing its projection on the xy plane. Impact parameters d_0, z_0 are the distance between origin and Point of closest approach on xy plane and the z coordinate of the Point of closest approach, respectively. [38]

where a is the intrinsic detector resolution, b the multiple scattering coefficient in units of [GeV μm] and the denominators in the equations the so-called pseudo-momenta, which take effect of multiple scattering into account [38]. The impact parameters d_0 and z_0 are collected in bins of the pseudo-momentum. By fitting a Gaussian to the binned impact parameters the resolution parameters from eq. 3.1 can be estimated.

3.4.3 Vertex Reconstruction

To reconstruct the decay or interaction vertex of a particle, reconstructed parameters of decaying particles are used. Not only is it possible to reconstruct the vertex, but also the momentum as well as the invariant mass of the decaying particle is reevaluated. Difference in decay time and decay length can also be calculated by a vertex fitter (see sec. 2.3.1). At basf2, there are two main vertex reconstruction techniques: the Kinematic Fit library KFit developed at Belle and the Reconstruction in an Abstract Vertices Environment RAVE, a standalone software from CMS, which are used for kinematic fits, while latter also serves for geometric fits, and the TreeFitter from the BaBar Collaboration. TreeFitter is used for entire decay chain fitting [36].

In kinematic fits the known properties of specific decay chains are applied to improve measurements, while kinematic constraints are acquired from Lagrangian Multipliers [36]. A χ^2 function is defined which is minimized iteratively in order to obtain parameter estimates on physical quantities. This procedure is usually applied in order to determine decay vertex positions.

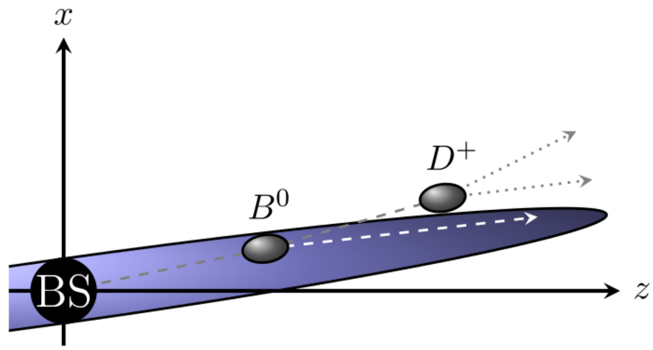

Figure 3.4: Schematic view of the tag-side B decay vertex in zx plane. A ellipsoid region centered around the beam-spot (BS) along the boost direction is defined. While B^0 decays more likely inside this region, decay vertices outside this region are more likely to be D mesons (here, D^+). [36]

Entire decay chains are fitted using the TreeFitter, where trees are parameterized and fitted globally. Because information can be passed along the whole tree in this module, modes rich in neutral and missing particles can also be accessed. As the entire chain is parameterized, χ^2 minimization is not used due to computation lengths. Instead, Kalman filtering algorithm is applied which brings down computation times significantly [36].

Moving on to a crucial application of vertex reconstruction in this analysis is as already described in section 2.3.1 the reconstruction of time variables using vertex information. The sensitivity on the vertex position has to be sufficient to resolve neutral B meson oscillations. The difference between the tag-side and signal-side B decaytime is defined as in eq. 2.57 and the sum of both times in eq. 2.56. Both equations depend on the vertex positions of the tag-side and signal-side B. As the tag-side B's vertex sensitivity dominates the resolution of Δt and Σt a precise determination of the vertex position plays an important role in mitigating uncertainty. In order to further optimize the χ^2 function's minimization, weights are introduced. These weights are constraints imposed upon the D meson's decay vertex. For this, an ellipsoid region is defined around the beam spot orientated along the boost direction in which the B^0 is more likely to decay to a D meson. For decay vertices outside this defined region the tracks originating from that point are assigned to the D. The following figure illustrates this beam spot constraint: More detailed description of the tag-side B meson's reconstruction can be found in Sec. **??**.

3.4.4 Flavor Tagging

B mesons are produced in pairs, in this case as $B^{0(*)}\overline{B}^{0(*)}$ pairs. We reconstruct one B meson fully on the signal channel (signal-side) the remaining reconstructed tracks and neutral ECL and

KLM clusters belong to the other B meson on the so-called tag-side. The information of the flavor of each B meson is crucial for the analysis, since we also want to investigate the time-dependent asymmetry as explained in section 2.3.3 and also the entanglement of the B mesons through their time evolution (see section 2.2.2). We determine the B_{tag} flavor and it consequently dictates the flavor of B_{sig} at the time of B_{tag} decay. The procedure is done using so called flavor tagging algorithms, short flavor tagger.

Flavor-specific decays, e.g. $B^0 \to D^- l^+ \nu_l$ are used to determine the flavor of a decaying B meson. These types of decays result in a final state, which can exclusively be reached from a specific B^0 state There are a lot of possibilities for flavor-specific modes. Reconstruction of all of them is not possible. Thus, the flavor tagger relays on inclusive techniques to gain information provided by signatures in flavor-specific decays.

Flavor Tagging Parameters

Some variables that quantify the goodness of the flavor tagger and which will later be included in the observable PDF (see sec. 4.2.2) are introduced here. We define the efficiency of the Flavor Tagger as the ratio between the number of events where the flavor tagger (N^{tag}) can assign a flavor to over all events (N):

$$\varepsilon = \frac{N^{\text{tag}}}{N}. \tag{3.2}$$

The case of the tag decision to be wrong is expressed by the fraction w, that can be used to express the number of tag-side B^0 mesons:

$$N^{\text{tag}}_{B^0} = \varepsilon(1-w)N_{B^0} + \varepsilon w N_{\overline{B}_0}, \tag{3.3}$$

$$N^{\text{tag}}_{\overline{B}^0} = \varepsilon(1-w)N_{\overline{B}^0} + \varepsilon w N_{B_0}. \tag{3.4}$$

Consequently, the observed asymmetry can be defined in terms of eqs. 3.3 and 3.4

$$a^{\text{obs}} = \frac{N^{\text{tag}}_{B^0} - N^{\text{tag}}_{\overline{B}^0}}{N^{\text{tag}}_{B^0} + N^{\text{tag}}_{\overline{B}^0}} = (1-2w)\frac{N_{B^0} - N_{\overline{B}^0}}{N_{B^0} + N_{\overline{B}^0}}.. \tag{3.5}$$

The statistical uncertainty for this value is given by

$$\delta a = \frac{\delta a^{\text{obs}}_{CP}}{1-2w} \overset{N^{\text{tag}}_{B^0} \approx N^{\text{tag}}_{\overline{B}^0}}{=} \frac{1}{\sqrt{N^{\text{tag}}}(1-2w)}. \tag{3.6}$$

Here the asymmetry is diluted by the term $(1-2w)$ which is the so-called dilution factor

$$r \equiv |1-2w|, \tag{3.7}$$

where $r = 0$ means no flavor information, this is the case for $\omega = 0.5$ and $r = 1$ that the Flavor Tagger determined the flavor with full certainty, hence $w = 0, 1$. By introducing N^{eff}, the effective number of tagged events and with that substituting the denominator from Eq. 3.6 we obtain

$$\delta a = \frac{1}{\sqrt{N^{\text{eff}}}} = \frac{1}{\sqrt{\varepsilon_{\text{eff}} \cdot N}}, \tag{3.8}$$

where ε_{eff} is the effective tagging efficiency, defined as

$$\varepsilon_{\text{eff}} = \varepsilon \cdot r^2. \tag{3.9}$$

As a result one can say that by maximizing the effective efficiency the statistical uncertainties are minimized. Therefore, in this analyses and also several CP-violation analyses the fits are performed in bins of the dilution factor r. The strength of flavor discrimination is maximal for r close to 1. This method is also applied when calibrating the flavor tagger. [38] The r-bins intervals are chosen to be

$$[0.000, 0.100, 0.250, 0.450, 0.600, 0.725, 0.875, 1.000]. \tag{3.10}$$

In the final step, the fact that a possible deviation arises for both w and ε when $q = \pm 1$ has to be considered. This is caused by the detector's charge-asymmetric performance. Thus, eq. 3.2 and w are extended to

$$\varepsilon = \frac{\varepsilon_{B^0} + \varepsilon_{\overline{B}^0}}{2}, \quad w = \frac{w_{B^0} + w_{\overline{B}^0}}{2}, \tag{3.11}$$

where w_{B^0} is the fraction of true B^0 wrongly tagged as $\overline{B}^0$. The differences read

$$\Delta\varepsilon = \varepsilon_{B^0} - \varepsilon_{\overline{B}^0}, \quad \Delta w = w_{B^0} - w_{\overline{B}^0}. \tag{3.12}$$

To account for the charge-asymmetry the r-bins are multiplied by $q = \pm 1$.

4 Analysis Strategy

This chapter explains how we reconstructed and selected events for the three main quantum states used in this analysis. In particular, it discusses how we obtained the time variables and describes the key algorithms applied in each step to obtain the time variables, such as the extraction of kinematic information (see section 2.3.1). Furthermore, it explains how the three $B^{0(*)}\bar{B}^{0(*)}$ pairs, were separated and how the physics model introduced in section 2.3.2 is reevaluated in terms of detector and reconstruction effects, allowing us to move from a purely theoretical model to one that can be observed in data. Finally, the procedure for simulating signal Monte Carlo samples used in this analysis is described, since the number of reconstructed B meson pairs in the generic Monte Carlo samples is too low for a meaningful study. A first, preliminary validation of the signal Monte Carlo dataset is also presented.

4.1 Event Reconstruction and Selection

In this section, the reconstruction process and selection requirements are discussed. The goal of the reconstruction process is to fully reconstruct the signal channel, which defines B_{sig}, and to obtain the flavor and vertex positions of the corresponding B_{tag}. For this purpose, we use a machine learning algorithm called the flavor tagger. The chosen decay channels for reconstructing the B_{sig} meson are

$$B^0 \to D^-\pi^+, \text{ with } D^- \to K^+\pi^-\pi^- \tag{4.1}$$

$$B^0 \to D^{*-}\pi^+, \text{ with } D^{*-} \to \bar{D}^0\pi_s^- \text{ and } \bar{D}^0 \to K^+\pi^- \tag{4.2}$$

$$B^0 \to D^{*-}\pi^+, \text{ with } D^{*-} \to \bar{D}^0\pi_s^- \text{ and } \bar{D}^0 \to K^+\pi^-\pi^+\pi^- \,. \tag{4.3}$$

The excited B meson cannot be reconstructed, since the photon energy of 45 MeV is too low to achieve a good reconstruction efficiency. As a result, reconstructing the B^*would most likely include a large amount of background. To separate the three possible B meson configurations, a different approach, explained in Section 4.1.2, is used.
These decay channels were chosen to align with the analysis by Abudinen et al. [39], even though

that analysis was performed at the $\Upsilon(4S)$ resonance.
The selected channels are hadronic decay modes with charged final-state particles, which makes reconstruction more precise, as charged particles are easier to detect and distinguish. The subscript s in π_s^- denotes the "slow" pion with low momentum, which arises from the small mass difference (about 5 MeV) between the D^* and its decay products in this channel [3].
Another decay channel used in the work of Abudinen et al. [39] is $B^0 \to D^{*-}\pi^+$, with $D^{*-} \to \bar{D}^0\pi_s^-$ and $\bar{D}^0 \to K^+\pi^-\pi^0$, is excluded here due to issues with the reconstruction of the π^0. The main problem was a large amount of background events; applying a tighter cut to reduce this background leads to a loss of about 40% of the signal data. Further details on this issue are discussed in Kilian Brückner's Bachelor's thesis [31].
Unless otherwise stated, all charge-conjugated decay channels are included in the following discussion. In the reconstruction procedure, the B mesons are reconstructed starting from the final-state particles in the decay chain. We begin by reconstructing pions and kaons from hits and tracks in the detector that originate from the same vertex and can be combined to form a D meson. The reconstructed D meson is then combined with an additional pion originating from the same vertex, allowing this common vertex to be identified as the B meson decay vertex. In the next section, the selection criteria for particle reconstruction are described.

4.1.1 Signal and Tag Side

The signal B meson is fully reconstructed from the final-state particles of the decay channel up to the B meson itself. The first step of the signal-side reconstruction is to find D^- and $\bar{D}^0$ candidates. To achieve this, we apply basic geometrical cuts on the decay products of the D mesons, as listed in Table 4.1. These cuts are applied to the pions and kaons and ensure that the particles decay inside the Belle detector.
The fiducial cuts are defined by the transverse distance to the interaction point dr, the vertex z-position dz, and the polar angle θ. It is also necessary to distinguish kaons from pions, which is done using particle identification (PID) cuts. Several methods for distinguishing charged hadrons in basf2 are described in [36]; these methods are based on the Belle II detector. Since this analysis uses Belle data, we employ the PID packages provided by b2bii, the basf2 module that allows for processing Belle data, as Belle mDST samples are converted into Belle II mDST format.
Each of the three PID packages in b2bii combines information collected from various sub-detector systems (CDC, ACC, TOF, ECL, KLM). The combination of individual likelihoods from each sub-detector system can be supplemented with external information, such as a priori probabilities of each particle type, which are read from the Belle database. Special Belle-legacy variables that reproduce the PID variables are introduced (see [35]). Pions and kaons are compared (specified by the indices 2 and 3 in Table 4.1), resulting in a variable ranging from 0 to 1, where values close to

0 represent pions and values close to 1 represent kaons.
The pions and kaons are then combined to form $D^{\pm}$ candidates, taking into account their kinematics. The four-momenta of the combined pions and kaons should match the expected four-momentum of the D meson. The $D^{\pm}$ candidates are subsequently combined with an additional pion to form B^0 candidates, which must lie within loose ΔE and M_{bc} windows.
The approach for decay channels involving a D^* meson is similar. The same cuts are applied to the final-state kaons and pions, with the addition of a list for "slow" pions. Here, the required momentum in the center-of-mass (CMS) frame must be less than 0.5 GeV. The kaons and pions are then combined to form a D^0 candidate, whose invariant mass must lie within the same mass window as for the $D^{\pm}$ candidates. The D^0 candidate, combined with a slow pion, forms a $D^{*\pm}$ candidate, which is required to lie within a loose mass window, and the energy release in the decay Q must be smaller than 15 MeV, as the mass difference between the D^* and its decay products is small [31]. The D^* candidates are then combined with pions to form B^0 candidates, using the same loose ΔE and M_{bc} windows.
In both reconstruction scripts, two separate vertex tree fits are performed. The purpose of the first vertex fit is to reduce the number of non-physical B^0 candidates. This is achieved by applying an interaction point and mass constraint on the $D^{\pm}$ mass, which improves the momentum resolution of the candidates. Afterward, and before the second vertex fit, tighter ΔE and M_{bc} cuts are applied to further reduce the number of non-physical B^0 candidates. The second vertex fit is performed without a mass constraint and updates the vertex positions of all daughter particles, resulting in improved vertex and momentum information.
The B_{tag} meson is reconstructed exclusively, meaning that it can decay generically into all possible final states. The B_{tag} candidates are taken from the Rest of Event (ROE), which consists of particles not associated with the signal-side candidate list. A mask with loose selection requirements for the ROE is taken from [35] to limit the number of possible B meson candidates. The mask applies cuts on the number of CDC hits (which must be greater than one) as well as on the particle momenta in both the CMS and laboratory frames.
The ROE is also important for continuum suppression (CS), since event-shape variables obtained from the ROE are used to distinguish $B^0\bar{B}^0$events from $q\bar{q}$ events. The CS variables are obtained by running the continuum suppression basf2 module, where the same mask is applied. Table 4.1 lists all cuts applied in the reconstruction file.

Cuts applied to all decay channels	
Fiducial cuts for $\pi^\pm$ and $K^\pm$	$dr < 0.5\,\text{cm}$, $\lvert dz\rvert < 3.0\,\text{cm}$, $17° < \theta < 150°$
PID cut for $\pi^\pm$	atcPIDBelle(3,2) < 0.4
PID cut for $K^\pm$	atcPIDBelle(3,2) > 0.6
Requirement for B^0	$M_{\text{bc}} > 5.0\,\text{GeV}$, $\lvert\Delta E\rvert < 1\,\text{GeV}$
Mask for ROE and CS	$n_{\text{CDCHits}} > 0$, $p_{\text{CMS}} \leq 3.2\,\text{GeV}$, $p \geq 0.05\,\text{GeV}$
Cuts applied to D^- decay channel	
Mass cut for $D^\pm$	$1.8597\,\text{GeV} < M < 1.8797\,\text{GeV}$
Narrowed cut after first Tree Fit	$5.25\,\text{GeV} < M_{\text{bc}} < 5.35\,\text{GeV}$, $\lvert\Delta E\rvert < 0.5\,\text{GeV}$
Cuts applied to D^* decay channels	
Special cuts for $\pi_s^\pm$	atcPIDBelle(3,2) < 0.4, $p_{\text{CMS}} < 0.5\,\text{GeV}$
Mass cut for D^0	$1.82\,\text{GeV} < M < 1.91\,\text{GeV}$
Cuts for $D^{*\pm}$	$1.90\,\text{GeV} < M < 2.10\,\text{GeV}$, $Q < 0.015\,\text{GeV}$
Narrowed cut after first Tree Fit	$5.20\,\text{GeV} < M_{\text{bc}} < 5.40\,\text{GeV}$, $\lvert\Delta E\rvert < 0.5\,\text{GeV}$

Table 4.1: Preselection cuts made in the reconstruction script [31].

The efficiencies for the preselection cuts as well as the amount of signal B mesons and the amount of background events, where we combined combinatorial and continuum background, are listed in Tab. 4.1.1. More details on the reconstruction efficiencies are given in Sec. 4.1.3 for each decay channel.

Quantity	$B^0 \to D^-\pi^+$	$\bar{D}^0 \to K^+\pi^-$	$\bar{D}^0 \to K^+\pi^-\pi^+\pi^-$
$n_{\text{available in MC}}$	32758	9116	19873
n_{signal}	10387	3774	4575
$n_{\text{background}}$	165944	275723	1318090
ε [%]	31.7	41.4	23.0

Table 4.2: Signal efficiency after the preselection cuts for the different decay channels have been applied. The background numbers include both continuum and combinatorial $\Upsilon(5S)$ background and are not separated further because of technical reasons. The number of events corresponds to the full $734\,\text{fb}^{-1}$ Monte Carlo data sample.

4.1.2 Separation of the different $\Upsilon(5S) \to B^{0(*)}\bar{B}^{0(*)}$ decays

An important part in this analysis is the separation of the three possible decay channels of the Υ(5S): $\Upsilon(5S) \to B^0\bar{B}^0$, $\Upsilon(5S) \to B^{0*}\bar{B}^0$+ c.c. and $\Upsilon(5S) \to B^{0*}\bar{B}^{0*}$, so that the different forms of entanglement discussed in Section 2.2.2 can be distinguished. In this section, we introduce the method used to separate these three channels by analyzing the kinematics of the possible decay modes. For that we introduce the beam-constrained mass M_{bc}

$$M_{\mathrm{bc}} = \sqrt{(E^{\Upsilon}_{\mathrm{beam}})^2 - (p^{\Upsilon}_{B^0})^2} \tag{4.4}$$

and the energy difference ΔE

$$\Delta E = E^{\Upsilon}_{B^0} - E^{\Upsilon}_{\mathrm{beam}} \,, \tag{4.5}$$

where Υ indicates that the corresponding variables are evaluated in the Υ(5S) CMS frame, $E^{\Upsilon}_{\mathrm{beam}}$ denotes the beam energy in the Υ(5S) CMS frame and is equal to half of the total Υ(5S) energy. Thus, the three decay cases can be distinguished by examining the energies and momenta of the reconstructed signal B meson in the Υ(5S) CMS frame. In the following CMS frame refers to the Υ(5S) CMS frame.

We begin with investigating the momenta:

In the CMS frame the momentum of the Υ(5S) is zero, meaning that the momenta of the $B^{0(*)}\bar{B}^{0(*)}$ mesons are equal in magnitude and opposite in direction $\vec{p_1} = -\vec{p_2}$. The total energy in the system is given by the Υ(5S) mass $m_{\Upsilon(5S)} = (10869 \pm 6)$ MeV. The four momenta are given by

$$P_{B_1} = \begin{pmatrix} E_{B_1} \\ \vec{p} \end{pmatrix} \,,\; P_{B_2} = \begin{pmatrix} E_{B_2} \\ -\vec{p} \end{pmatrix} \,,\; P_{\Upsilon} = \begin{pmatrix} m_{\Upsilon(5S)} \\ \vec{0} \end{pmatrix} \,. \tag{4.6}$$

From energy–momentum conservation in the decay, we get the expression for the invariant mass:

$$P^2_{\Upsilon} = (P_{B_1} + P_{B_2})^2 = m^2_{\Upsilon(5S)} \tag{4.7}$$

$$= E^2_{B_1} + E^2_{B_2} + 2E_{B_1}E_{B_2} \tag{4.8}$$

$$= m^2_{B_1} + m^2_{B_2} + 2\sqrt{|\vec{p}|^4 + |\vec{p}|^2(m^2_{B_1} + m^2_{B_2}) + m^2_{B_1}m^2_{B_2}} + 2|\vec{p}|^2 \tag{4.9}$$

where we used $\vec{p_1} \cdot \vec{p_2} = \cos(\theta = 180°)|\vec{p}|^2 = -|\vec{p}|^2$ and the relativistic momentum energy relation $E^2 = m^2 + p^2$ with $c = 1$. The momentum of the B meson depends only on the masses of B_1, B_2 and the Υ(5S). Note that B_1 and B_2 can each correspond to either a ground-state B meson or an excited B^* meson. When solving eq. 4.7 one obtains for the momentum of the $B^{(*)}$ mesons in the CMS:

$$p = \frac{\sqrt{m^4_{B_1} + m^4_{B_2} - 2m^2_{B_1}m^2_{B_2} + m^4_{\Upsilon(5S)} - 2m^2_{B_1}m^2_{\Upsilon(5S)} - 2m^2_{B_2}m^2_{\Upsilon(5S)}}}{2m_{\Upsilon(5S)}} \,. \tag{4.10}$$

When plugging in the corresponding masses of $m_{B^*} = (5324.75 \pm 0.20)$ MeV, $m_{B^0} = (5279.72 \pm 0.08)$ MeV and $m_{\Upsilon(5S)} = (10885.2^{+2.6}_{-1.6})$ MeV [3], for B_1/B_2, in the respective decay channels, we obtain the momenta of the B mesons in the CMS frames as listed in Tab. 4.3. Since we only

Table 4.3: Momenta of the B mesons in the CMS.

Decay channel	Momentum [MeV]
$B\bar{B}$	$p_B = 1321.53$
$B^*\bar{B}$	$p_{B^*} = p_{B^0} = 1228.08$
$B^*\bar{B}^*$	$p_{B^*} = 1125.99$

reconstruct the B mesons and not the excited B mesons, we also have to take the photon of the electromagnetic transition from $B^{*0} \to \gamma B^0$ into account. The emission of the photon changes the momentum of the B meson depending on the direction of the emission. For simplification, we only look at the two extreme cases were the photon is emitted parallel and anti-parallel to the flight direction of the B meson to calculate the upper and lower limit of the momenta and with that for M_{bc} of the reconstructed B meson. The resulting values for the M_{bc} of the three cases are given in tab. 4.4. We can also distinguish the cases by looking at the photon missing energy, so by looking at ΔE. Here we compare the $B^{0(*)}$ meson energy to half of the $\Upsilon(5\text{S})$ energy in the CMS. For the calculation of the $B^{0(*)}$ meson energy, we again use the relativistic energy–momentum relation. The B meson momentum in the CMS frame is taken from the previously calculated values, which also depend on the direction of the emitted photon. When we only look at the B meson that was not excited and didn't emit a photon before, ΔE should be exactly zero since all of the energy from the $\Upsilon(5\text{S})$ decay is entirely transferred into the production of the B meson and its kinetic energy. However, if the B meson originates from an excited B meson that has previously emitted a photon, then ΔE is not zero, since the energy from the $\Upsilon(5\text{S})$ decay is not only distributed between the production and the kinetic energy of the B mesons, but also into the kinetic energy of the photon. All of the theoretical limits for each case for ΔE and M_{bc} are given in tab. 4.3. Also the values are plotted in fig. 4.1. As can be seen, the calculated values of ΔE and M_{bc} lie on a straight line described by $\Delta E = m_{B^0} - M_{\text{bc}}$. When examining the data, where M_{bc} is plotted against ΔE, the data points are also found to follow this line.Thus, the three decay modes can be distinguished by moving along this theoretical line and defining elliptical regions around it. This approach has already been studied in [40]. Since the separation of these channels is also important in our analysis, Kilian Brückner investigated the same method in his Bachelor's thesis [31], and additionally explored improvements to the separation using boosted decision trees (BDTs). He used generic Monte Carlo data and optimized the cuts required for both background suppression and signal separation between the different cases. The variables ΔE and M_{bc} were used as input features for training the BDTs, together with reconstructed B mesons from the same decay channels that are employed in this analysis (see [31] for details). Because the same decay channels, selection cuts, and generic Monte Carlo samples are used here, we can directly apply his methods in our analysis.

Table 4.4: Theoretical maximum and minimum values for M_{bc} and ΔE for the different cases.

Decay channel	**Direction of photon emission**	ΔE [MeV]	M_{bc} [MeV]
$\Upsilon(5\text{S}) \to B\bar{B}^0$	None emitted	0	5279.72
$\Upsilon(5S) \to B^{0*}\bar{B}^0$+c.c.	parallel	−31.95	5312.46
	back to back	−11.56	5291.61
	B^0 detected	−21.93	5302.24
$\Upsilon(5S) \to B^{0*}\bar{B}^{0*}$+c.c.	parallel	−53.35	5334.17
	back to back	−34.58	5315.14

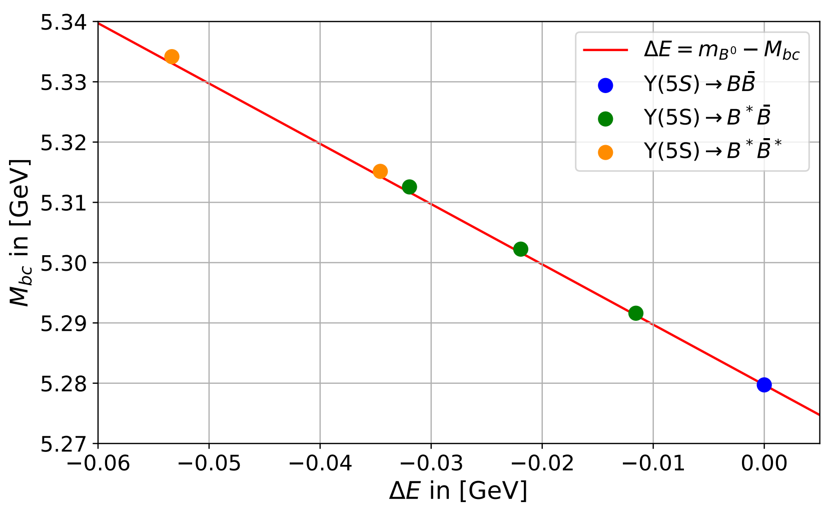

Figure 4.1: Theoretical ΔE and M_{bc} values as upper and lower limit for each decay of Υ(5S). The values fall on a line described by $\Delta E = m_{B^0} - M_{\text{bc}}$.

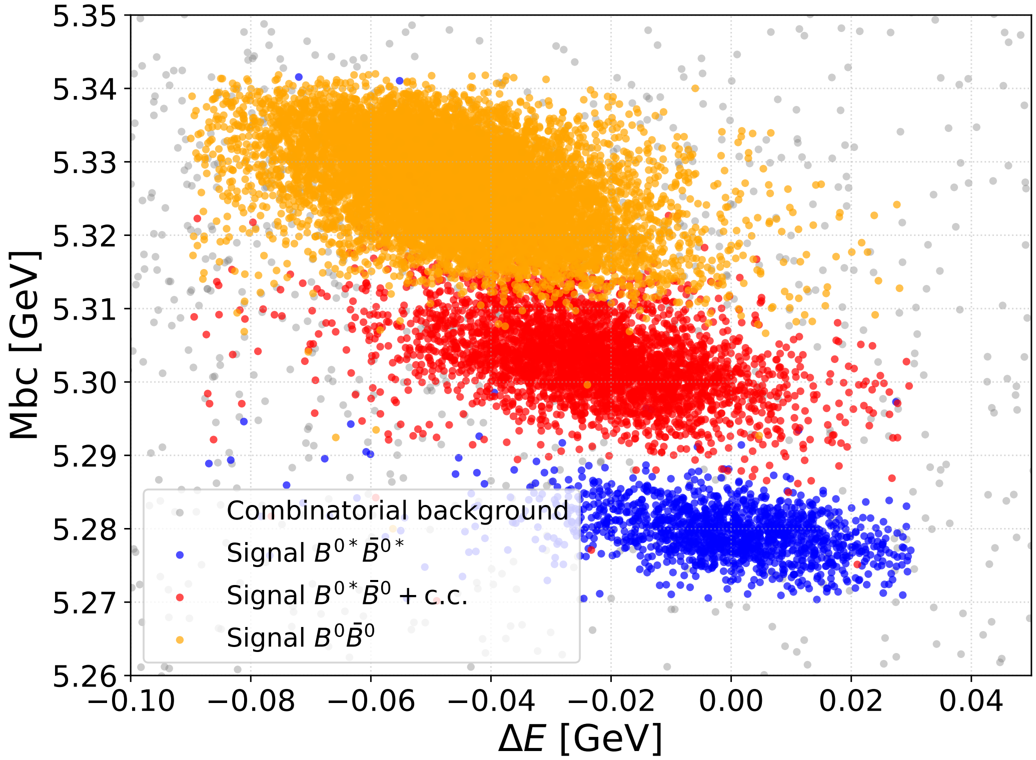

Figure 4.2: Reconstructed invariant mass M_{bc} as a function of ΔE for three decay channels (see legend). Grey dots indicate the combinatorial background.

4.1.3 Background studies and Reconstruction Efficiency

All of the cuts in section 4.1.1 are only made in the reconstruction script, which is also called steering file. The Signal and Background events after these loosely set reconstruction script cuts can be seen in fig. 4.4. After the reconstruction, additional tighter cuts are made in the so called Offline analysis. The cuts are shown in table 4.5. All of the chosen cuts in the offline analysis for this analysis were studied in the Bachelor Thesis of Kilian Brückner [31] and are taken over for this thesis when dealing with generic Monte Carlo data, because the same reconstruction script, the same decay channels as well as the same generic Monte Carlo Data provided by the Belle collaboration is used. Since this work here primarily focuses on simulating Signal Monte Carlo data, to optimize the number of reconstructed signal B mesons, and testing the physics model on it, the background studies which are made on generic Monte Carlo data weren't established so far. One goal of the analysis [31] was to differentiate background events such as combinatorial background, continuum background and beam induced backgrounds or background coming from e^-e^+ scattering from signal events. The latter isn't as relevant for this thesis as the other two, since it is mostly handled by the Belle trigger system [35].

Continuum background and Combinatorial Background are both called physics backgrounds. Combinatorial background means that final particles are wrongly combined to a D or B meson even though the final particles are correct. This happens for example when an additional intermediate particle was part of the decay chain as for example in the case of $D^- \to [\bar{K}^{0*} \to K^-\pi^+]\pi^+$ instead of $D^- \to K^+\pi^-\pi^-$. The reconstruction script includes this decay as well. This process can also result in a true B meson. This decay channel has to be excluded in the final selection cuts after the reconstruction.

Continuum background is the dominant source of background and contains $e^-e^+ \to q\bar{q}$ events with $q = u, d, s, c$. The resulting quarks can hadronized and match the final states of the B mesons resulting in wrongly detected signal B mesons.

The cuts and variables to cut on were chosen and optimized by using an differential evolution algorithm which is a stochastic based optimization algorithm and searches large solution spaces. It was used to eliminate any influence of variables that depend on each other. The algorithm is explained in more detail in [31] and [41]. The optimization metric of the differential evolution algorithm was chosen to be a figure of merit (FOM), which aims to optimize the significance od the resulting signal yield [1]

$$FOM = \frac{S}{\sqrt{S+B}}\,, \tag{4.11}$$

with S being the number of signal events and B the number of background events. The chosen variables to cut on in the offline analysis are:

1. M_{bc} and ΔE, which are explained in sec.4.1.2. These cuts exclude background events that are not reconstructed B mesons. The ΔE range is asymmetric, i.e., shorter on the lower side, to reduce backgrounds from B decays with missing daughters [2].

2. The invariant mass on the D^- and in the D^* channels on the D^* as well as on the D^- invariant mass. This allows to differentiate wether wrong daughter particles were included in the recombination. That's why these cuts especially reduce the number of combinatorial backgrounds, but also the majority of the continuum background (see for more details [31]).

3. Energy released in the decay of the D^*: $Q = M(D^{*-}) - M(\bar{D}^0) - M(\pi_s^-)$. Additionally to the invariant mass cut, this cut allows to separate more continuum background. It connects the D^* and D^0 momentum measurements. Since the uncertainty of the D^* momentum is mostly dominated by the D^0 momentum measurement because the energy release in the D^* decay is low and one can measure the π_s^- momentum pretty precisely, one can cancel out the D^0 momentum measurement uncertainty by looking at Q, making a tighter cut possible [1].

4. D^- significance of flight distance. It is given by $d_{\mathrm{flight}}/\sigma_{\mathrm{flight}}$ and is the ratio between flight distance of the D^- and the significance of its flight distance. The goal of this cut is to

eliminate events containing a D^- with momentum that points in the opposite direction to the traveled distance [39]. This cut allows for further discrimination of the continuum background.

5. Event shape variables for continuum suppression: Thrust axis, which direction is the projection of all maximum momenta of the decay products of the B meson candidates, the angle θ_T between thrust axis of the reconstructed B meson and the thrust axis of the Rest of Events, the ratio between the second and zeroth Fox-Wolfram moment $R2 = H2/H0$. The Fox-Wolfram moments for a group of N event particles with momenta $\vec{p}_i$ is defined as $H_K = \Sigma_{i,j}^{N} |\vec{p}_i||\vec{p}_j| P_k(\cos\theta_{ij})$ with P_k being the $k-$th Legendre Polynomial [1]. In fig. 4.3 one can see the difference between the event shape of the B meson events and the continuum event. Since the quarks in continuum events hadronize and produce jets, that are pointing into the same direction as the large momentum of the quark, one can distinguish them from the B meson events, where the decay products are emitted more uniformly because of the lower momentum of the $B^{(*)}$ meson.

All of the final cuts are shown in Tab. 4.5.

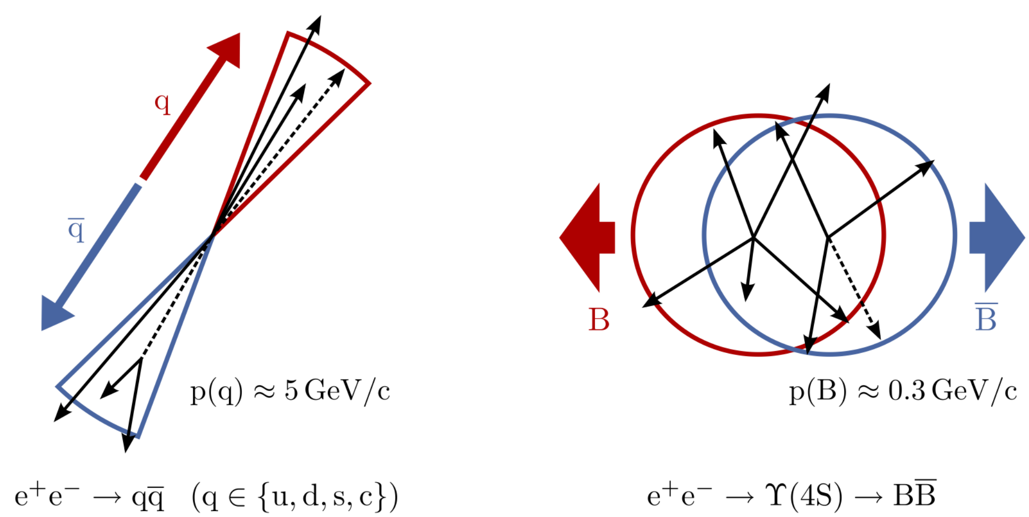

Figure 4.3: Continuum and B meson events shape at the Υ(4S) (credit: Markus Röhrken) [35].

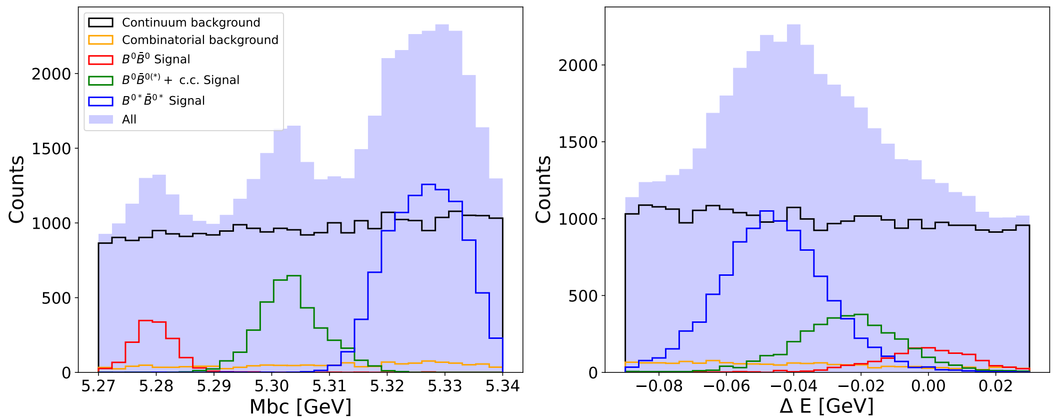

Figure 4.4: The projections of ΔE and M_{bc} from Fig. 4.2 onto the respective axes are shown here. Background includes continuum and combinatorial background. The cuts from Tab. 4.5 and Tab. 4.1 are applied. The decay channels are the ones listed in 4.1.

Table 4.1.1 shows the reconstruction efficiencies for the three decay channels. These correspond only to the efficiencies obtained after running the reconstruction script, i.e., before applying the final selection cuts listed in Table 4.5. The total reconstructed efficiencies after the final selection cuts are listed in Tabs. 4.6, 4.7 and 4.8 for each reconstructed decay channel.

Cuts applied to all decay channels	
Tightened ΔE cut	-0.09 GeV $< \Delta E <$ 0.03 GeV
Tightened M_{bc} cut	5.27 GeV $< M_{\mathrm{bc}} <$ 5.342 GeV
Cuts applied to $B^0 \to D^-\pi^+$ decay channel	
Thrust axis angle	$\lvert\cos\theta_T\rvert < 0.747$
Thrust magnitude of B meson	$\mathrm{thrust}_B < 0.964$
Fox–Wolfram ratio R_2	$R_2 < 0.470$
D^- invariant mass	1.859 GeV $< M_{D^-} <$ 1.8804 GeV
Signed significance of D^- flight distance	$d_{\mathrm{flight}}/\sigma(d_{\mathrm{flight}}) > 0$
Cuts applied to $\bar{D}^0 \to K^+\pi^-$ decay channel	
Thrust axis angle	$\lvert\cos\theta_T\rvert < 0.793$
Thrust z-angle	$\lvert\cos\theta_z\rvert < 0.897$
Fox–Wolfram ratio R_2	$R_2 < 0.313$
D^{*-} invariant mass	1.9859 GeV $< M_{D^{*-}} <$ 2.0536 GeV
$\bar{D}^0$ invariant mass	1.8363 GeV $< M_{\bar{D}^0} <$ 1.8923 GeV
Energy released in D^* decay (Q value)	0.0041 GeV $< Q <$ 0.0083 GeV
Cuts applied to $\bar{D}^0 \to K^+\pi^-\pi^+\pi^-$ decay channel	
Thrust axis angle	$\lvert\cos\theta_T\rvert < 0.769$
D^{*-} invariant mass	1.994 GeV $< M_{D^{*-}} <$ 2.0362 GeV
$\bar{D}^0$ invariant mass	1.8443 GeV $< M_{\bar{D}^0} <$ 1.8813 GeV
Energy released in D^* decay (Q value)	0.005 GeV $< Q <$ 0.0072 GeV

Table 4.5: Final cuts for all decay channels and variables [31].

The efficiencies after the final cuts were studied in detail in [31]. The total efficiencies for the reconstruction including the final cuts are calculated as the product of the reconstruction efficiencies from Table 4.1.1 and the individual cut efficiencies from Table 4.5 taken from the analysis in [31]. Since the same cuts are applied in this analysis, we do not recalculate them. Only the efficiencies after the reconstruction script differ, due to the additional vertex fit applied to the tag-side B meson (resulting in about 87.9% less signal data).

Cut	n(signal)	$n(\Upsilon(5S)$ background) & n(Continuum)	ε [%]
Preselection	10387	165944	31.7
ΔE and M_{bc}	10387	4870 & 161074	100.0[1]
D^- invariant mass	9431	1241 & 50017	90.8
D^- flight significance	8582	823 & 33469	91.0
Continuum suppression	6350	554 & 5635	74.0
Total		–	**19.4**

Table 4.6: Reconstruction efficiencies ε for the $B^0 \to D^-\pi^+$ decay channel. ε is calculated for each reconstruction step. The total efficiency is computed by comparing the final number of reconstructed signal events to the number of generated events listed in Table 4.1.1. Background is not separated into continuum and $\Upsilon(5S)$ components at preselection due to technical reasons.

Cut	n(signal)	$n(\Upsilon(5S)$ background) & n(Continuum)	ε [%]
Preselection	3774	275723	41.4
ΔE and M_{bc}	3136	593 & 10424	83.1
D^{*-} and D^- invariant mass	3082	455 & 8343	98.3
Q	2891	177 & 6577	93.8
Continuum suppression	2217	119 & 1556	76.7
Total		–	**24.1**

Table 4.7: Reconstruction efficiencies ε for the $D^0 \to K^+\pi^-$ decay channel. ε is calculated for each reconstruction step. The total efficiency is computed by comparing the final number of reconstructed signal events to the number of generated events listed in Table 4.1.1. Background is not separated into continuum and $\Upsilon(5S)$ components at preselection due to technical reasons.

4.2 Observable PDF

In chapter 2 we discussed the physical quantities of all the entangled and disentangled cases and derived the different PDFs for each case as a function of Δt as well as Σt. We did not take measurement uncertainties that change the physical PDF into account. Such reconstruction effects are wrongly determined Flavor of the tag B meson B_{tag}, detector response and kinematic smearing. From now on we only focus on the Δt dependency of the $C = -1$ case and the disentangled case, since this work builds upon the existing analysis of partial spontaneous entanglement at the $\Upsilon(4S)$ as in [42] and [2], where this resolution function model has already been used. A further goal, which could be pursued as a continuation of this work, is to find a suitable resolution model for the measurement of Σt, as well as to implement the $C = +1$ case into the given fit framework.

Cut	n(signal)	$n(\Upsilon(5S)$ background) & n(Continuum)	ε [%]
Preselection	4575	1318090	23.0
ΔE and M_{bc}	3788	3524 & 46096	82.8
D^{*-} and D^- invariant mass	3557	1319 & 18332	93.9
Q	3183	331 & 8193	89.5
Continuum suppression	2467	237 & 2114	77.5
Total		–	**24.1**

Table 4.8: Reconstruction efficiencies ε for the $\bar{D}^0 \to K^+\pi^-\pi^+\pi^-$ decay channel. ε is calculated for each reconstruction step. The total efficiency is computed by comparing the final number of reconstructed signal events to the number of generated events listed in Table 4.1.1. Background is not separated into continuum and $\Upsilon(5S)$ components at preselection due to technical reasons.

An important accomplishment would be to perform a two-dimensional fit of the B meson time distributions, either by fitting Δt and Σt simultaneously, or by using a linear combination of both to extract t_1 and t_2. Due to time constraints, this could not be accomplished within this analysis. The detector effects are modeled by the Resolution Function $R(\delta\Delta t, \sigma_{\Delta t})$, which is a distribution of residuals $\delta\Delta t = \Delta t - \Delta t^{\mathrm{MC}}$, described by the difference of true decay time difference and reconstructed decay time difference. One observes the discrepancy of true and reconstructed values because of combined uncertainty on the vertex position as well as tracks coming from intermediate charm decays on tag-side [2].

4.2.1 Flavor Tagger parameters in the PDF

We want to include the wrongly identified flavor of the B mesons by including the Flavor Tagger parameters from Sec. 3.4.4 into the fit function and with that its impact on the observable PDF. When using the Flavor Tagger Variables from Sec. 3.4.4 and using them for the spontaneous disentangled (SD) function and with that the partial spontaneous dismantlement (PSD) Δt distributions from eq. 2.102 for Opposite Flavor (OF) events and eq. 2.99 for Same Flavor (SF) events and eq. 2.111 for the PSD function, we obtain for the adapted SD function

$$\begin{aligned} P^{\mathrm{obs}}_{SD}(\Delta t; q_{\mathrm{sig}}, q_{\mathrm{tag}}) = \frac{\varepsilon}{8}\, e^{-\Gamma\Delta t}\Big[&2(1 - q_{\mathrm{tag}}\Delta w + q_{\mathrm{tag}}\mu(1-2w)) \\ &- [q_{\mathrm{tag}}(1-2w) + \mu(1 - q_{\mathrm{tag}}\Delta w)]q_{\mathrm{sig}} \\ &\times \big(f_{\cos}\cos(\Delta m\,\Delta t) + f_{\sin}\sin(\Delta m\,|\Delta t|)\big)\Big]\,, \end{aligned} \tag{4.12}$$

with $\mu = \Delta\epsilon/2\epsilon$, and q_{tag} and q_{sig} being the flavor of the tag-side and signal-side B meson. $\Delta\epsilon$, w, and ϵ are the Flavor Tagger Parameters described in Sec. 3.4.4. $f_{\cos}$ and $f_{\sin}$ are the prefactors of the trigonometric functions of eq. 2.102 for OF events and eq. 2.99 for SF events. The Δt distribution for the PSD model can then be computed by inserting eq. 4.12 in the equation for the PSD model (see eq. 2.111). This approach was chosen to be the same as in [42] and [38], since the wrongly detected flavor information are integrated in the fit framework as shown in eq. 4.12.

4.2.2 Resolution Function

To include the detector response we use the same model for the resolution function as in [2]. The resolution function is a linear combination of three components: two outlier parts denoted by the subscript OL and one core part:

$$R(\delta\Delta t;\sigma_{\Delta t}) = (1-f_{\mathrm{OL}})R_{\mathrm{core}}(\delta\Delta t;\sigma_{\Delta t}) + f_{\mathrm{OL}}R_{\mathrm{OL}}(\delta\Delta t;\sigma_{\Delta t}), \tag{4.13}$$

with f_{OL} the fraction of outlier events. Moreover, $R_{\mathrm{core}}(\delta\Delta t;\sigma_{\Delta t})$ is the sum of two single Gaussians $G(x;\mu;\sigma)$ and a Gaussian convoluted with the right- and left-side exponential tail $\exp_{\pm}(x)$, with $x>0$ or $x<0$:

$$\begin{aligned}
R_{\mathrm{core}}(\delta\Delta t;\sigma_{\Delta t}) =&(1-f_{\mathrm{tail}})\cdot G(\delta\Delta t;\mu_{\mathrm{main}}\cdot\sigma_{\Delta t}, s_{\mathrm{main}}\cdot\sigma_{\Delta t})\\
&+ f_{\mathrm{tail}}(1-f_{\mathrm{exp}})\cdot G(\delta\Delta t;\mu_{\mathrm{tail}}\cdot\sigma_{\Delta t}, s_{\mathrm{tail}}\cdot\sigma_{\Delta t})\\
&+ f_{\mathrm{tail}}\cdot f_{\mathrm{exp}}\cdot G(\delta\Delta t;\mu_{\mathrm{tail}}\cdot\sigma_{\Delta t}, s_{\mathrm{tail}}\cdot\sigma_{\Delta t})\\
&\otimes((1-f_{\mathrm{R}})\mathrm{exp}_{\mathrm{L}}(\delta\Delta t/c\cdot\sigma_{\Delta t}) + f_{\mathrm{R}}\mathrm{exp}_{\mathrm{R}}(-\delta\Delta t/c\cdot\sigma_{\Delta t}))
\end{aligned} \tag{4.14}$$

with $\sigma_{\Delta t}$ being the vertex fit uncertainty on Δt. The mean and width of the tight and wide gaussians are denoted with the subscripts main and tail. The constant c models the length of the exponential tails. The fractions of events that belong to either the exponential part, tail part (Gaussian and exponential tail) or right exponential part are given by the parameters f_{exp}, f_{tail} and f_{R}. f_{tail} is given as in [2]

$$f_{\mathrm{tail}}(\sigma) = f_{\mathrm{max}}\cdot\mathrm{erf}(\sigma,\mu=f_{\mu}), \tag{4.15}$$

where erf is the error function, which causes a smooth transition between small and large tail fractions for $\sigma_{\Delta t}$ [2]. The OL part of eq 4.13 is given by

$$R_{\mathrm{OL}}(\delta\Delta t;\sigma) = G(\delta\Delta t, 0, \sigma_{\mathrm{OL}}). \tag{4.16}$$

The analytical convolution of the resolution function with the physics PDF from 2.2.2 is a crucial step to obtain the observed PDF and is described in [43] and [42]. Also a short derivation is given in the appendix. The choice of the resolution's parametrisation in [2] was compared to an alternative parametrization called the BaBar shape, which requires fewer parameters that can be left to float in the fit. But it has been shown to be less accurate than the approach used in this thesis, because it introduces a small bias to mixing parameter Δm [2].

4.3 Likelihood Function and Fit Method

The goal of a model fitting framework is to determine fit modeling parameters θ by maximizing the agreement of a set of data points to a probability distribution described by a set of parameters $\vec{\theta}$. The measurement of the metric of the goodness or the disagreement of the predicted model with the experimental data is called loss function. In our case we want to extract physical parameters from the observed Δt distribution. To do so we define our loss function as the likelihood function L, in particular the extended negative log-likelihood (NLL), which is minimized in order to estimate the parameters of the model [44]:

$$L = -\Sigma_i^n \ln(f(\theta|x_i))\,, \tag{4.17}$$

with $f(\theta|x_i)$ being the probability density function evaluated at event x_i and parameter θ [44]. with the experimental data is referred to as loss function [44]. The probability density function is given by the physical PDF convoluted with the resolution function as explained in section 4.2.2. It is constructed by using zfit [44], a python based model fitting library based on TensorFlow [45] [42]. The fit is performed using the Minuit algorithm implemented within the minuit library [46].

4.4 Validation of the Signal MC sample

So far only generic Monte Carlo Belle data was provided on the $\Upsilon(5S)$. Since the actual amount of signal data, especially in the $B\bar{B}$ and $B^*\bar{B}+$ c.c. case was too low to study proper entanglement effects as well as the computing time for reconstructing events was really high, we needed to simulate Belle Signal Monte Carlo data, containing only events of the chosen decay channels. In this section the procedure of simulating Signal Monte Carlo data is explained. Since the software that is used to reconstruct the events and obtain event variables such as the Flavor of the B mesons, time information and vertex information, is mainly written for Belle2 data and the $\Upsilon(4S)$ decay case, it was needed to rewrite some functions and variables.

4.4.1 Simulating Belle Signal Monte Carlo Data

As explained in sec. 3.4.1 we need to first generate B decays using the event generator EvtGen, a versatile tool specifically designed for simulating particle decays. For that we generate Signal Monte Carlo (MC) data.
The event generator EvtGen has so far only used the model VSS_BMIX which describes the decay of a $C = -1$ vector particle into two scalar particles such as $\Upsilon(4\mathrm{S}) \to B^0\bar{B}^0$, using $B^0\bar{B}^0$ like coherent mixing. The two possible daughter particles must be charge conjugates and have the same lifetime. Their mass difference is supplied as an argument to the model, in units of $\hbar/s$ which in our case is the mass difference Δm [37]. Since we also want to consider $C = +1$ decays as well as decays of the $\Upsilon(5\mathrm{S})$ to particles and their charge conjugated excited particles, we need to introduce a new mixing model called PHSP_BB_MIX. This mixing model allows to generate decays like

$$\Upsilon(5\mathrm{S}) \to B^{0(*)}_{(s)}\bar{B}^{0(*)}_{(s)}(X)\,, \tag{4.18}$$

with (X) being an additional particle. It takes as input the C eigenvalue of the $B^{0(*)}(s)\bar{B}^{0(*)}_{(s)}$ pair and the mixing parameter $\Delta m_{(s)}$. This model does not represent the physics accuratley and should be used with care as already mentioned in [47], but it should be sufficiently accurate for our purpose. The limitations are:

1. All daughters of the $\Upsilon(5\mathrm{S})$ are assumed to be spinless which is not true for the excited states.

2. The mixing dosen't happen with the B mesons, but instead with the direct decay products of the $\Upsilon(5\mathrm{S})$, which can also be the excited B mesons B^*. For that the direct decay products have the same properties as the B^0 and undergo the same mixing. Then they decay into B mesons with no lifetime. These new particles are called B0heavy which represents the B^{0*} and B0long which represents the B^0, that is a direct decay product of the $\Upsilon(5\mathrm{S})$ in the $\Upsilon(5\mathrm{S}) \to B^0\bar{B}^0$ and $\Upsilon(5\mathrm{S}) \to B^{0*}\bar{B}^0+$ c.c. case. This solution is chosen for implementation simplicity, but the $B^{*0} \to B^0\gamma$ vertices are displaced from their true position [47].

To implement this mixing model, several modifications had to be made in the basf2 software. For this purpose, the software was installed locally, allowing changes to be made in the particle decay table (PDL) as well as in the generic decay file, which describes all possible decays of a B meson. The changes in the particle definition table are as follows:

1. The B^0 and $\bar{B}^0$ particles are assigned a zero lifetime. The particle B^0 is now renamed B0test with Particle Identification Number 5011. We had to introduce this completely new particle, B0test, because simply setting the lifetime of the predefined B^0 in the PDL to zero did not work: the locally modified PDL was overwritten during event generation, and EvtGen's internal PDL reset the B^0 lifetime to its original value. As a consequence, the B

mesons would oscillate twice: once immediately after the $\Upsilon(5S)$ decay, and a second time after B0long or B0heavy[2] decayed into B^0. This caused the reconstructed asymmetry mixing frequency and B^0 lifetime to be incorrect by halving the true mixing frequency and lifetime in the reconstructed time distributions.

2. (anti-)B0long has the B^0 properties with the non-zero lifetime and decays to B0test.

3. (anti-)B0heavy is a B^{*0} with the B^0 lifetime and without spin. It decays to B0test and γ.

4. The standard decay file, DECAY.DEC, which describes all possible decay modes of the Bnmeson, had to be modified for the new particle B0test, so that it decays through all channels in exactly the same way as the B^0. This is important because we want the tag-side B meson to decay generically, while the signal-side B meson decays only into the specified decay channel.

Also a globaltag with smearing of beam parameters and generation flags is needed which is called b2bii_beamParameters_with_smearing.
After event generation, which describes purely the physical process, the Belle detector simulation is applied. This is performed using a Geant3-based detector simulation (for more details see: [48]). For this step, only the EvtGen-produced GEN files are required as input, and the output consists of Belle Signal MC mDST files. These files should then be converted to Belle II mDST format to be used in the reconstruction scripts. Since the events were generated at generator level with basf2 using a global tag that includes beam smearing, it is necessary to disable smearing in the Belle simulation by removing the bpsmear module from the basf gsim scripts. The following differences must also be considered: when converting the simulation results back to Belle II format, it is recommended to disable the conversion of beam parameters (convertBeamParameters = False). Because the BELLE_NOMINA_BEAM table cannot store an arbitrary covariance matrix, the covariance matrix of the interaction point (BeamSpot) is not guaranteed to be identical after conversion.

4.4.2 Flavor tagging variables

In basf2, many functions are written assuming that the mother particle is the $\Upsilon(4S)$, rather than the $\Upsilon(5S)$. Because of this, most functions and variables obtained from basf2 need to be checked to determine whether this assumption affects them. The process of determining which variables and functions were affected, as well as rewriting the necessary functions and obtaining the correct variable information, was a difficult and time-consuming part of this thesis.

[2]These names are misleading: long and heavy have no relation with the mass eigenstates of the $B^0\bar{B}^0$ system. B0long is a B^0 with a non-zero lifetime, B0heavy has the same spin and lifetime as a B^0, but the mass of the B^{0*}.

In the case of the flavor information of the other B meson, this is relevant. In basf2, the variable FlavorOfTheOtherBmeson is used to obtain the Monte Carlo information of the flavor of the tag-side B meson. However, since the source code of this variable requires the mother particle to be the $\Upsilon(4S)$, we do not obtain any value in the case of the $\Upsilon(5S)$. Therefore, it was necessary to find a way to determine certain variables, which are not provided in the $\Upsilon(5S)$ case, manually. A schematic overview of the procedure is shown in fig. 4.7.
The first problem was that we knew all of the signal B meson MC variables but had little information about the tag side B meson. The approach was that in addition to the reconstructed B meson list, we also extracted B mesons from the fillParticleListFromMC which is used to create and fill a particle list directly from Monte Carlo (MC) truth information and not from reconstructed detector data that match a given decay descriptor [35]. Out of this list we got the MC information for two B meson candidates that were labeled with B_1 and B_2. To match each MC particle out of the list to the sig or tag B meson, we labeled each particle with an particle ID, so that we could then compare the IDs with the sig B meson ID. This allows us to obtain all MC information for both the sig and the tag B meson by matching the IDs see fig. 4.7.
To evaluate the performance of the flavor tagger the variable qrGNN is analyzed. For each decay case of the $\Upsilon(5S)$. The flavor tagging algorithm is not sensitive to entanglement effect since it takes only the momentum and tracks of the particles into account which are the decay products of the tag side B meson [49].

The problem with the flavor tagger was that the number of SF and OF events was nearly identical, which is not physically expected. This is because the ratio can be calculated for each qrGNN bin, and in the purest bin—i.e., when qrGNN can determine the flavor of the tag-side B meson with at least 85% accuracy the ratio should be exactly 22% in the $C = -1$ case. One can calculate this ratio with

$$\text{ratio} = \frac{P(B^0 B^0) + P(\bar{B}^0 \bar{B}^0)}{P(\bar{B}^0 B^0) + P(B^0 \bar{B}^0)} \tag{4.19}$$

when plugging in the probability function derived in eq. 2.67 and eq. 2.66.

However, this was not observed, see fig. 4.5. Here, the blue curve represents the case where the signal-side B meson is a $\bar{B}^0$, while the red curve corresponds to the signal-side B meson being a B^0. When looking at the qrGNN output, one observes that at values close to -1, meaning that the Flavor Tagger identifies the tag-side B meson as a $\bar{B}^0$ with nearly 100% purity, the number of same-flavor (SF) events is larger than the number of opposite-flavor (OF) events, as indicated by comparing the red and blue curves. The same behavior appears at qrGNN output values close to $+1$. This leads to a ratio of SF to OF events greater than 100%. Therefore, it was investigated whether this issue originates from the signal Monte Carlo (MC) sample. As references, the generic Monte Carlo data provided by the Belle collaboration, as well as the $\Upsilon(4S)$ signal MC data for the decay $\Upsilon(4S) \to B^0 \bar{B}^0$, were used. When examining the ratio between Same Flavor and Opposite

Flavor events as a function of the qrGNN bin, a linear, monotonically decreasing behavior following a function of the form $ax + b$ can be observed see fig. 4.6. This behavior is also expected for the Υ(5S) case. From this, it can be concluded that the flavor tagger does not yet perform correctly on the pure signal Monte Carlo data, and that further calibration is required concerning the decay products of the tag side B meson or the ROE objects on which the flavor tagger operates. This issue needs to be further studied and refined within the scope of the Υ(5S) analysis. A first attempt to correct it was made by adjusting the number of SF events: using the $ax+b$ function obtained from the generic data, where the behavior is known to be correct, SF events were randomly removed to match the expected ratio.

In fig. 4.8, 4.9 and 4.10 the qrGNN for all corrected Signal MC cases is shown. The blue and red histogram show the distribution for $q_{\mathrm{tag}^{\mathrm{MC}}} = \pm 1$, which is the MC information of the flavor of the tag side B meson, respectively. The combined histogram is shown in black. All figures show the characteristic shapes of the qrGNN variables, also seen in [49]. But this is only the case for the $C = -1$ case. For the $C = +1$ case we don't have a reference, since this case was not investigated before. The histograms show a strong peak |qrGNN| values close to ± 1. This means the qrGNN-bin in intervals 3.10 with highest purity is the most densely populated. For lower |qrGNN| values the blue and red distributions becomes mostly flat until qrGNN$= 0$. For $q_{\mathrm{tag}^{\mathrm{MC}}} = \pm 1$ and qrGNN < 0 (> 0), drops off but is non-zero due to mistagged events.

4.4.3 Δt^{MC} distributions

The goal of this analysis is to use the already existing fitframework that was used in [2] and [42] for the $\Upsilon(4\mathrm{S})$ analysis to test the SPD model and with that validate the theory that is obtained here, to see if by mixing the $C = \pm 1$ states, one can create a disentangled state with a specific disentanglement fraction ζ. For that it is crucial to reconstruct the proper decay time difference Δt, which is the decay time difference of the B mesons in their own restframe. The theoretical Δt distributions have been discussed in chapter 2.
To obtain the correct Δt variable we again have to define our own variable, since basf2 uses an approximation for obtaining Δt in the $\Upsilon(4\mathrm{S})$ case, which can not be used in the $\Upsilon(5\mathrm{S})$ analysis, since they neglect the additional boost of the $\Upsilon(n\mathrm{S})$ on the B mesons, which separates the B mesons in every direction and allows us to measure both Δt as well as Σt.
In section 2.3.1 we calculated the time distributions out of the kinematics of the B mesons. As a reminder the formula is given as

$$\Sigma t = \frac{\Delta xy}{\beta_B \sin(\theta_{\mathrm{CMS}})\gamma_B} \tag{4.20}$$

$$\Delta t = \frac{\Delta z}{\gamma_B \gamma \beta} - \frac{\Delta xy \cot(\theta_{\mathrm{CMS}})}{\beta_B \beta}\,. \tag{4.21}$$

With

$$\Delta x = (x_{B_1} - x_{B_2})\cos(\alpha) + (z_{B_1} - z_{B_2})\sin(\alpha) \tag{4.22}$$

$$\Delta z = (z_{B_1} - z_{B_2})\cos(\alpha) - (x_{B_1} - x_{B_2})\sin(\alpha)\,, \tag{4.23}$$

and

$$\Delta xy = \sqrt{\Delta x^2 + \Delta y^2}\,. \tag{4.24}$$

Now, we need to derive all relevant variables from the vertex and momentum information. One important point to consider is that, during the conversion of Belle MDST samples to BelleII MDST samples, the correct interaction point (IP) was not transferred. Therefore, it is crucial to set the IP constraint to False in the vertex fit within the reconstruction script. Otherwise, only events within a cylinder around the BelleII detector IP (from the $\Upsilon(4\mathrm{S})$ setup) would be considered, which does not correspond to the actual IP of the Belle detector used in the $\Upsilon(5\mathrm{S})$ case.
Next, we have to transform the momentum, energy, and position variables of the signal-side and tag-side B mesons into the rest frame of the $\Upsilon(5\mathrm{S})$. These quantities are required to determine the Lorentz factors β_B and γ_B, which are given by

$$\beta_B = \frac{p_{\mathrm{CMS}}}{\sqrt{E^2_{\mathrm{CMS}} - p^2_{\mathrm{CMS}}}} \tag{4.25}$$

$$\gamma_B = \frac{1}{\sqrt{1-\beta^2}}\,, \tag{4.26}$$

with p_{CMS} and E_{CMS} being the absolute momentum and energy of the signal B meson in the $\Upsilon(5\mathrm{S})$ rest frame.
After that, we need to calculate the polar angle θ_{CMS} in the $\Upsilon(5\mathrm{S})$ rest frame. This is done by considering the momentum vector of the signal B meson in the $\Upsilon(5\mathrm{S})$ rest frame and applying

$$\theta_{\mathrm{CMS}} = \arccos\left(\frac{p_{\mathrm{z,CMS}}}{p_{\mathrm{CMS}}}\right) . \tag{4.27}$$

The final step is to correctly determine the distance Δxy in the transverse plane. In the case of MC truth studies, Δxy is defined exactly as in 4.24, meaning it is by construction always positive. However, when using reconstructed quantities, Δxy and therefore also Σt can become negative. This also affects the calculation of Δt, since Δt depends on Δxy (see eq. 4.21).
A negative sign in the reconstructed case can occur when the momentum vector of the signal B meson in the $\Upsilon(5\mathrm{S})$ rest frame, is oriented parallel to the vertex difference vector between the tag and signal B mesons (see Fig. 4.11). Therefore, we must include a condition in the formula for Δxy that checks whether the scalar product of the B meson momentum vector points parallel or antiparallel to the connection vector between the sig and tag B mesons in the $\Upsilon(5\mathrm{S})$ rest frame . If it is antiparallel, the sign remains positive; if it is parallel, this indicates a reconstruction error, and the sign must be flipped to negative. This mainly occurs for B meson pairs that decay very close to each other.

In fig. 4.12, 4.13 and 4.14, the Δt^{MC} distributions for full entanglement for each case is shown. The OF and SF events are plotted in red and blue, respectively. The x-axis shows the Δt^{MC} distributions in the range of -10 ps and $+10$ ps, the y-axis shows the number of events. The distributions of the Signal MC follow the expected shape shown in fig. 2.3. Additionally, the asymmetry from eqs. 2.115 and 2.114 is plotted in the lower plots as black data points. We fitted the PSD model from eq. 2.111 to the Δt^{MC} distributions. Since we only look at MC truth information and because of that no detector resolution effects should be seen, the PSD model only depends on the physical PDFs from eqs. 2.102 and 2.102 for OF events and eqs. 2.99 and 2.99 for SF events. As expected the ζ value is 0 for these cases, since we expect full entanglement. The theory curve with the fit result parameters is plotted as solid red and blue lines. Additionally the time dependent asymmetry was also fitted to the data points and can be seen in the lower plot as solid red line. Here we fitted the eq. 2.114 for the $C = -1$ case and eq. 2.115 for the $C = +1$ case. The fit results for the mixing frequency is as expected around the theoretical values of 0.506 ps. In tabel 4.9 the fit results are shown. As a clear overlap of the fitted curves with the data points can be seen, this naive validation is concluded as successful.
In addition we also plotted the Σt distributions for the different cases (see. figs. 4.16, 4.17, 4.18 and 4.19). The x-axis now shows the Δt^{MC} distributions in the range of 0 ps and 15 ps, the y-axis shows the number of events. The distributions of the Signal MC follow the expected shape shown

in fig. 2.4. Additionally, the asymmetry from eqs. 2.116 and 2.117 is plotted in the lower plots as black data points. We again fitted the PSD model from eq. 2.111 to the $\sum t^{\mathrm{MC}}$ distributions. Since we only look at MC truth information and because of that no detector resolution effects should be seen, the PSD model only depends on the physical PDFs from eqs. 2.107 and 2.87 for OF events and eqs. 2.105 and 2.86 for SF events. As expected the ζ value is 0 for these $B^0\bar{B}^0$, $B^{0*}\bar{B}^0$+ c.c. and $B^{0*}\bar{B}^{0*}$ cases, since we expect full entanglement. For the equally mixed case, $\zeta = 1$ as expected, since we created by the equal mixture of $C = \pm 1$ states a disentangled state. The theory curve with the fit result parameters is plotted as solid red and blue lines. Additionally the time dependent asymmetry was also fitted to the data points and can be seen in the lower plot as solid red line. Here we fitted the eq. 2.114 for the $C = -1$ case and eq. 2.115 for the $C = +1$ case. The fit results for the mixing frequency and ζ are not in the expected region around the theoretical values for the $C = -1$ cases. They show a significant deviation from the expected theoretical values of $\zeta = 0$, as well as from the expected mass difference Δm. This discrepancy is particularly pronounced in the BB case, where the fitted value of ζ is close to 10%. The origin of this deviation must be investigated in more detail in future studies. Since this behavior is not observed in the Δt distributions, one can conclude that a technical issue in the reconstruction of the Σt for the $C = -1$ case is a possible explanation. It may also be necessary to use a different fit model to accurately describe the data.

	$B^0\bar{B}^0$	$B^{*0}\bar{B}^0$+c.c.	$B^{*0}\bar{B}^{*0}$	50/50 Mix
Δt: ζ	0.00 ± 0.01	0.00 ± 0.07	0.00 ± 0.01	1.00 ± 0.12
Δt: Δm [ps^{-1}]	0.510 ± 0.001	0.506 ± 0.001	0.510 ± 0.001	0.510 ± 0.001
Δt: $\frac{\chi^2}{\mathrm{ndof}}$ $\zeta \mid \Delta m$	1.0|1.4	1.1|1.2	1.0|1.2	1.3|1.5
Σt: ζ	0.068 ± 0.007	0.003 ± 0.001	0.034 ± 0.007	1.000 ± 0.191
Σt: Δm [ps^{-1}]	0.534 ± 0.002	0.517 ± 0.006	0.524 ± 0.002	0.520 ± 0.001
Σt: $\frac{\chi^2}{\mathrm{ndof}}$ $\zeta \mid \Delta m$	1.0|1.9	3.8|2.1	0.9|1.9	1.0|2.7

Table 4.9: Fitted parameters of the Δt and Σt distributions and time-dependent asymmetries for each case. The fit is performed using Minuit, with the loss function defined as a least-squares function. The uncertainties are obtained from the Hesse error matrix.

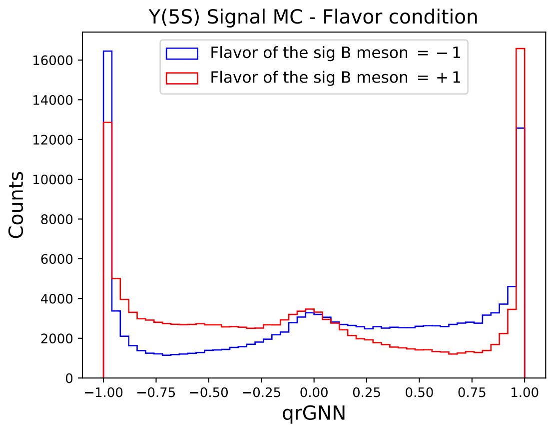

(a) $\Upsilon(5S)$ signal MC, $C = -1$ (physically not possible ratio).

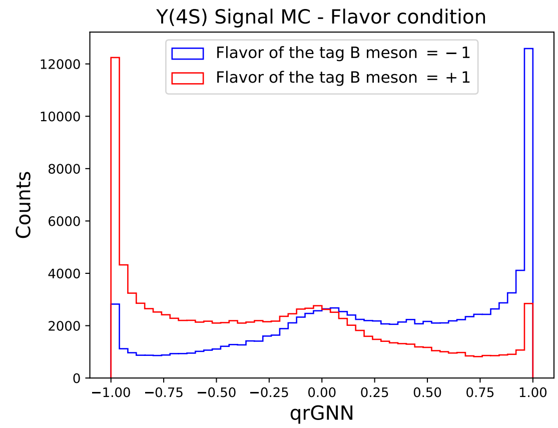

(b) $\Upsilon(4S)$ signal MC, $C = -1$ (physically correct ratio).

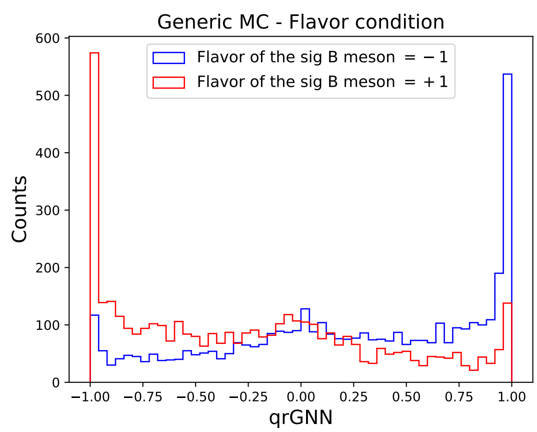

(c) $\Upsilon(5S)$ generic MC, $C = -1$ (Belle sample).

Figure 4.5: Comparison of the flavor tagger output qrGNN for different Monte Carlo samples and $C = -1$ configurations. The blue curve shows the qrGNN output under the condition that the signal-side B meson has flavor -1, while the red curve corresponds to flavor $+1$. The ratio of SF to OF events differs between the samples as described in the subfigures.

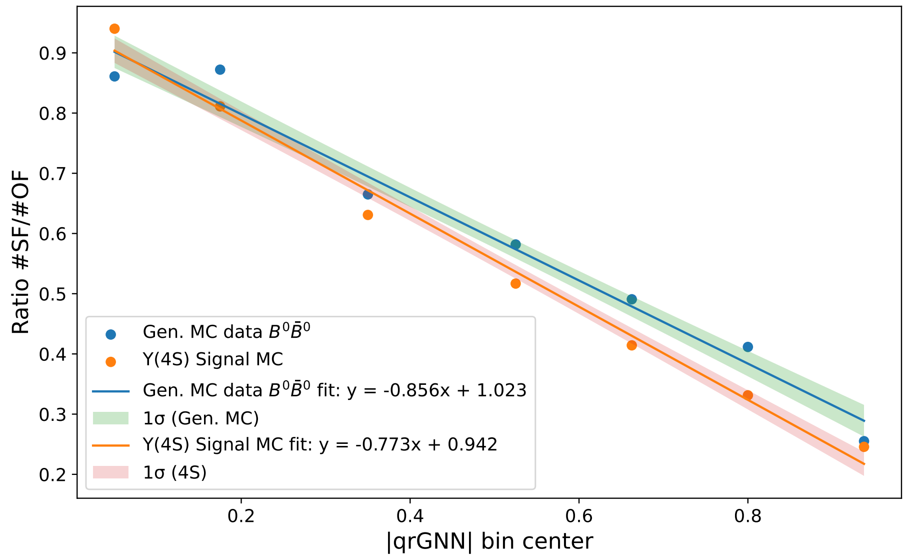

(a) Ratio of SF and OF events from the $\Upsilon(4S)$ signal MC sample for the $C = -1$ case (orange) and from the Belle generic $B^0\bar{B}^0$ sample (blue).

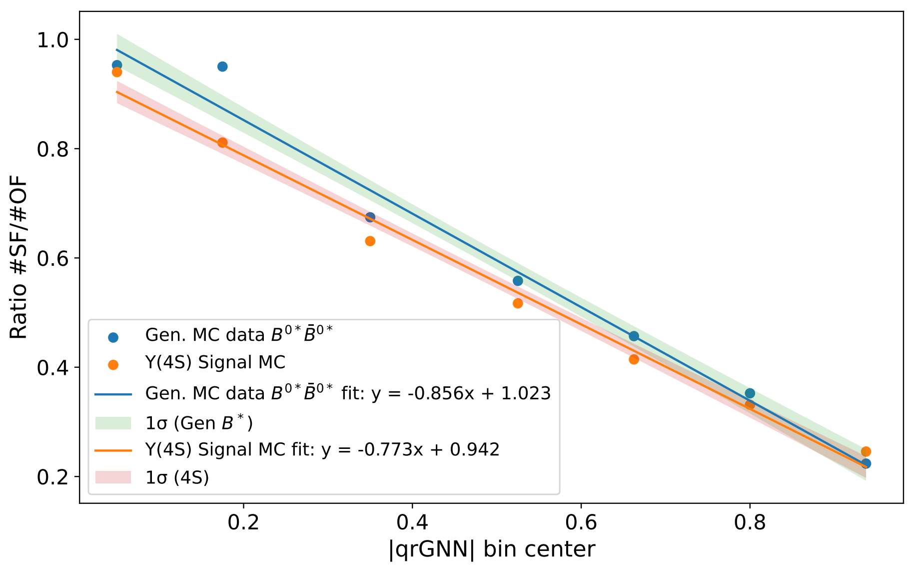

(b) Ratio of SF and OF events from the $\Upsilon(4S)$ signal MC sample for the $C = -1$ case (orange) and from the Belle generic $B^{*0}\bar{B}^{*0}$ sample (blue).

Figure 4.6: Comparison of the ratio between SF and OF events for signal $\Upsilon(4S)$ and generic Belle MC samples. A fit function of the form $ax + b$ was fitted to the ratio as a function of the |qrGNN| bin center.

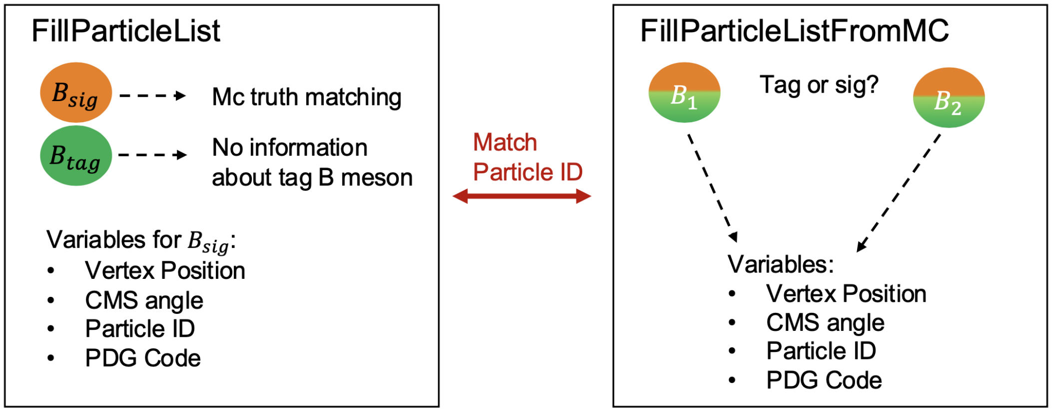

Figure 4.7: Approach to determine MC information of the tag side B meson by matching the particle IDs from the B mesons out of the reconstructed B meson list and the B mesons from the MC Truth list.

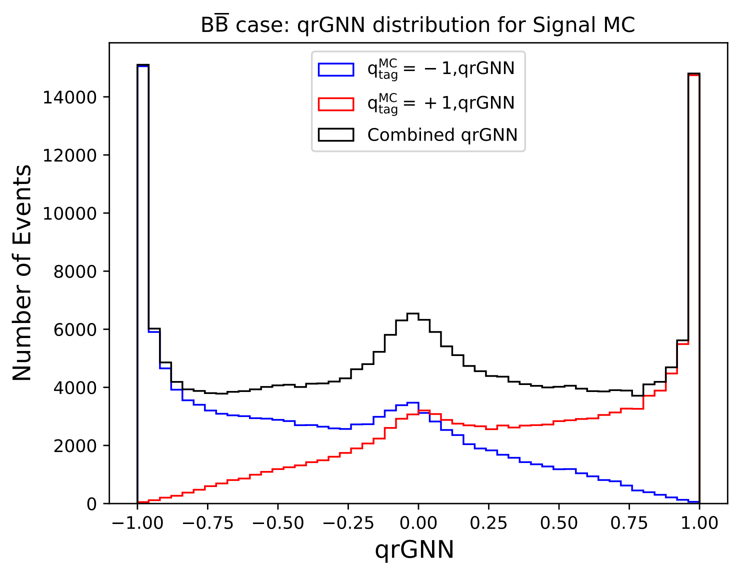

Figure 4.8: qrGnn distribution for fully entangled Signal MC of the $\Upsilon(5S) \to B^0\bar{B}^0$ decay. The red (blue) histograms represents the distribution for $q_{\rm tag}^{\rm MC} = -1$ ($q_{\rm tag}^{\rm MC} = +1$). The black histogram shows the sum of these two distributions.

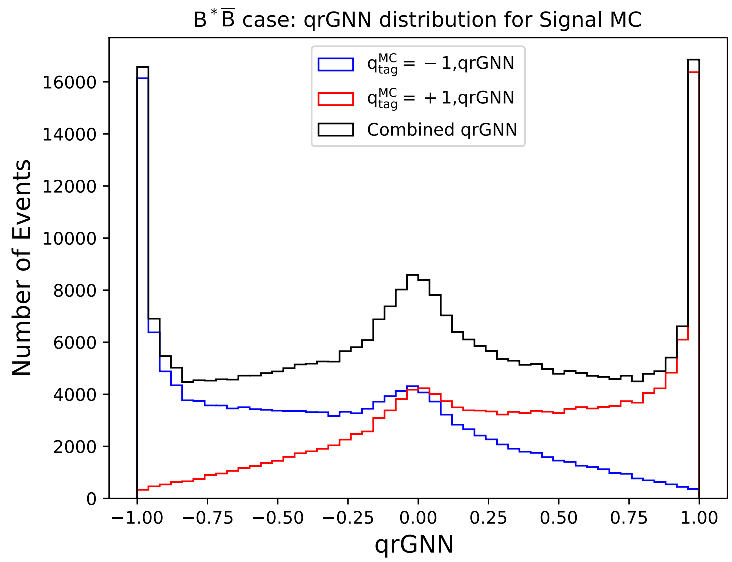

Figure 4.9: qrGnn distribution for fully entangled Signal MC of the $\Upsilon(5S) \rightarrow B^{0*}\bar{B}^{0}$+c.c. decay. The red (blue) histograms represents the distribution for $q_{tag}^{MC} = -1$ ($q_{tag}^{MC} = +1$). The black histogram shows the sum of these two distributions.

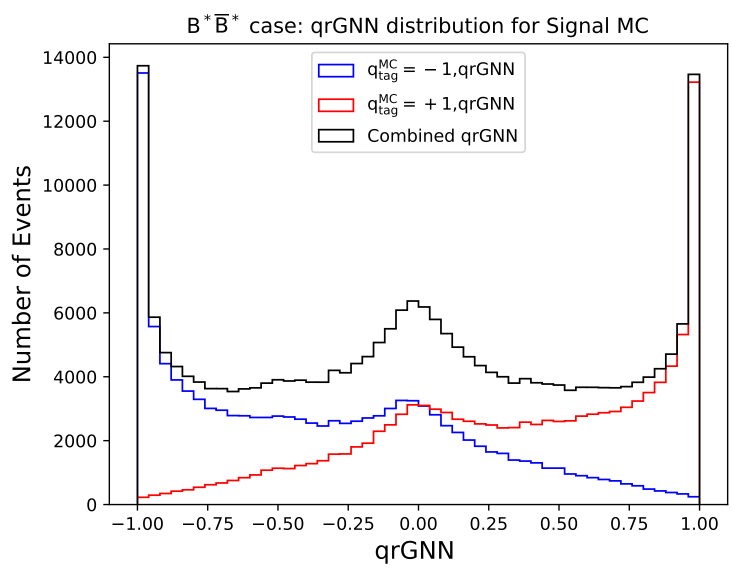

Figure 4.10: qrGnn distribution for fully entangled Signal MC of the $\Upsilon(5S) \rightarrow B^{0*}\bar{B}^{0*}$ decay. The red (blue) histograms represents the distribution for $q_{tag}^{MC} = -1$ ($q_{tag}^{MC} = +1$). The black histogram shows the sum of these two distributions.

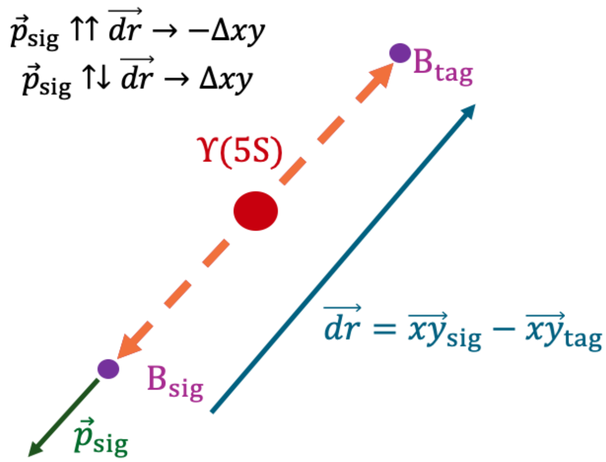

Figure 4.11: Sketch for showing wether one needs to apply a minus sign in the formula for Δxy. One checks whether the scalar product of the B meson momentum vector points parallel or antiparallel to the connection vector between the sig and tag B mesons in the $\Upsilon(5S)$ rest frame.

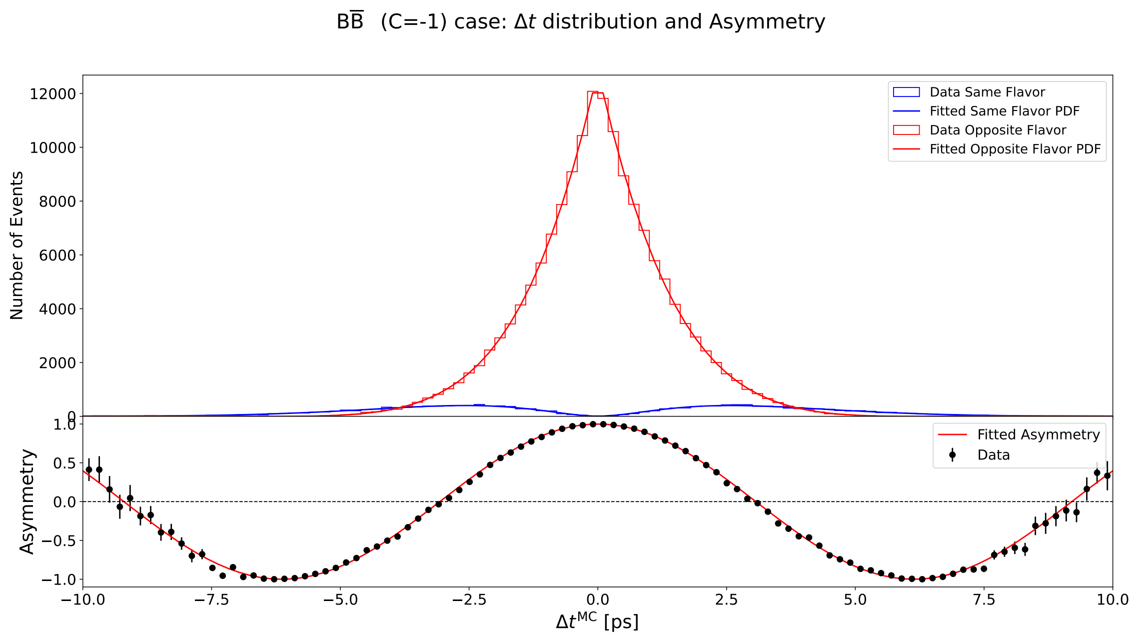

Figure 4.12: Signal MC Δt distribution for the fully entangled $\mathrm{B^0\bar{B}^0}$ (C = -1) case as well as the time dependent asymmetry as a function of Δt. The pure physics PDFs from eq. 2.69 for OF events and eq. 2.68 for SF events are fitted to the Signal MC Data points and are shown by the solid lines. This was done to validate the distribution shape of the parameters. For the Δt distribution the Signal MC Data is shown by histograms (red for OF and blue for SF events). Both distributions have Poisson errors, from which the uncertainty of the asymmetry can be calculated.

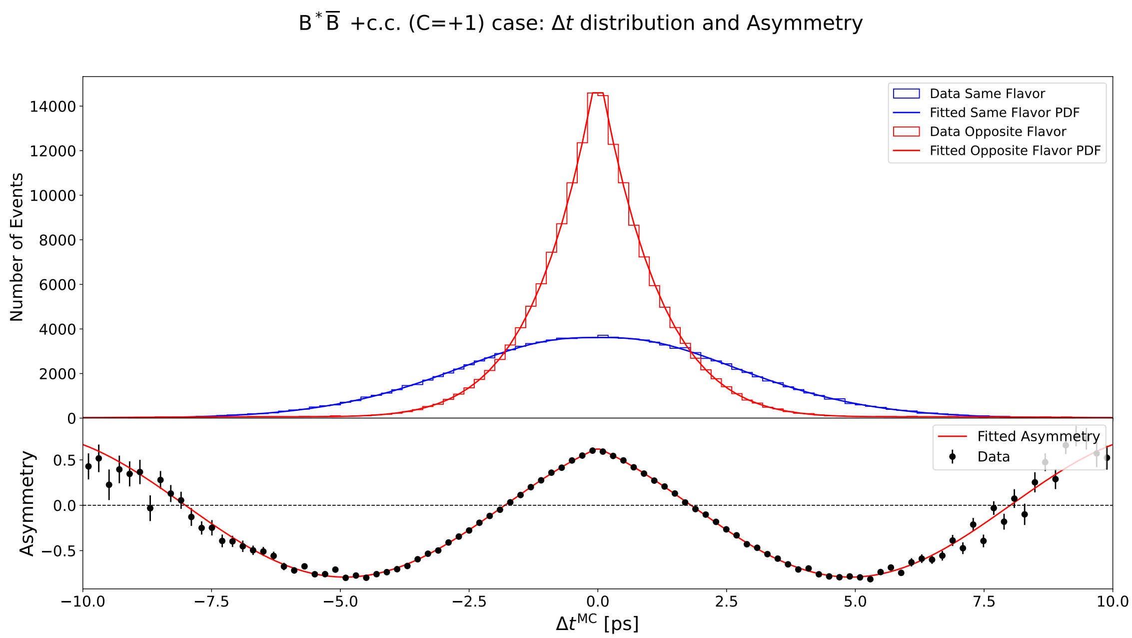

Figure 4.13: Signal MC Δt distribution for the fully entangled $B^{0*}\bar{B}^{0}$ + c.c. (C = +1) case as well as the time dependent asymmetry as a function of Δt. The pure physics PDFs from eq. 2.83 for OF events and eq. 2.81 for SF events are fitted to the Signal MC Data points and are shown by the solid lines. This was done to validate the distribution shape of the parameters. For the Δt distribution the Signal MC Data is shown by histograms (red for OF and blue for SF events). Both distributions have Poisson errors, from which the uncertainty of the asymmetry can be calculated.

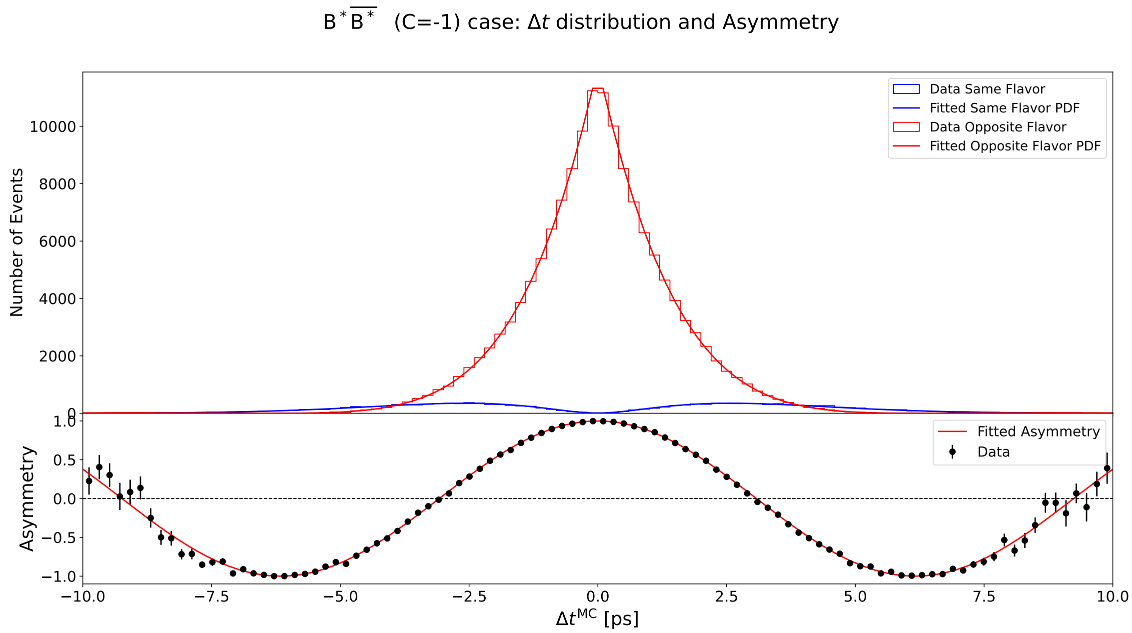

Figure 4.14: Signal MC Δt distribution for the fully entangled $B^{0*}\bar{B}^{0*}$ (C = -1) case as well as the time dependent asymmetry as a function of Δt. The pure physics PDFs from eq. 2.69 for OF events and eq. 2.69 for SF events are fitted to the Signal MC Data points and are shown by the solid lines. This was done to validate the distribution shape of the parameters. For the Δt distribution the Signal MC Data is shown by histograms (red for OF and blue for SF events). Both distributions have Poisson errors, from which the uncertainty of the asymmetry can be calculated.

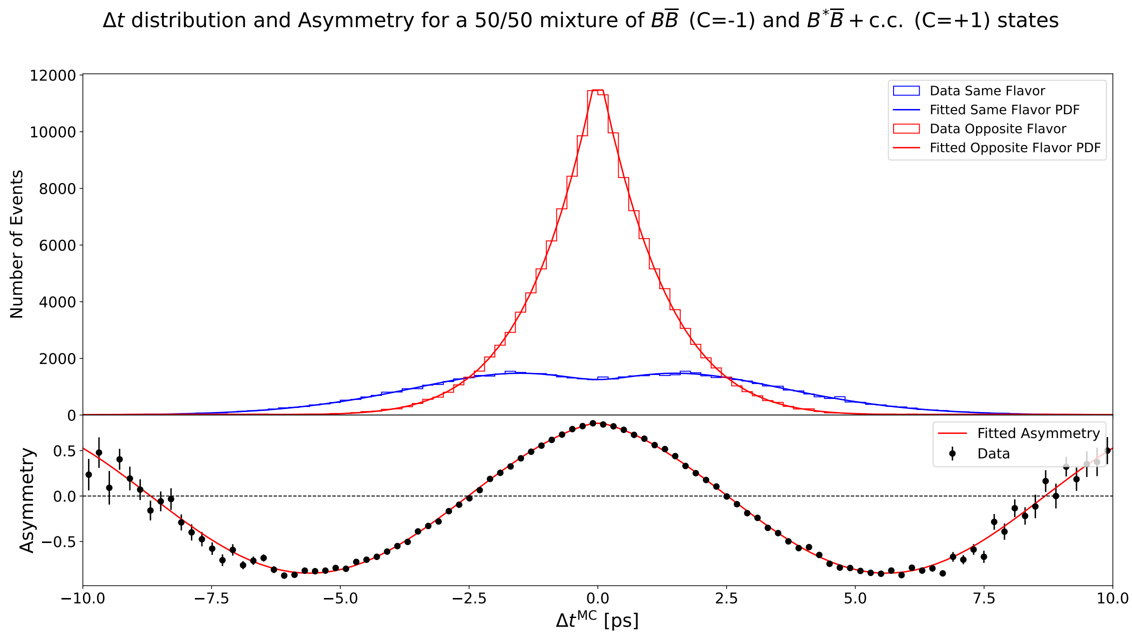

Figure 4.15: Signal MC Δt distribution for a 50/50 mixture of the fully entangled $B^0\bar{B}^0$ (C = -1) case and fully entangled $B^{0*}\bar{B}^0$ + c.c. (C = -1) case as well as the time dependent asymmetry as a function of Δt. The pure physics PDFs from eq. 2.102 for OF events and 2.99 for SF events are fitted to the Signal MC Data points and are shown by the solid lines. This was done to validate the distribution shape of the parameters. For the Δt distribution the Signal MC Data is shown by histograms (red for OF and blue for SF events). Both distributions have Poisson errors, from which the uncertainty of the asymmetry can be calculated. The mixture is equal to a fully disentangled case as shown in fig. 2.3

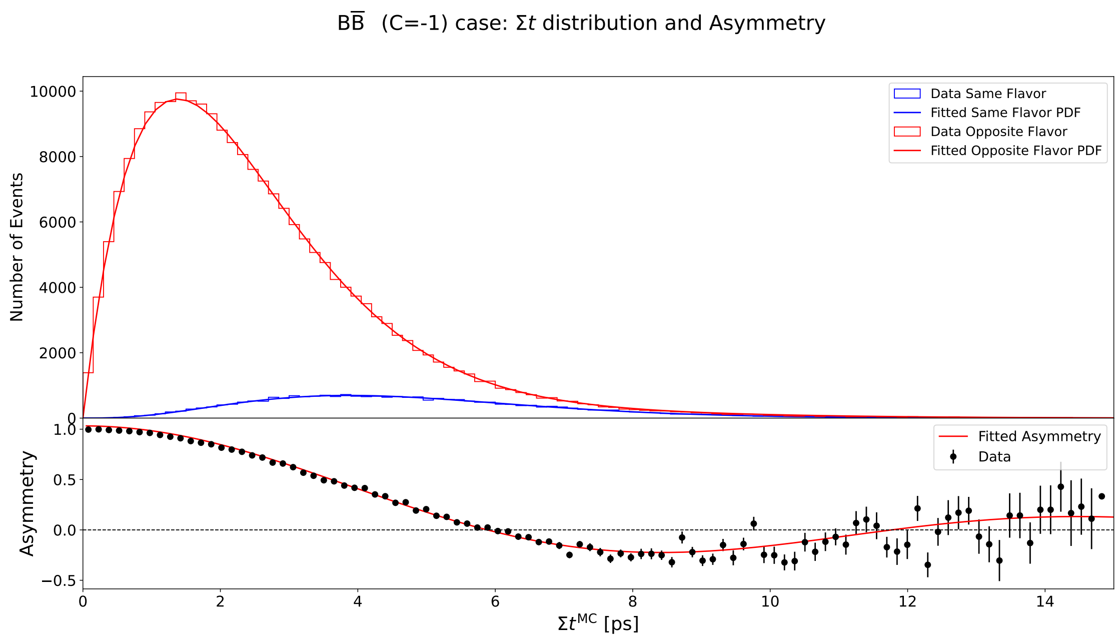

Figure 4.16: Signal MC Σt distribution for the fully entangled $B^0\bar{B}^0$ (C = -1) case as well as the time dependent asymmetry as a function of Σt. The pure physics PDFs from eq. 2.72 for OF events and eq. 2.71 for SF events are fitted to the Signal MC Data points and are shown by the solid lines. This was done to validate the distribution shape of the parameters. For the Σt distribution the Signal MC Data is shown by histograms (red for OF and blue for SF events). Both distributions have Poisson errors, from which the uncertainty of the asymmetry can be calculated.

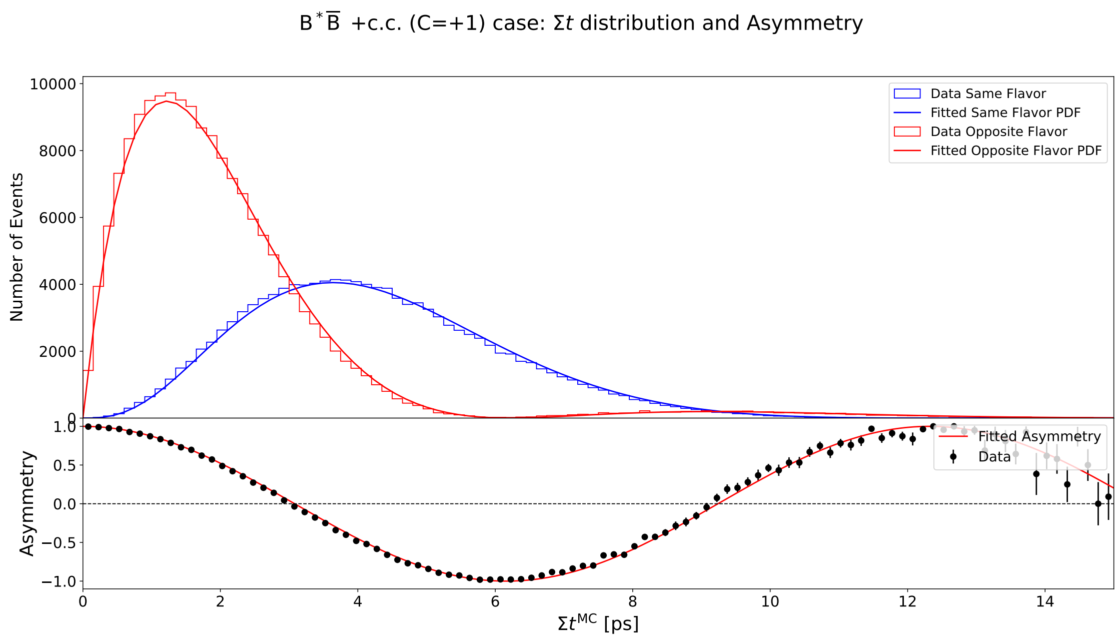

Figure 4.17: Signal MC Σt distribution for the fully entangled $B^{0*}\bar{B}^0$+ c.c. ($C = +1$) case as well as the time dependent asymmetry as a function of Σt. The pure physics PDFs from eq. 2.87 for OF events and eq. 2.86 for SF events are fitted to the Signal MC Data points and are shown by the solid lines. This was done to validate the distribution shape of the parameters. For the Σt distribution the Signal MC Data is shown by histograms (red for OF and blue for SF events). Both distributions have Poisson errors, from which the uncertainty of the asymmetry can be calculated.

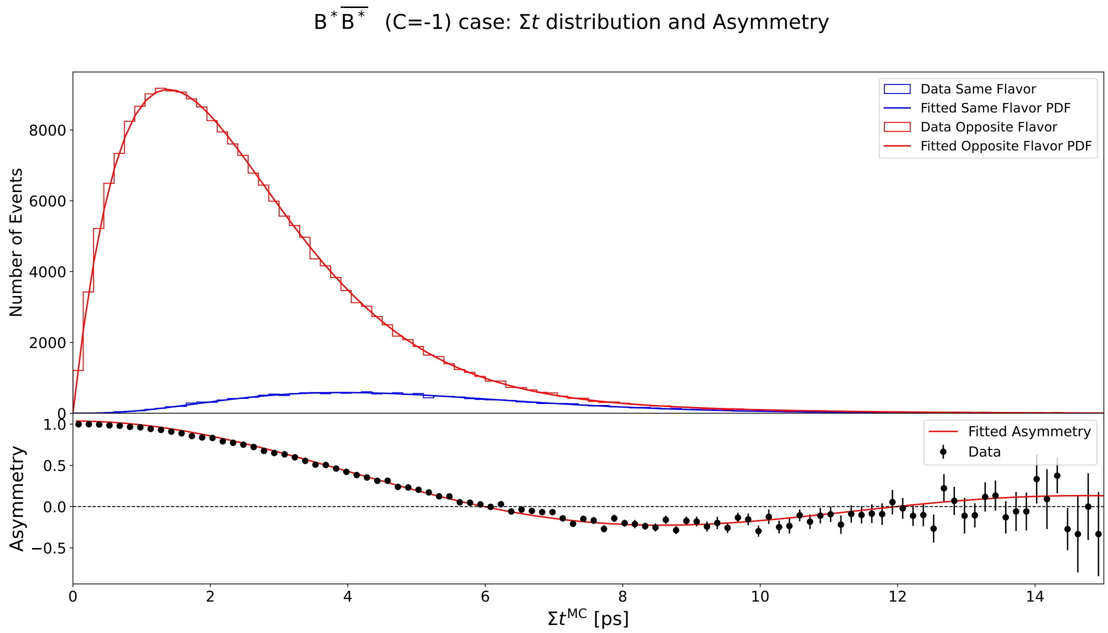

Figure 4.18: Signal MC Σt distribution for the fully entangled $B^{0*}\bar{B}^{0*}$ (C = -1) case as well as the time dependent asymmetry as a function of Σt. The pure physics PDFs from eq. 2.72 for OF events and eq. 2.71 for SF events are fitted to the Signal MC Data points and are shown by the solid lines. This was done to validate the distribution shape of the parameters. For the Σt distribution the Signal MC Data is shown by histograms (red for OF and blue for SF events). Both distributions have Poisson errors, from which the uncertainty of the asymmetry can be calculated.

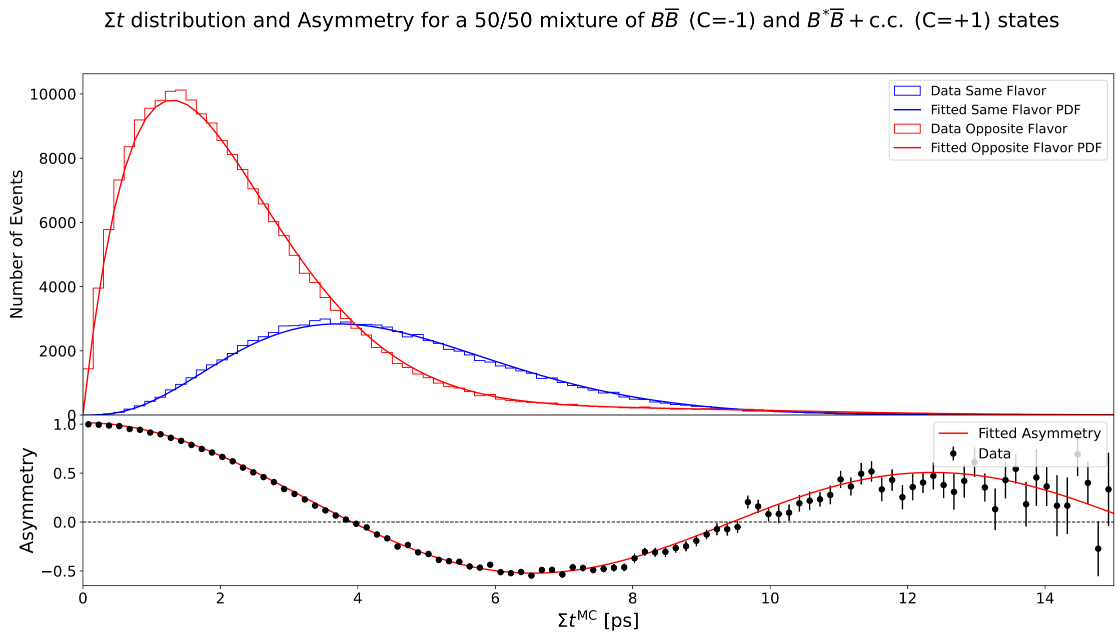

Figure 4.19: Signal MC Δt distribution for a 50/50 mixture of the fully entangled $B^0\bar{B}^0$ (C = -1) case and fully entangled $B^{0*}\bar{B}^0$ + c.c. (C = -1) case as well as the time dependent asymmetry as a function of Σt. The pure physics PDFs from eq. 2.107 for OF events and 2.105 for SF events are fitted to the Signal MC Data points and are shown by the solid lines. This was done to validate the distribution shape of the parameters. For the Σt distribution the Signal MC Data is shown by histograms (red for OF and blue for SF events). Both distributions have Poisson errors, from which the uncertainty of the asymmetry can be calculated. The mixture is equal to a fully disentangled case as shown in fig. 2.4

5 Studies of Entanglement and Disentanglement Models on Signal MC

The main goal is to reuse the framework developed to study entanglement effects and model quantum disentanglement on the Υ(4S) and apply it to the Υ(5S). We aim to test the derived theory of creating disentangled states by mixing the different $C = -1$ and $C = +1$ states, as well as to confirm that the simulated Signal MC data are fully entangled by examining the disentanglement fraction ζ. This is done by fitting the observable Δt to obtain best-fit estimates for the parameter ζ, which represents the fraction of partial spontaneous disentanglement (PSD). Since the PDF contains many variables, including resolution function parameters, an initial calibration of their values is required. This is achieved by performing so-called residual fits on the observable $\delta\Delta t$, as described in Sec. 5.1.1, before moving on to the Δt fits. In the single Δt fits presented in Sec. 5.1.2, the physics parameter ζ is fitted simultaneously with the resolution function parameters and the flavor tagging parameters.

Due to time constraints, it was not possible to test a two-dimensional fit, e.g., fitting Δt and Σt simultaneously, which would allow a more precise exploration of disentanglement. Additionally, the framework for the $C = +1$ case and for Σt considerations has not yet been established. These are goals for ongoing and future analyses.

5.1 Fits on Signal MC

The analysis presented in the main part is performed on Signal MC generated for full entanglement $C = -1$ cases as well as the mixture of fully entangled $C = \pm 1$ cases so that the resulting endstate is a fully disentangled state . The real Belle data size corresponds to an integrated luminosity $\int \mathcal{L} \mathrm{d}t \sim 121.4$ fb^{-1}. The Signal MC sample size is given in Tab. 5.1. We calculated the luminosity with the formula

$$\int \mathcal{L} \mathrm{d}t = \frac{N(\texttt{isSignal == 1})}{\sigma_{e^- e^+ \to b\bar{b}}} \tag{5.1}$$

with $\sigma_{e^-e^+\to b\bar{b}} = (0.340 \pm 0.016)$ nb [1] and N (`isSignal == 1`) is the amount of signal $B/\bar{B}$ mesons after reconstruction. For comparison the amount of B mesons in real data in each decay

Signal MC	$\int \mathcal{L}\mathrm{d}t$	N (`isSignal == 1`)
$B^0\bar{B}^0$	$\sim 6.5 \cdot 10^{11}$ fb^{-1}	$\sim 2.2 \cdot 10^5$
$B^{0*}\bar{B}^{0*}$	$\sim 7.8 \cdot 10^{11}$ fb^{-1}	$\sim 2.7 \cdot 10^5$
Equal mixture of $C = \pm 1$ states	$\sim 8.8 \cdot 10^{11}$ fb^{-1}	$\sim 3.0 \cdot 10^5$

Table 5.1: Integrated luminosities and approximate number of events after applying condition isSignal $==$ 1 for Signal MC for the three different cases.

are listed in table 5.2. For that the branching fractions of the $\Upsilon(5S) \to B^{0(*)}\bar{B}^{0(*)}$ were taken from tab. 2.2 are taken. The branching fractions of the reconstructed decay channels from sec. 4.1 are taken from [50]

Signal MC	decay channel	N (B)
$B^0\bar{B}^0$	$D^-\pi^+$	566401
$B^{0*}\bar{B}^0$+c.c.		392368
$B^{0*}\bar{B}^{0*}$+c.c.		141088
$B^0\bar{B}^0$	$D^{*-} \to K^+\pi^-$	24155
$B^{0*}\bar{B}^0$+c.c.		167327
$B^{0*}\bar{B}^{0*}$+c.c.		60167
$B^0\bar{B}^0$	$D^{*-} \to K^+\pi^-\pi^+\pi^-$	41063
$B^{0*}\bar{B}^0$+c.c.		284455
$B^{0*}\bar{B}^{0*}$+c.c.		102284

Table 5.2: Amount of B mesons in the real data, corresponding to an integrated Luminosity of $\int \mathcal{L}\mathrm{d}t \sim 121.4$ fb^{-1} in each reconstructed decay channel.

5.1.1 $\delta\Delta$t Residual Fit

Here, a fit to the Δt residuals $\delta\Delta t$ is performed. It is given by the difference of the measured reconstructed values needed for the calculation of Δt and the MCtruth information of said values to calculate Δt^{MC}. The decay time difference's sensitivity is limited by signal-side and tag-side vertex resolution. Because the residual fit on $\delta\Delta t$ is independent of flavor and disentanglement effects this first fit is used to gauge the nuisance parameters introduced in sec. 4.2.2 needed for later studies. As a result the fit parameters should not differ significantly by looking at the disentangled and entangled sample. The fit to Eq. 4.13 is performed for all qrGNN-bins, while parameters describing main, tail, and exponential parts are shared across qrGNN-bins 0-5 and get a broader range for qrGNN-bin 6. Parameter f_{OL} is shared across all qrGNN-bins. In the following we will only consider the expression qr for qrGNN bins.

In Figs. 5.1 the shapes for residual fits are displayed for the 6$^{\text{th}}$ qr bin. We chose this bin because it is the most populated and provides the best confidence in the flavor tagger output for the tag-side B meson. The other qr bins are shown in the Appendix A.1. Tab. 5.3 shows the fit parameters for all seven qr-bins for the $\mathrm{B^0\bar{B}^0}$, $\mathrm{B^{0*}\bar{B}^{0*}}$ ($C = -1$) cases, and the disentangled case in the Signal MC, respectively. The data points with error bars are shown along with their fits to Eq. 4.13 in solid lines. The lower plots displaying the pulls show the discrepancies between data and fit.

The fits for all MC samples across all qr-bins look reasonable. When looking at the pulls no big systematic under-/overshooting of data points visible.
However, one can observe that, especially on the right flank of the residual fits, the fit lies slightly above the data points, which leads to a negative pull. This means that the reconstructed Δt values tend to be slightly smaller than the true ones for $\Delta t < 0$. Since Δt primarily depends on the polar angle θ and Δz see eq. 4.21, the effect could be caused by an incorrectly estimated uncertainty on θ or related quantities entering the overall Δt error. At the moment, the uncertainty is calculated using Gaussian error propagation. This is only a possible explanation for the more negative pull observed on this side. In general, this effect should be investigated in more detail in future systematic error studies. As expected, there are no significant deviations in the parameter values between different fractions of disentanglement.

This is only a consideration to explain the more negative pull observed on this side. In general, this effect should be investigated in more detail in future systematic error studies. As expected, there are no significant deviations in the parameter values between different fractions of disentanglement.

5.1.2 Δt Fit on Signal MC data

One accomplishment of this work is, on the one hand, to validate the simulated signal MC data not only at the MC truth level but also to investigate whether entanglement behavior can be observed in reconstructed MC data, additionally taking into account the detector resolution. The other goal was to test whether a mixture of $C = \pm 1$ states can be measured to show resolvable disentanglement behavior.
For this purpose, we used the fitframework for the Υ(4S) case, in which the fitted parameter ζ determines the maximum possible disentanglement in the datasets. Since we can construct our entanglement ourselves by mixing the cases, the value of ζ provides a validation of our theory on

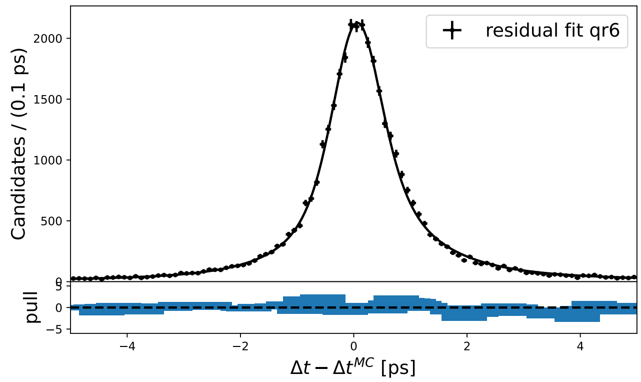

(a) $\mathrm{B}^0\bar{\mathrm{B}}^0$ $C = -1$ entangled case.

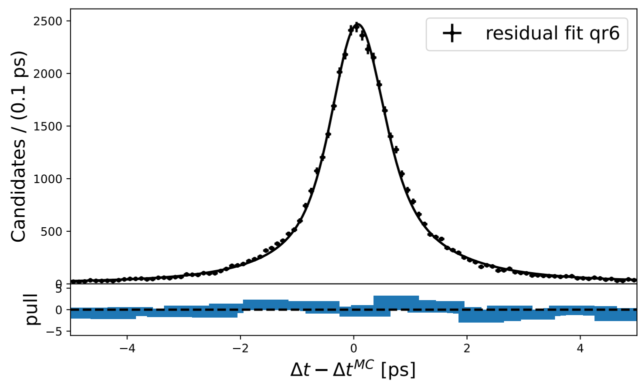

(b) $\mathrm{B}^{0*}\bar{\mathrm{B}}^{0*}$ $C = -1$ entangled case.

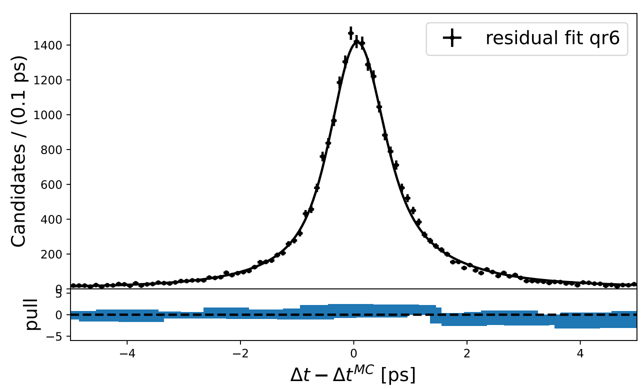

(c) Disentangled case. Equal mixture of $C = \pm 1$ states

Figure 5.1: Residual fits for Signal MC with full entanglement for the $\mathrm{B}^0\bar{\mathrm{B}}^0$, $\mathrm{B}^{0*}\bar{\mathrm{B}}^{0*}$ ($C = -1$) cases, and the disentangled case. The single figures show the fits in different qr bins (6th bin, from left to right). We chose this bin because it is the most populated and provides the best confidence in the flavor tagger output for the tag-side B meson.

Parameter	$\mathbf{B^0\bar{B}^0}$ (entangled)	$\mathbf{B^{0*}\bar{B}^{0*}}$ (entangled)	**Mixed** $C = \pm 1$ (disentangled)
f_{OL}	0.0011 ± 0.0002	0.0019 ± 0.0002	0.0004 ± 0.0002
μ_{Main}	0.2766 ± 0.0058	0.2916 ± 0.0055	0.2824 ± 0.0068
μ_{Tail}	0.8275 ± 0.0241	0.7525 ± 0.0223	0.8437 ± 0.0292
σ_{Main}	1.3046 ± 0.0091	1.3162 ± 0.0085	1.3251 ± 0.0094
σ_{Tail}	3.5167 ± 0.0500	3.5234 ± 0.0418	3.6944 ± 0.0517
f_{Tail}	0.3792 ± 0.0122	0.7425 ± 0.0219	0.6462 ± 0.0272
f_{exp}	0.2175 ± 0.0039	0.2276 ± 0.0036	0.2103 ± 0.0042
c_1 [ps^2]	13.8206 ± 0.3775	13.5133 ± 0.2791	15.5245 ± 0.4053
$f_{\mathrm{Tail,\ R}}$	0.5531 ± 0.0065	0.5490 ± 0.0061	0.5534 ± 0.0079
$f_{\mathrm{Tail},\mu}$	0.0052 ± 0.0057	0.0015 ± 0.0013	0.0022 ± 0.0014
$f_{\mathrm{Tail},\sigma}$	0.0021 ± 0.0033	0.0381 ± 0.0746	0.0142 ± 0.0048
$\mu^{(6)}_{\mathrm{Main}}$	0.1947 ± 0.0119	0.2137 ± 0.0106	0.1888 ± 0.0143
$\mu^{(6)}_{\mathrm{Tail}}$	0.5875 ± 0.0498	0.3797 ± 0.0383	0.5284 ± 0.0535
$\sigma^{(6)}_{\mathrm{Main}}$	1.3045 ± 0.0173	1.2703 ± 0.0140	1.2734 ± 0.0198
$\sigma^{(6)}_{\mathrm{Tail}}$	3.6589 ± 0.0924	3.5054 ± 0.0614	3.5715 ± 0.0949
$f^{(6)}_{\mathrm{Tail}}$	0.3840 ± 0.0155	0.8097 ± 0.0278	0.7130 ± 0.0373
$f^{(6)}_{\mathrm{exp}}$	0.2136 ± 0.0088	0.2056 ± 0.0068	0.1980 ± 0.0090
$c^{(6)}_1$ [ps^2]	12.3945 ± 0.5533	11.7274 ± 0.3997	13.3325 ± 0.6711
$f^{(6)}_{\mathrm{Tail,\ R}}$	0.5536 ± 0.0146	0.5914 ± 0.0123	0.5676 ± 0.0169

Table 5.3: Fit parameter estimates from $\delta\Delta t$ residual fits on Signal MC for the $\mathrm{B^0\bar{B}^0}$ (entangled), $\mathrm{B^{0*}\bar{B}^{0*}}$ (entangled), and equally mixed $C = \pm 1$ (disentangled) configurations. Superscript (6) denotes parameters obtained from the 6th qr-bin fitted separately.

the formation of entanglement in the $B^0\bar{B}^0$ system. To do this, we fit the PSD model from eq. 2.111, which includes the parameter ζ, to the reconstructed Δt distributions for the fully entangled $B^0\bar{B}^0$, $B^{*0}\bar{B}^{*0}$, and disentangled case (consisting of a equal mixture of $C = \pm 1$ states). We again distinguish between all qr bins as well as same-flavor (SF) and opposite-flavor (OF) events, because entanglement and disentanglement can be differentiated in the case of SF events best when looking at the Δt distributions. In the entangled $C = -1$ case, the PDF for $\Delta t = 0$ is also zero. In the disentangled case, this is not the case. See theory plots for illustration 2.3.
One can also apply the fit to obtain the precise parameter values for mixing parameters such as Δm and τ as demonstrated in Ref. [2] and not measure the disentanglement fraction ζ.
Here, ζ is the main physics parameter left to float in the fit, as Δm and τ are fixed to PDG world averages[1] [3]

$$\Delta m_d = (0.5065 \pm 0.0019)\ \mathrm{ps}^{-1}, \quad \tau_B = (1.519 \pm 0.004)\ \mathrm{ps}. \tag{5.2}$$

As OL and Tail parameters (except f_{Tail}) have been fixed in the previous residual fits to values from Tab. 5.3, only core parameters are left free in the resolution function.

In the Fit the data is divided into 7 bins of dilution factor r, as it has been done in the resolution fit, with intervals given in 3.10, with r-bin 6 having the highest purity of tagging efficiency. In addition, the data is split into the different flavor combinations: $B^0\bar{B}^0$ and B^0B^0 and charge conjugate, to investigate possible asymmetries between B^0_{tag} and $\bar{B}^0_{\mathrm{tag}}$, as pointed out in Ref. [51]. The combined parameter $\mu_i = (\varepsilon_{B^0_{\mathrm{tag}}} - \varepsilon_{\overline{B}^0_{\mathrm{tag}}})/(\varepsilon_{B^0_{\mathrm{tag}}} - \varepsilon_{\overline{B}^0_{\mathrm{tag}}})$ is the weighted average of wrong tag fractions with $q_{\mathrm{tag}} = +1$ and -1. This results in a total of 28 qr-bins that are fitted simultaneously.

Flavor tagger parameters, such as wrong tag fractions, the uncertainty on the mistag as well as efficiency are also free parameters in the fit. Only in the 6th bin, the wrong tag fractions had to be fixed to MCtruth values. We did this, because the value of ζ and the values of the wrong-tag fractions counteract each other. A decrease in the wrong-tag fractions leads to an increase in ζ, which distorts the result if both parameters are left free in this case. Therefore, the MC truth data were used to calculate the wrong-tag fractions. This approach is justified here since we do not aim to perform a detailed analysis of the wrong-tag fractions in this sample, but rather to determine the degree of (dis)entanglement, which is given by ζ. However, one goal of future analyses could be to study the correlation between these two quantities in more detail. The calculated wrong tag fractions out of MC information in each qr-bin are:

[1] These are also the values which are used for Signal MC generation.

$$\begin{aligned}
\text{Fully entangled } B^0\bar{B}^0 \text{ case:} \quad & w^+ = [0.483, 0.448, 0.391, 0.315, 0.237, 0.127, 0.022], \\
& w^- = [0.464, 0.433, 0.373, 0.297, 0.218, 0.125, 0.012], \\
\text{Fully entangled } B^{0*}\bar{B}^{0*} \text{ case:} \quad & w^+ = [0.484, 0.442, 0.370, 0.279, 0.217, 0.139, 0.0256], \\
& w^- = [0.478, 0.424, 0.346, 0.282, 0.210, 0.129, 0.023], \\
\text{Equally mixed } C = \pm 1 \text{ case:} \quad & w^+ = [0.481, 0.440, 0.382, 0.298, 0.242, 0.145, 0.036], \\
& w^- = [0.473, 0.438, 0.370, 0.294, 0.221, 0.137, 0.037].
\end{aligned}$$

We calculated the wrong tag fractions by the formula

$$w^{\pm} = \frac{N(q_{\text{tag}} = \pm 1 \ \& \ q_{\text{tag}} \neq q_{\text{tag}}^{\text{MC}})}{N(q_{\text{tag}}^{\text{MC}} = \pm 1)} \,. \tag{5.3}$$

Free parameter ζ, and f_{Tail} are shared across all qr-bins, core parameters and μ_i are shared across respective r intervals and finally $w_i^{\pm}$ are specific for q_{tag} for all bins up to bin 5. To avoid the fit to hit parameter limits the allowed parameter space for ζ is extended to $[-0.3,\ 1.3]$.

The plots in figs. 5.2 show the fits to the Signal MC $B^0\bar{B}^0$ case for the best quality qr-bin 6, in figs. 5.3 the fits to the Signal MC $B^{0*}\bar{B}^{0*}$ case for the best quality qr-bin 6 , while plots in Figs. 5.4 show the fits to the Signal MC of the equally mixed $C = \pm 1$ state case for the best quality qr-bin 6. The fit parameters for both cases are summarized in Tab. 5.4. For both full entanglement and disentanglement Signal MC, the remaining qr-bin 0-5 alongside fits to the Signal MC samples for the three cases, can be found in the Appendix A.2.

The fitted shapes for same-flavor and opposite-flavor events for the fully entangled $B^{0(*)}\bar{B}^{0(*)}$ and the mixed $C = \pm 1$ cases are consistent with the expectations from the physics PDFs shown in Fig. 2.3. Examining the pulls, no systematic under- or overshooting is visible for the opposite-flavor events. For the same-flavor events, especially for the B^0B^0 and the B mesons resulting from the $B^{0*}\bar{B}^{0*}$ sample, the fit slightly undershoots, as indicated by the positive pull distribution. This could be due to incorrect normalization, since the BB and $B\bar{B}$ samples are fitted simultaneously, sharing the same normalization. Furthermore, the positive wrong-tag fractions are higher than the negative wrong-tag fractions in the last bin, which may also introduce a bias in the fit normalization. This may explain why the fits for the equally mixed case do not show overshooting, as the pull distribution shows no systematic under- or overshooting in this case, and the negative and positive wrong-tag fractions are nearly equal. Moreover, the expected values for the PSD fraction ζ are within the fitted ζ's 1.03σ uncertainty for the equally mixed case. Thus, we can conclude that mixing the two different data samples of $C = \pm 1$ states results in a visible and detectable difference in the ζ value, indicating a fully disentangled sample. For the entangled $B^0\bar{B}^0$ case, the fitted value deviates by about 4.2σ and for the $B^{0*}\bar{B}^{0*}$ case by about 3.5σ from the expected value 0. This discrepancy requires further study in future analyses.

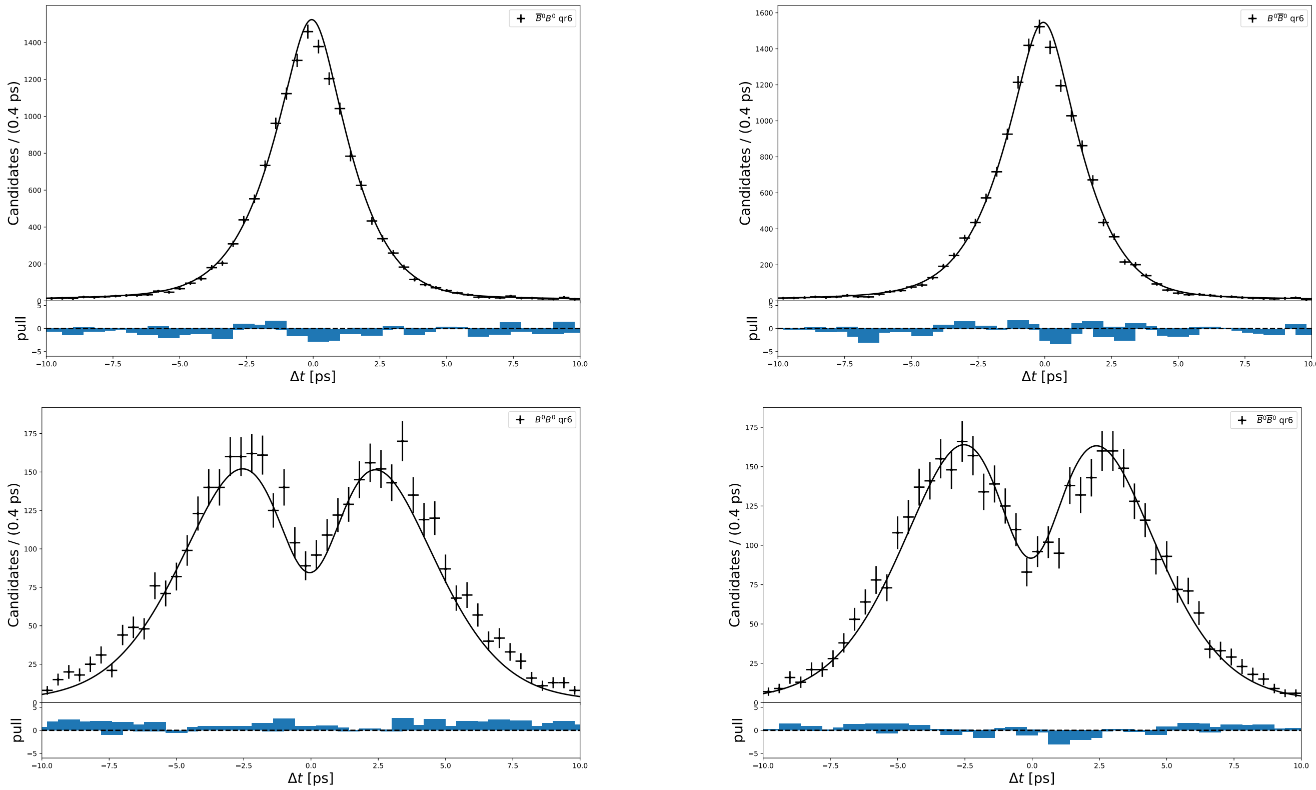

Figure 5.2: Δt-distribution fitted to Signal MC data for the full entanglement $B^0\bar{B}^0$ case. Data points with error bars show Signal MC data for $|qr| > 0.875$, so for the 6th qr-bin, solid line shows the fit. The lower plot show the pulls.

5.1.3 Δt Fit on Signal MC data for the $C = +1$ case

In the section above, we used the existing fit framework to fit the PSD model to the antisymmetric $C = -1$ states and to the equally mixed sample corresponding to a disentangled state. For this, we had to adjust the fit as described above, but the convolution of the physics PDF with the resolution function did not need to be reevaluated, since the physics PDF remains unchanged in the $C = -1$ case. Now we want to further test our hypothesis that a disentangled state is created by mixing the two different $C = -1$ and $C = +1$ cases. This was already demonstrated in Sec. 5.1.2, where the obtained ζ value is 1 when fitting the PSD model to the equally mixed sample. We also aim to obtain information about the fraction of disentanglement for the $C = +1$ case, e.g. $\Upsilon(5\mathrm{S}) \to B^{0*}\bar{B}^0$, decays, using the same fit framework, we assume that the PDF of the

Parameter	Fit estimate	
ζ	0.0540	$\pm$ 0.0128
μ_6	-0.0214	$\pm$0.0052
$\mu^{(6)}_{M1}$	-0.1038	$\pm$ 0.0263
$\mu^{(6)}_{T1}$	-1.3463	$\pm$ 0.1249
$\sigma^{(6)}_{M1}$	1.3040	$\pm$ 0.0397
$\sigma^{(6)}_{T1}$	4.5190	$\pm$ 0.2019
$f^{(6)}_{\mathrm{T}}$	0.2551	$\pm$ 0.0141

Fully entangled $B^0\bar{B}^0$ case.

Parameter	Fit estimate	
ζ	1.0155	$\pm$ 0.0150
μ_6	-0.0169	$\pm$ 0.0045
$\mu^{(6)}_{M1}$	-0.1558	$\pm$ 0.0213
$\mu^{(6)}_{T1}$	-1.3125	$\pm$ 0.1137
$\sigma^{(6)}_{M1}$	1.2799	$\pm$ 0.0341
$\sigma^{(6)}_{T1}$	4.8549	$\pm$ 0.2092
$f^{(6)}_{\mathrm{T}}$	0.4220	$\pm$ 0.0219

Equal mixture of $C = \pm 1$ states.

Parameter	Fit estimate	
ζ	0.0493	$\pm$ 0.0139
μ_6	-0.0142	$\pm$ 0.0057
$f^{(6)}_{\mathrm{OL}}$	0.00630	$\pm$ 0.00218
$\sigma^{(6)}_{0,\mathrm{OL}}$	28.062	$\pm$ 9.062
$\mu^{(6)}_{M1}$	-0.1341	$\pm$0.0329
$\mu^{(6)}_{T1}$	-0.9808	$\pm$ 0.2088
$\sigma^{(6)}_{M1}$	1.2708	$\pm$ 0.0633
$\sigma^{(6)}_{T1}$	4.1169	$\pm$ 0.3021
$f^{(6)}_{\mathrm{T}}$	0.2725	$\pm$ 0.0252
$c^{(6)}_1$	11.2666	$\pm$ 1.2661
$f^{(6)}_{\mathrm{TR}}$	0.4381	$\pm$ 0.0323

Fully entangled $B^{0*}\bar{B}^{0*}$ case.

Table 5.4: Δt fit parameters for Signal MC with the fully $B^0\bar{B}^0$ entangled sample, the fully $B^{0*}\bar{B}^{0*}$ entangled sample and the equal mixture of $C = \pm 1$ states (disentangled) sample. Superscript 6 expresses the parameter's 6th qr-bin specific value. ζ is the fraction of disentanglement and is fit simultaneously across all qr-bins, same for f_{Tail}.

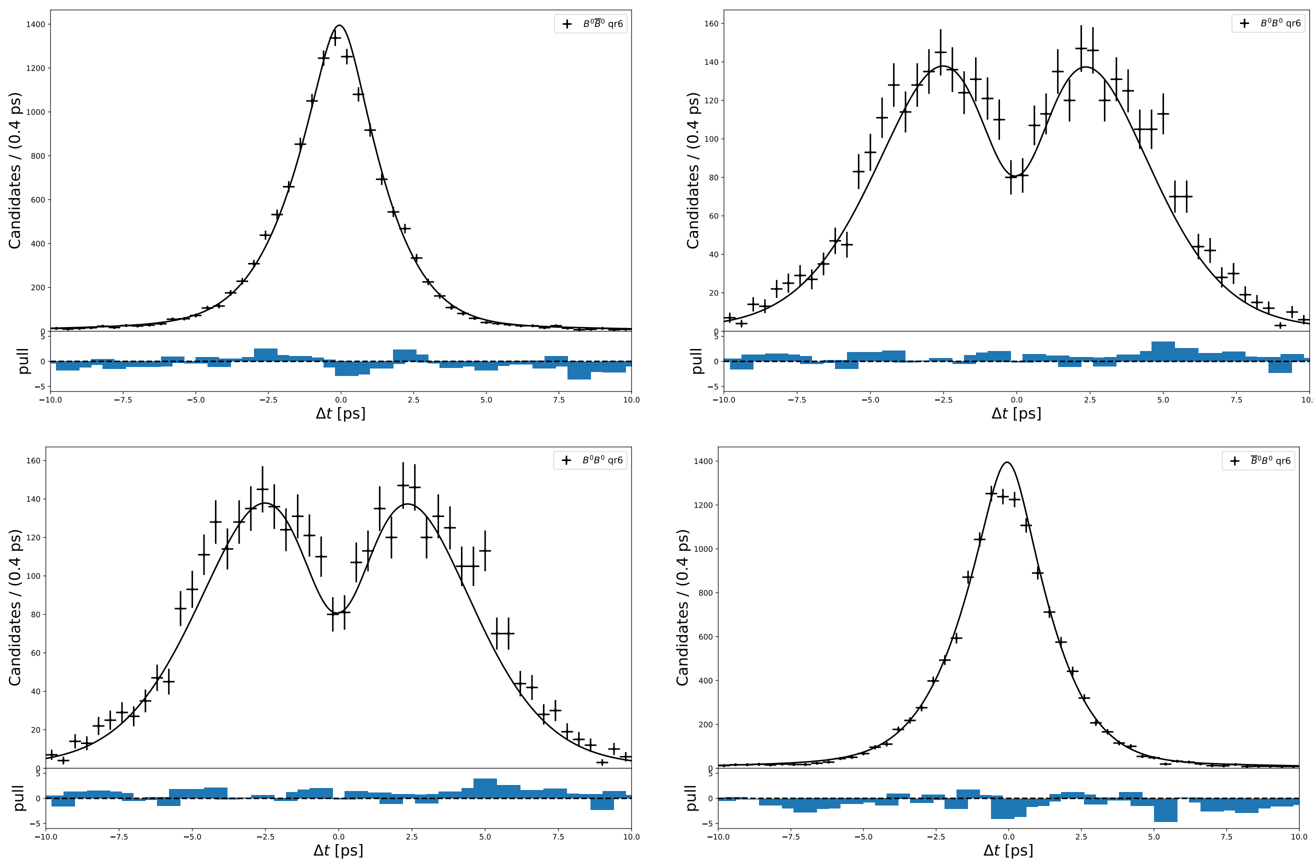

Figure 5.3: Δt-distribution fitted to Signal MC data for the full entanglement $B^{0*}\bar{B}^{0*}$ case. Data points with error bars show Signal MC data for $|qr| > 0.875$, so for the 6th qr-bin, solid line shows the fit. The lower plots show the pulls.

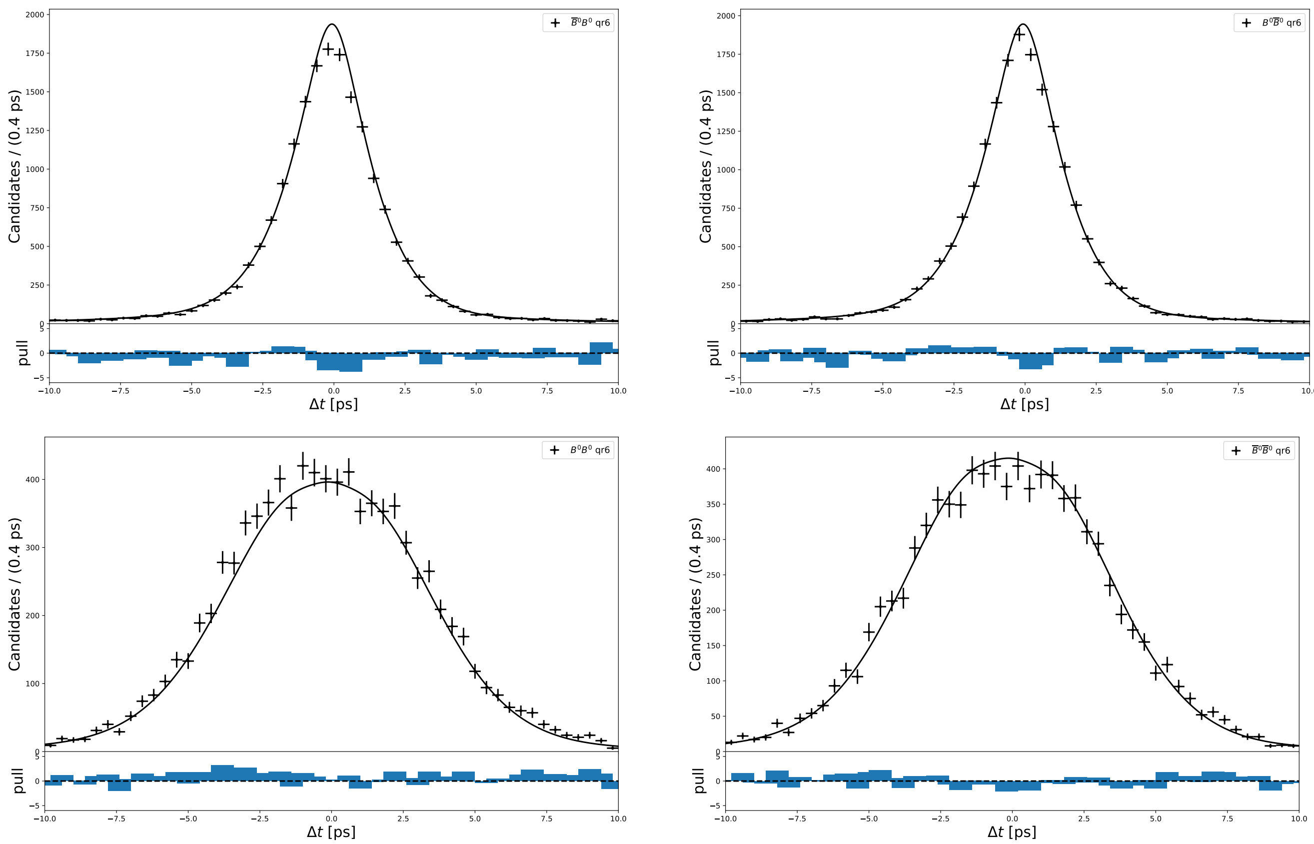

Figure 5.4: Δt-distribution fitted to Signal MC data for the equally mixed $C = \pm 1$ (disentangled) sample. Data points with error bars show Signal MC data for $|qr| > 0.875$, so for the 6th qr-bin, solid line shows the fit. The lower plots show the pulls.

Parameter	Fit estimate	
ζ	2.0037	$\pm$ 0.0149
μ_6	-0.0045	$\pm$ 0.0045
$\mu_{M1}^{(6)}$	-0.1035	$\pm$ 0.0250
$\mu_{T1}^{(6)}$	-1.0111	$\pm$ 0.0775
$\sigma_{M1}^{(6)}$	1.0770	$\pm$ 0.0389
$\sigma_{T1}^{(6)}$	3.6880	$\pm$ 0.1571
$f_{\mathrm{T}}^{(6)}$	0.9551	$\pm$ 0.0482

Table 5.5: Δt fit parameters for Signal MC with the fully $B^{0*}\bar{B}^0+$ c.c. entangled sample. Where the disetnangled function in the PSD model was modeld to be a equal mixture of $C = \pm$ entangled states. Superscript 6 expresses the parameter's 6th qr-bin specific value. ζ is the fraction of disentanglement and is fit simultaneously across all qr-bins, same for f_{Tail}.

disentangled case should consist of a mixture of the PDFs of the $C = +1$ and $C = -1$

$$PDF_{SD} = \frac{1}{2}PDF_{C=-1} + \frac{1}{2}PDF_{C=+1}\,. \tag{5.4}$$

When plugging eq. 5.4 into the PSD model function 2.111, we get

$$PSD = PDF_{C=-1} - \frac{1}{2}\zeta PDF_{C=-1} + \frac{1}{2}\zeta PDF_{C=+1} \tag{5.5}$$

where $PSD = PDF_{C=+1}$, when $\zeta = 2$. By fitting the already established fit framework to the $C = +1$ case as a function of Δt, we expect ζ to be 2. This has been done as explained in the sections above (see Sec. 5.1.2). The wrong-tag fractions for the $C = +1$ case are

$$w^+ = [0.475, 0.431, 0.372, 0.292, 0.241, 0.164, 0.0488],$$
$$w^- = [0.493, 0.444, 0.363, 0.293, 0.229, 0.161, 0.0481].$$

The resulting fits for the 6th qr bin are shown in Fig. 5.5. They agree with the expected distribution from theory (see Fig. 2.3 for reference). The fit parameters are listed in Tab. 5.5. The value of $\zeta$is, as expected, in the region of 2, lying within the 2.5σ range. This further validates our hypothesis that a completely disentangled state can be created by mixing two fully entangled $C = \pm 1$ states, and that this effect remains measurable under detector resolution effects. It also confirms that the simulated signal MC for the $C = +1$ case behaves as a fully entangled state. All remaining fit plots as well as fit parameters for the different qr bins are shown in Appendix A.2.

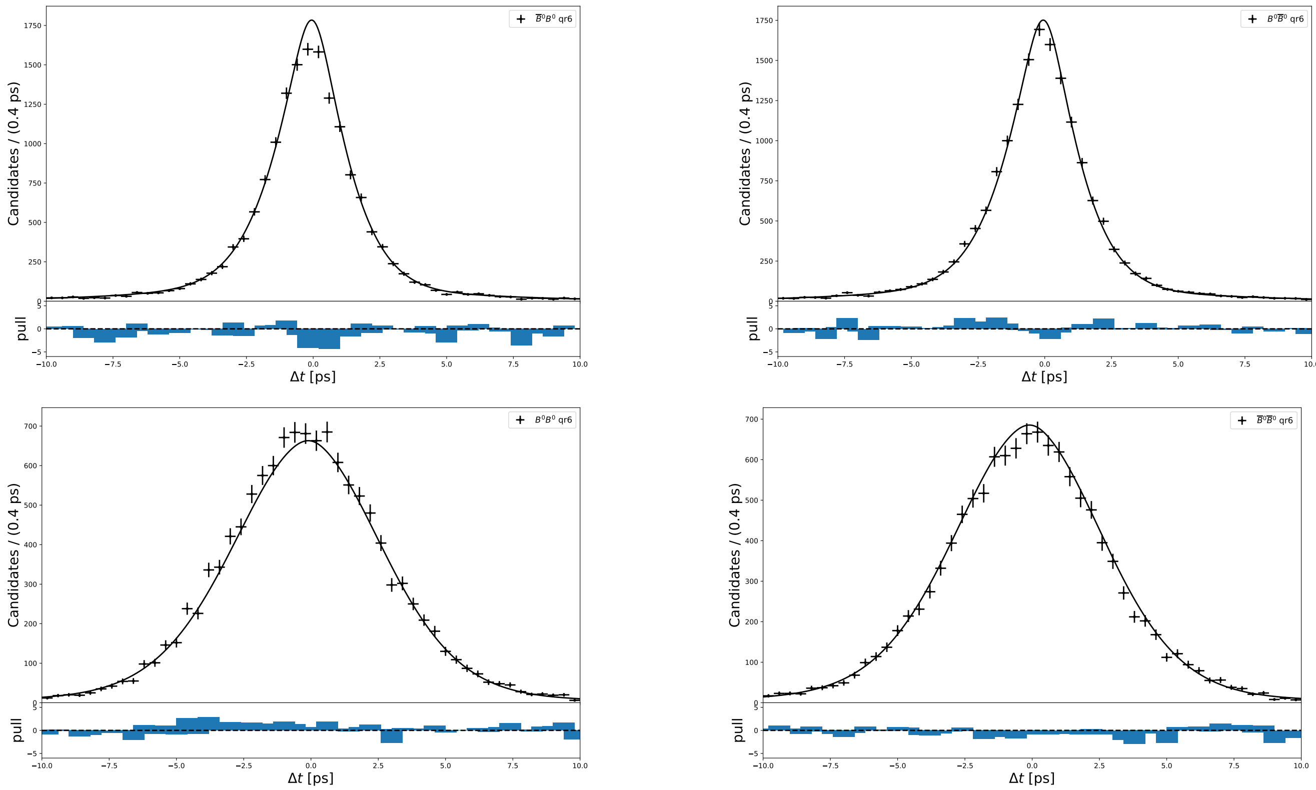

Figure 5.5: Δt-distribution fitted to Signal MC data for the full entanglement $B^{*0}\bar{B}^0$ case. Data points with error bars show Signal MC data for $|qr| > 0.875$, so for the 6th qr-bin, solid line shows the fit. The lower plot show the pulls.

6 Conclusion and Outlook

In this thesis, we investigated the entanglement and disentanglement of neutral B-meson pairs produced in the $\Upsilon(5\mathrm{S})$ resonance. We studied the quantum-mechanical properties such as the quantum numbers of the different states that can arise after the decays, i.e.

$$\Upsilon(5\mathrm{S}) \to B^0\bar{B}^0\ (C=-1), \quad \Upsilon(5\mathrm{S}) \to B^0\bar{B}^{0*} + \text{c.c.}\ (C=+1), \quad \Upsilon(5\mathrm{S}) \to B^{0*}\bar{B}^{0*}\ (C=-1).$$

These decays result in different wavefunctions describing the propagation of the B-meson pairs. We obtained an antisymmetric wavefunction for the $C=-1$ case and a symmetric wavefunction for the $C=+1$ case. From these wavefunctions, we calculated the time-dependent probabilities of the B-meson pairs for both same-flavor and opposite-flavor cases, as well as for fully entangled and fully disentangled states.

Furthermore, we derived time-dependent asymmetries that allow us to distinguish between the different entanglement configurations ($C=+1$, $C=-1$, and disentangled states). In particular, we demonstrated that these three cases can be differentiated not only by reconstructing the decay-time difference Δt, as has been done so far in all $\Upsilon(4\mathrm{S})$ entanglement analyses, but also by reconstructing the sum of the decay times Σt. This enables us to study time distributions and asymmetries as functions of both Δt and Σt, thereby increasing our ability to distinguish between the different entanglement configurations. To reconstruct these time variables, we derived the kinematics of the $\Upsilon(5\mathrm{S}) \to B^{0(*)}\bar{B}^{0(*)}$ system.

Another important result was the mixing of the two fully entangled $C=-1$ and $C=+1$ states to create a fully disentangled state. To achieve this, we separated the decay channels using the variables M_{bc} and ΔE, which required a detailed kinematic study of the $\Upsilon(5\mathrm{S})$ center-of-mass system. Additionally, we introduced selection cuts in generic Monte Carlo (MC) samples and provided an overview of the available MC data. Since the generic MC did not contain enough signal B-meson events, we generated dedicated signal MC samples. This process involved understanding the old Belle data simulation framework, rewriting several variables (such as Δt and flavor information), adjusting the output of the flavor tagger, and modifying the existing fitting framework to test a model of partial spontaneous disentanglement.

We successfully created and validated three different signal MC samples corresponding to the various entanglement configurations, and verified the MC truth information against theoretical predictions, finding good agreement. Using the Υ(4S) fitting framework, we investigated the disentanglement behavior of these samples without relying on MC truth, taking detector resolution effects into account.

$$\Upsilon(5\mathrm{S}) \to B^0\bar{B}^0 : \zeta = 0.054 \pm 0.013, \tag{6.1}$$

$$\Upsilon(5\mathrm{S}) \to B^{0*}\bar{B}^{0*} : \zeta = 0.049 \pm 0.014, \tag{6.2}$$

$$\Upsilon(5\mathrm{S}) \to B^{0*}\bar{B}^0 + \mathrm{c.c.} : \zeta = 1.016 \pm 0.015, \tag{6.3}$$

$$\text{Eqaul mixture of } C = \pm 1 \text{ states} : \zeta = 2.000 \pm 0.015. \tag{6.4}$$

Due to time constraints, we did not analyze the $C = +1$ case in detail, nor the dependence on Σt. Consequently, a full two-dimensional fit in $(\Delta t, \Sigma t)$ space couldn't be performed. This is an important goal for future studies. Other objectives include improving the flavor tagger performance at the Υ(5S), performing background and systematic studies, and investigating in more detail whether the electromagnetic transition $B^* \to \gamma B$ destroys at least partially the entanglement.

An interesting outlook would be to perform a CHSH inequality test at the Υ(5S), since it is now possible to select decay times large enough for the inequality to be violated. However, several loopholes may appear, such as the fair-sampling problem if the Belle detector resolution is insufficient, or the inability to determine the decay time of the B mesons with arbitrary precision (see [52] for more details). One might need, in principle, an extremely powerful X-ray laser to induce B-meson decays at chosen times [53]. Additionally, quantum tomography, which is full reconstruction of the states density matrix [54], could be explored.

In conclusion, the Υ(5S) resonance provides an interesting environment to study quantum-mechanical phenomena such as entanglement and disentanglement properties of neutral B-meson pairs.

A Analysis on Signal MC sample

A.1 $\delta\Delta t$ fits for all qrGNN bins on Signal MC

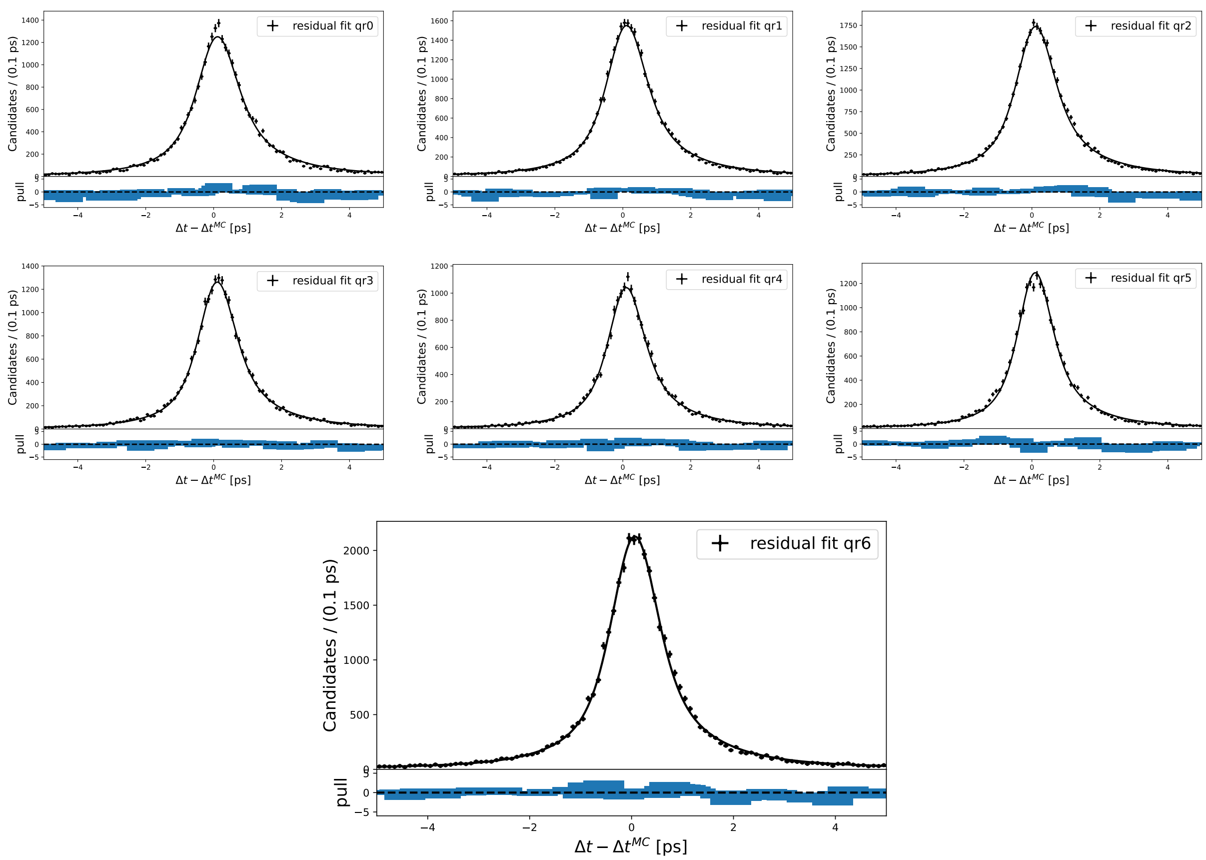

Figure A.1: Residual fits for Signal MC with full entanglement for the $B^0\bar{B}^0$ (C=-1) case. Single figures show the fits on different qr-bins 0-6 (left to right, top to bottom).

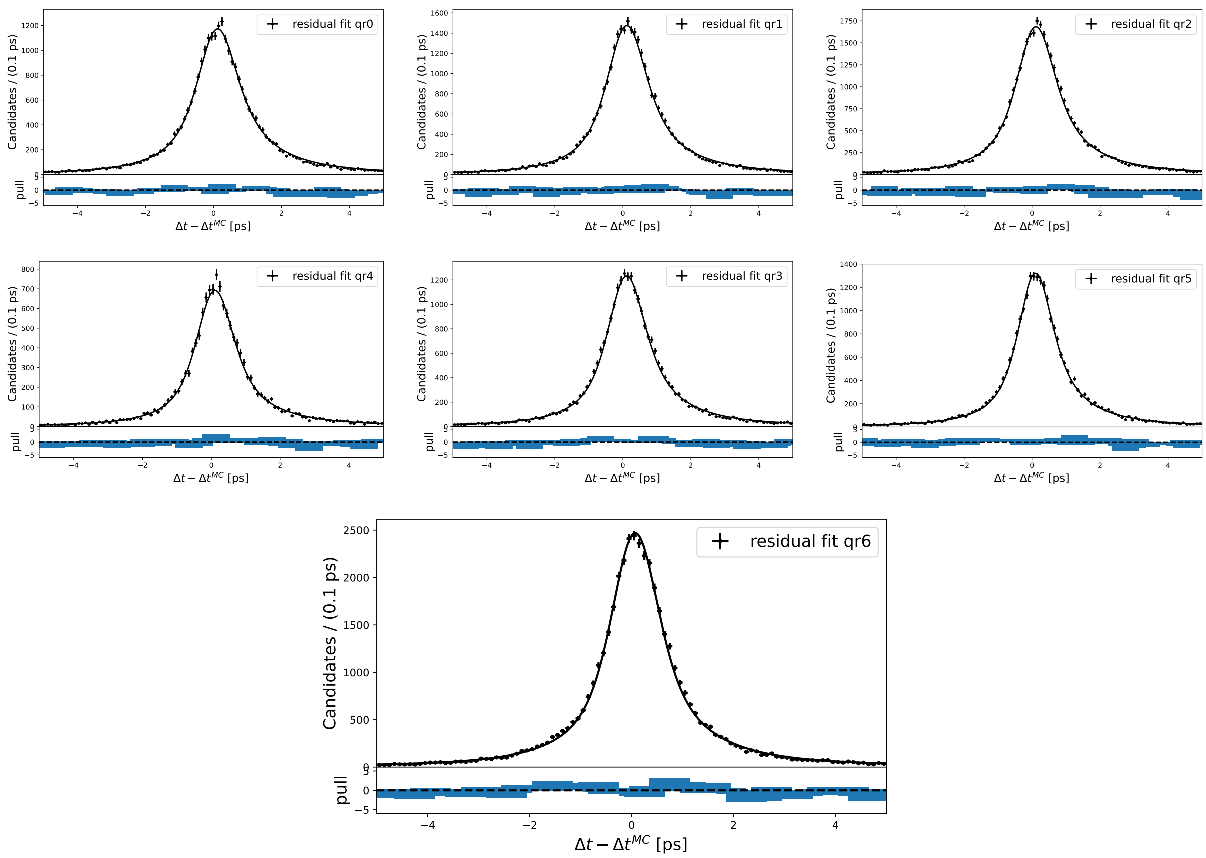

Figure A.2: Residual fits for Signal MC with full entanglement for the $B^{0*}\bar{B}^{0*}$ (C=-1) case. Single figures show the fits on different qr-bins 0-6 (left to right, top to bottom).

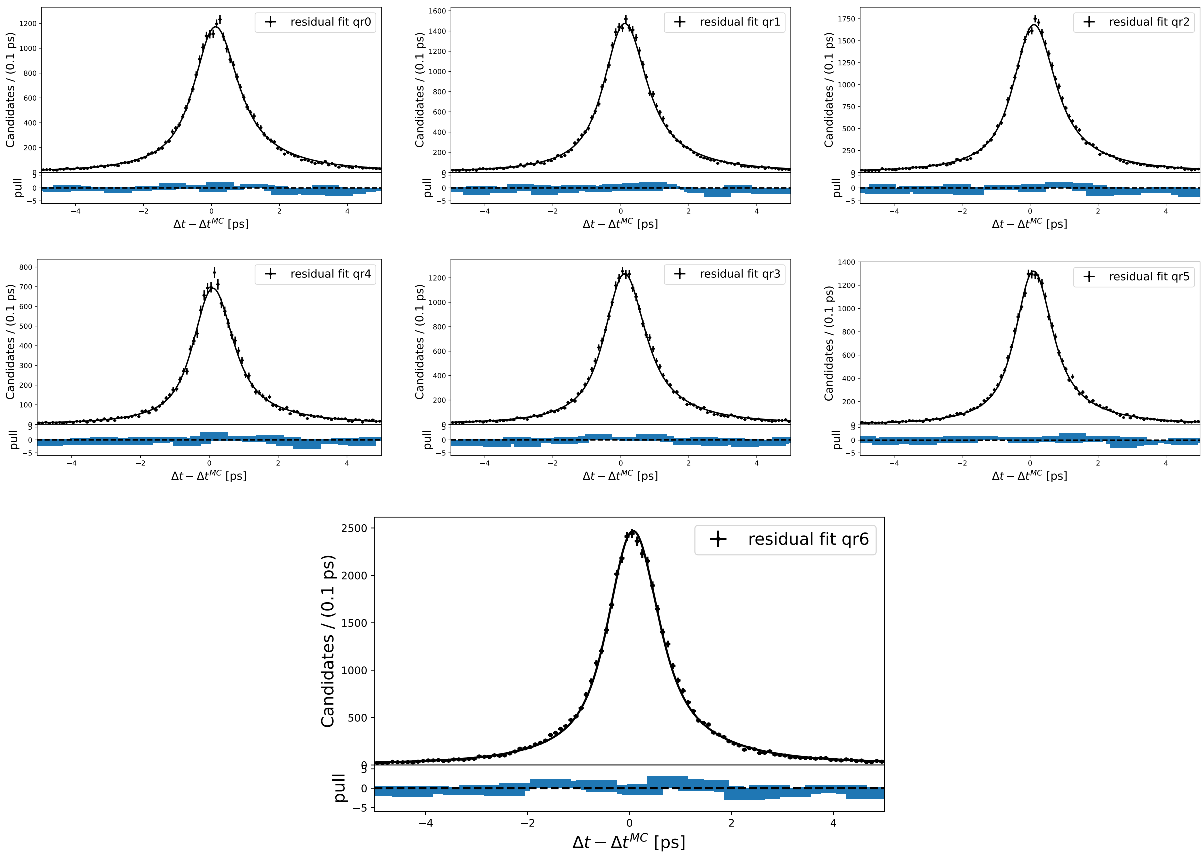

Figure A.3: Residual fits for Signal MC with full entanglement for the disentangled case (equal mixture of $C = \pm 1$ states). Single figures show the fits on different qr-bins 0-6 (left to right, top to bottom).

A.2 Δt fit plots

Parameter	Value $\pm$ Error
ζ	0.0540 ± 0.0128
wp_0	0.4813 ± 0.0050
wn_0	0.4599 ± 0.0047
μ_0	-0.0493 ± 0.0079
μ_{M1}	-0.1663 ± 0.0133
μ_{T1}	-1.1090 ± 0.0399
σ_{M1}	1.0069 ± 0.0155
σ_{T1}	2.8669 ± 0.0506
$fracT$	0.3431 ± 0.0057
wp_1	0.4437 ± 0.0046
wn_1	0.4344 ± 0.0044
μ_1	-0.0376 ± 0.0072

Parameter	Value $\pm$ Error
wp_2	0.3705 ± 0.0043
wn_2	0.3841 ± 0.0042
μ_2	-0.0267 ± 0.0069
wp_3	0.2951 ± 0.0050
wn_3	0.3080 ± 0.0049
μ_3	-0.0392 ± 0.0081
wp_4	0.2187 ± 0.0054
wn_4	0.2348 ± 0.0054
μ_4	-0.0265 ± 0.0090
wp_5	0.1302 ± 0.0046
wn_5	0.1368 ± 0.0047
μ_5	-0.0140 ± 0.0082
μ_6	-0.0214 ± 0.0052
μ_{M1}^{qr6}	-0.1038 ± 0.0263
μ_{T1}^{qr6}	-1.3463 ± 0.1249
σ_{M1}^{qr6}	1.3040 ± 0.0397
σ_{T1}^{qr6}	4.5190 ± 0.2019
$fracT^{qr6}$	0.2551 ± 0.0141

Table A.1: All Δt fit parameters for Signal MC on the fully $B^0\bar{B}^0$ entangled sample. Superscript 6 expresses the parameter's 6th qr-bin specific value. ζ is the fraction of disentanglement and is fit simultaneously across all qr-bins, same for f_{Tail}

.

Parameter	Value ± Error
ζ	0.0493 ± 0.0139
wp_0	0.4770 ± 0.0052
wn_0	0.4592 ± 0.0050
μ_0	-0.0369 ± 0.0082
$fracOL$	0.0111 ± 0.0011
$\sigma 0OL$	49.8432 ± 13.6275
μ_{M1}	-0.2351 ± 0.0230
μ_{T1}	-1.3068 ± 0.2323
σ_{M1}	1.1571 ± 0.0426
σ_{T1}	2.9794 ± 0.3209
$frac_T$	0.1811 ± 0.0316
$frac_{Exp}$	0.3472 ± 0.0526
c_1	11.8976 ± 0.5345
f_{TR}	0.4435 ± 0.0174
wp_1	0.4357 ± 0.0047
wn_1	0.4323 ± 0.0046
μ_1	-0.0398 ± 0.0075

Parameter	Value± Error
wp_2	0.3737 ± 0.0046
wn_2	0.3817 ± 0.0044
μ_2	-0.0490 ± 0.0072
wp_3	0.3036 ± 0.0053
wn_3	0.2992 ± 0.0052
μ_3	-0.0328 ± 0.0086
wp_4	0.2246 ± 0.0056
wn_4	0.2369 ± 0.0056
μ_4	-0.0184 ± 0.0095
wp_5	0.1345 ± 0.0050
wn_5	0.1457 ± 0.0049
μ_5	-0.0359 ± 0.0087
μ_6	-0.0142 ± 0.0057
$frac_{OL}^{qr6}$	0.0063 ± 0.0022
σ_{OL}^{qr6}	28.0618 ± 9.0619
μ_{M1}^{qr6}	-0.1341 ± 0.0329
μ_{T1}^{qr6}	-0.9808 ± 0.2088
σ_{M1}^{qr6}	1.2708 ± 0.0633
σ_{T1}^{qr6}	4.1169 ± 0.3021
$frac_T^{qr6}$	0.2725 ± 0.0252
c_1^{qr6}	11.2666 ± 1.2661
f_{TR}^{qr6}	0.4381 ± 0.0323

Table A.2: All Δt fit parameters for Signal MC on the fully $B^{0*}\bar{B}^{0*}$ entangled sample. Superscript 6 expresses the parameter's 6th qr-bin specific value. ζ is the fraction of disentanglement and is fit simultaneously across all qr-bins, same for f_{Tail}.

Parameter	Value $\pm$ Error
ζ	1.0155 ± 0.0150
wp_0	0.4737 ± 0.0059
wn_0	0.4601 ± 0.0054
μ_0	-0.0577 ± 0.0100
μ_{M1}	-0.1847 ± 0.0114
μ_{T1}	-1.1198 ± 0.0359
σ_{M1}	1.0814 ± 0.0143
σ_{T1}	3.4326 ± 0.0530
$frac_T$	0.6214 ± 0.0094
wp_1	0.4402 ± 0.0053
wn_1	0.4325 ± 0.0050
μ_1	-0.0462 ± 0.0092

Parameter	Value $\pm$ Error
$wp2$	0.3666 ± 0.0051
$wn2$	0.3838 ± 0.0048
μ_2	-0.0359 ± 0.0087
$wp3$	0.2786 ± 0.0062
$wn3$	0.2984 ± 0.0058
μ_3	-0.0453 ± 0.0103
$wp4$	0.2117 ± 0.0069
$wn4$	0.2378 ± 0.0066
μ_4	-0.0381 ± 0.0114
$wp5$	0.1229 ± 0.0066
$wn5$	0.1476 ± 0.0062
μ_5	-0.0341 ± 0.0103
μ_6	-0.0169 ± 0.0045
μ_{M1}^{qr6}	-0.1558 ± 0.0213
μ_{T1}^{qr6}	-1.3125 ± 0.1137
σ_{M1}^{qr6}	1.2799 ± 0.0341
σ_{T1}^{qr6}	4.8549 ± 0.2092
$fracT^{qr6}$	0.4220 ± 0.0219

Table A.3: All Δt fit parameters for Signal MC on the equally mixed $C = \pm 1$ (disentnagled) sample. Superscript 6 expresses the parameter's 6th qr-bin specific value. ζ is the fraction of disentanglement and is fit simultaneously across all qr-bins, same for f_{Tail}.

Parameter	Value ± Error
ζ	2.0037 ± 0.0149
wp_0	0.4880 ± 0.0090
wn_0	0.4724 ± 0.0086
μ_0	-0.0228 ± 0.0169
μ_{M1}	-0.1716 ± 0.0119
μ_{T1}	-1.1706 ± 0.0338
σ_{M1}	1.1400 ± 0.0132
σ_{T1}	3.6831 ± 0.0339
f_T	1.0000 ± 0.0001
wp_1	0.4264 ± 0.0085
wn_1	0.4222 ± 0.0077
μ_1	-0.0525 ± 0.0153
wp_2	0.3571 ± 0.0080
wn_2	0.3690 ± 0.0074
μ_2	-0.0394 ± 0.0143
wp_3	0.2656 ± 0.0101
wn_3	0.2884 ± 0.0092
μ_3	-0.0486 ± 0.0170
wp_4	0.2186 ± 0.0115
wn_4	0.2507 ± 0.0104
μ_4	-0.0525 ± 0.0188
wp_5	0.1410 ± 0.0105
wn_5	0.1693 ± 0.0099
μ_5	-0.0273 ± 0.0166
μ_6	-0.0045 ± 0.0045
$\mu_{M1}^{(6)}$	-0.1035 ± 0.0250
$\mu_{T1}^{(6)}$	-1.0111 ± 0.0775
$\sigma_{M1}^{(6)}$	1.0770 ± 0.0389
$\sigma_{T1}^{(6)}$	3.6880 ± 0.1571
$f_T^{(6)}$	0.9551 ± 0.0482

Table A.4: All Δt fit parameters for Signal MC on the $\mathrm{B}^{0*}\bar{\mathrm{B}}^0$+c.c. ($C = +1$) sample. Superscript 6 expresses the parameter's 6th qr-bin specific value. ζ is the fraction of disentanglement and is fit simultaneously across all qr-bins, same for f_{Tail}.

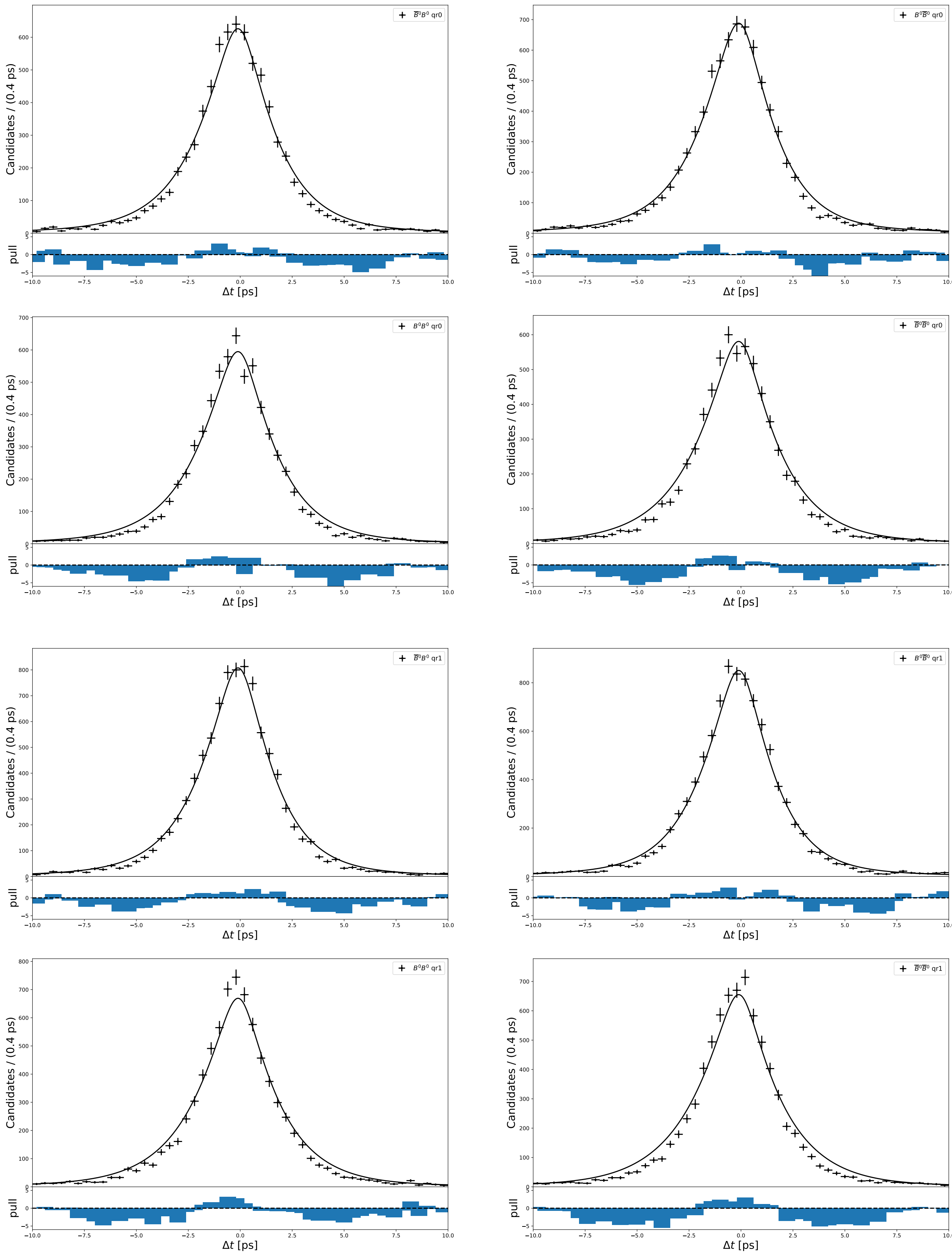
$\overline{B}^0B^0$ qr0
$B^0\overline{B}^0$ qr0
B^0B^0 qr0
$\overline{B}^0\overline{B}^0$ qr0
$\overline{B}^0B^0$ qr1
$B^0\overline{B}^0$ qr1
B^0B^0 qr1
$\overline{B}^0\overline{B}^0$ qr1
Candidates / (0.4 ps)
pull
Δt [ps]

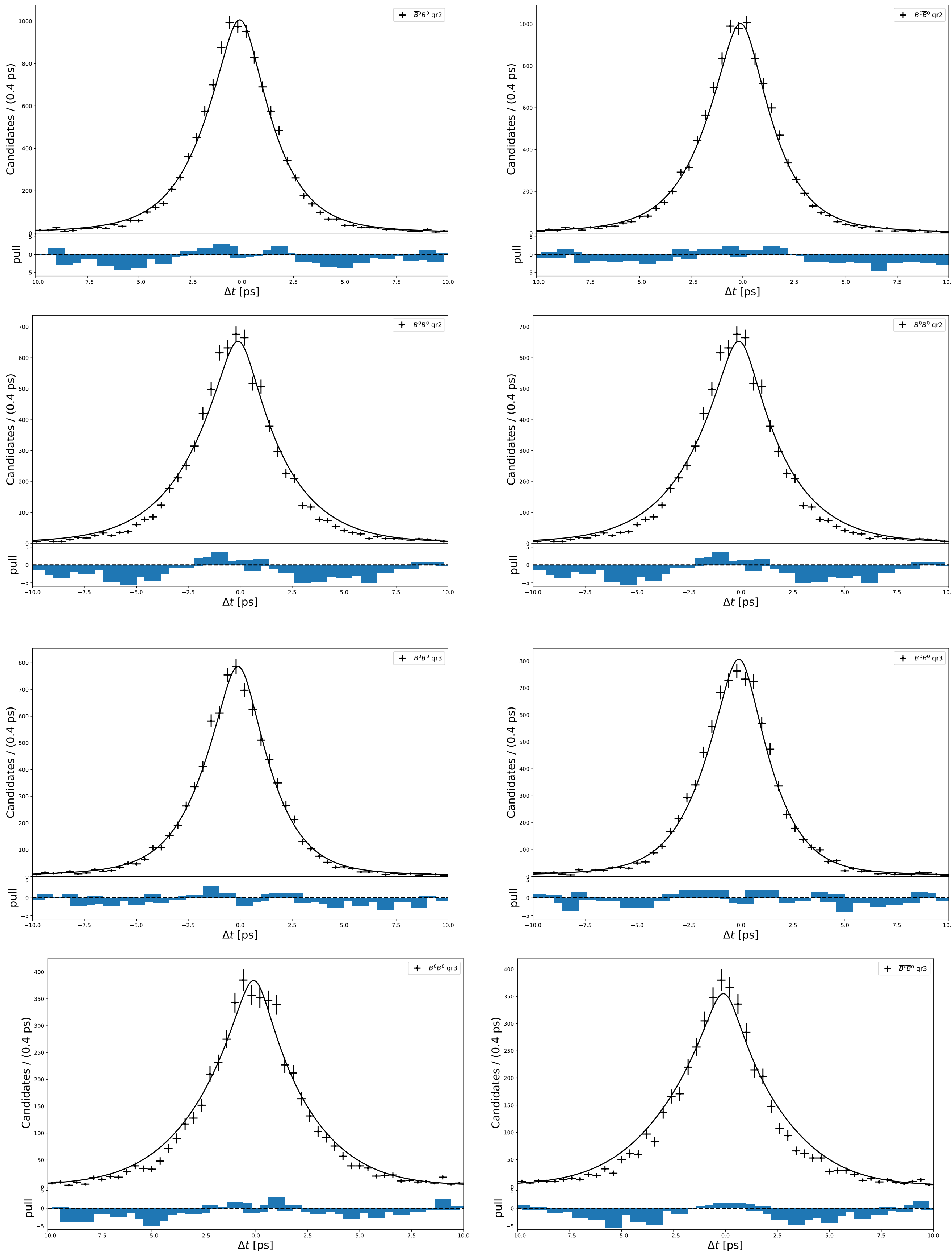

$\overline{B}^0 B^0$ qr2
$B^0 \overline{B}^0$ qr2
$B^0 B^0$ qr2
$B^0 B^0$ qr2
$\overline{B}^0 B^0$ qr3
$B^0 \overline{B}^0$ qr3
$B^0 B^0$ qr3
$\overline{B}^0 \overline{B}^0$ qr3
Candidates / (0.4 ps)
pull
Δt [ps]

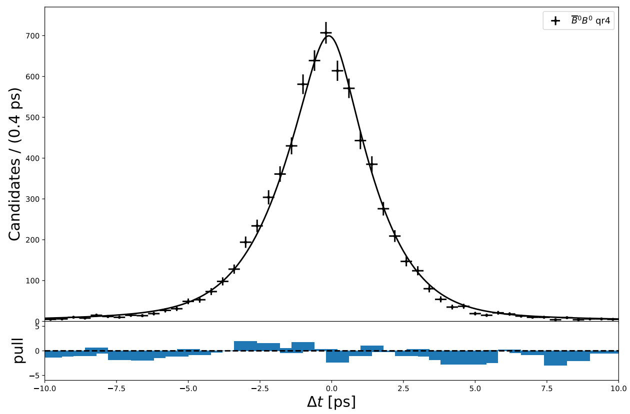

$\overline{B}^0B^0$ qr4
Candidates / (0.4 ps)
pull
Δt [ps]

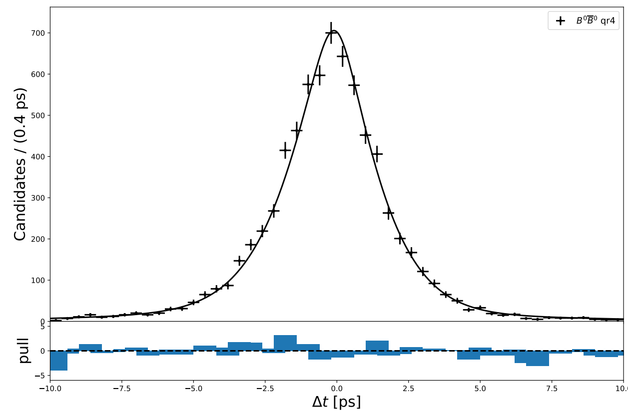

$B^0\overline{B}^0$ qr4
Candidates / (0.4 ps)
pull
Δt [ps]

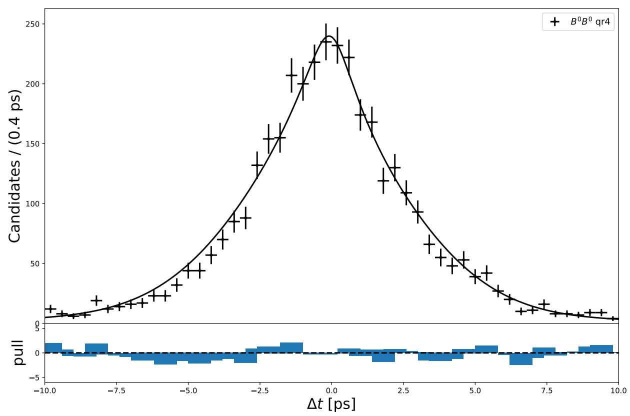

B^0B^0 qr4
Candidates / (0.4 ps)
pull
Δt [ps]

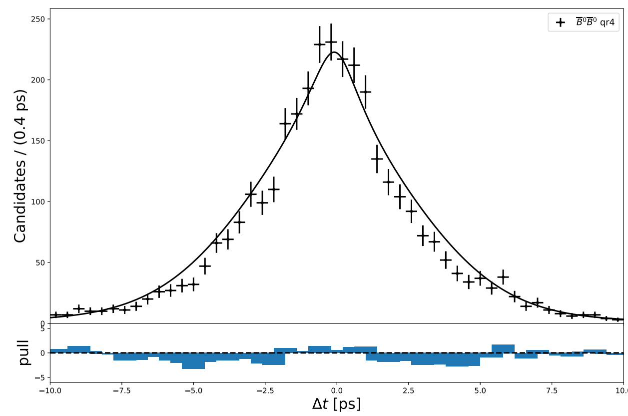

$\overline{B}^0\overline{B}^0$ qr4
Candidates / (0.4 ps)
pull
Δt [ps]

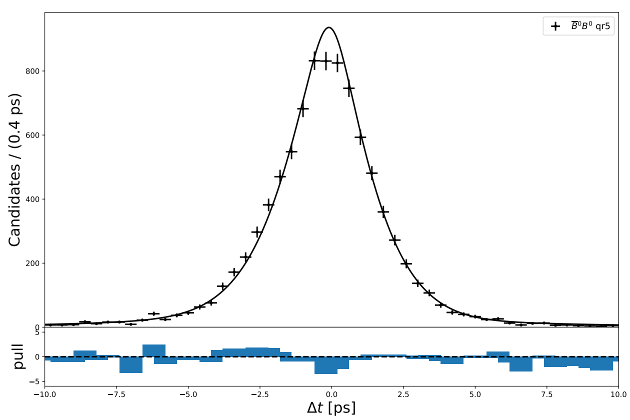

$\overline{B}^0B^0$ qr5
Candidates / (0.4 ps)
pull
Δt [ps]

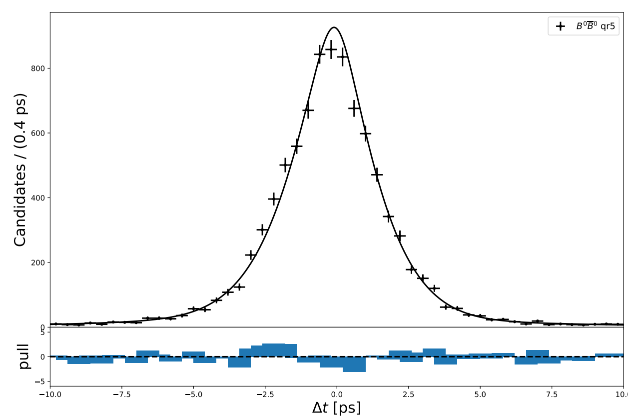

$B^0\overline{B}^0$ qr5
Candidates / (0.4 ps)
pull
Δt [ps]

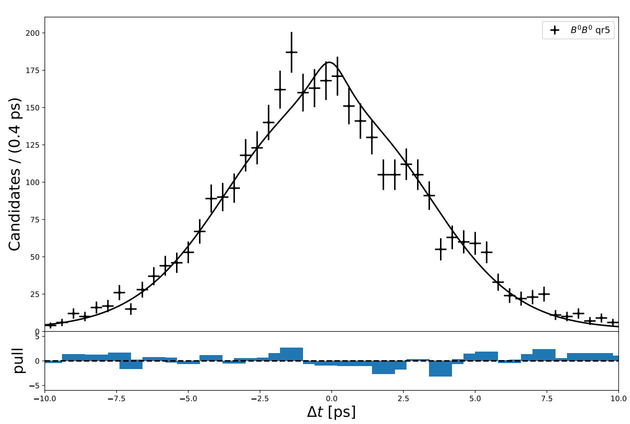

B^0B^0 qr5
Candidates / (0.4 ps)
pull
Δt [ps]

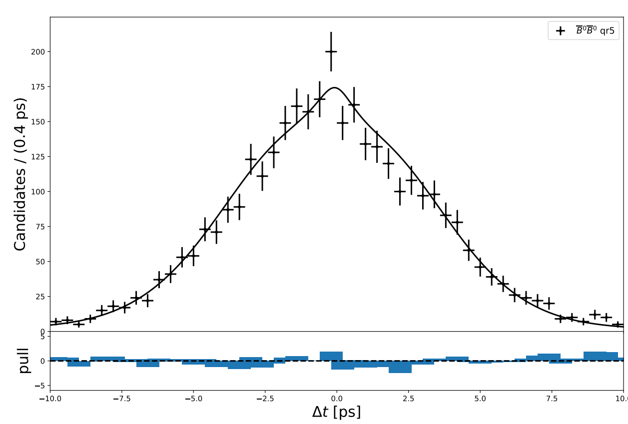

$\overline{B}^0\overline{B}^0$ qr5
Candidates / (0.4 ps)
pull
Δt [ps]

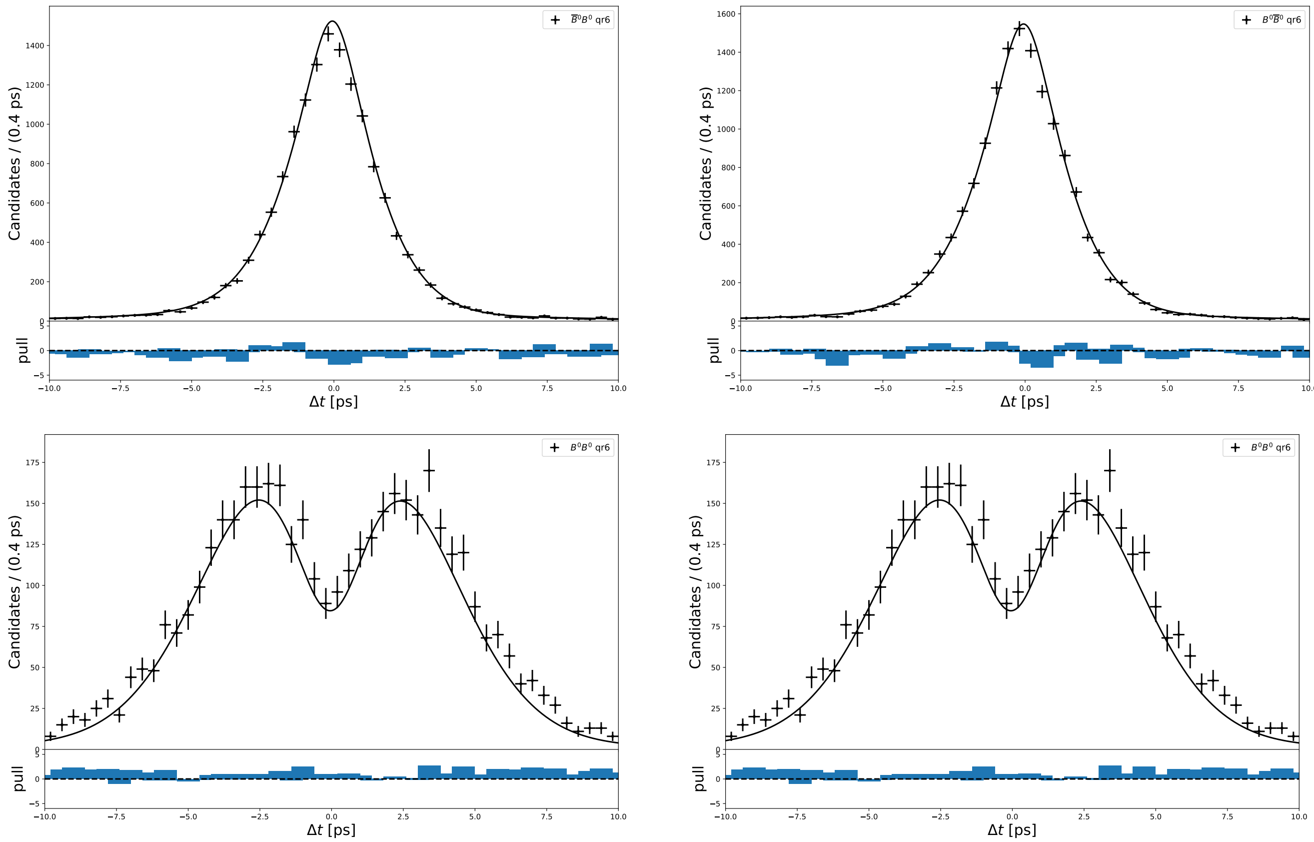

Figure A.4: Δt-distribution fitted to $B^0\bar{B}^0$ Signal MC data for all qr bins and four flavor combinations (left to right, top to bottom). Error bars show Signal MC data binned in qr bins and solid line shows the fit. The lower plot show the pulls.

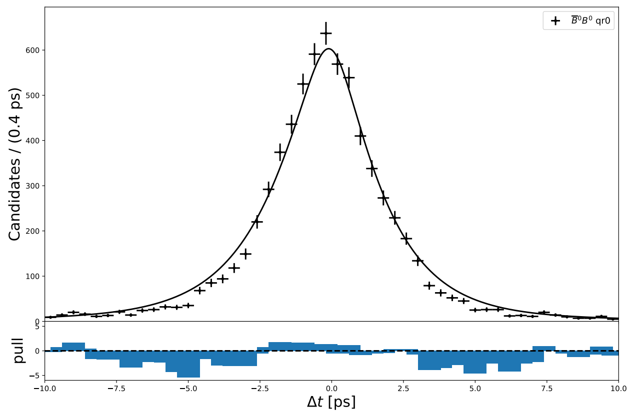
$\overline{B}^0B^0$ qr0
Candidates / (0.4 ps)
pull
Δt [ps]

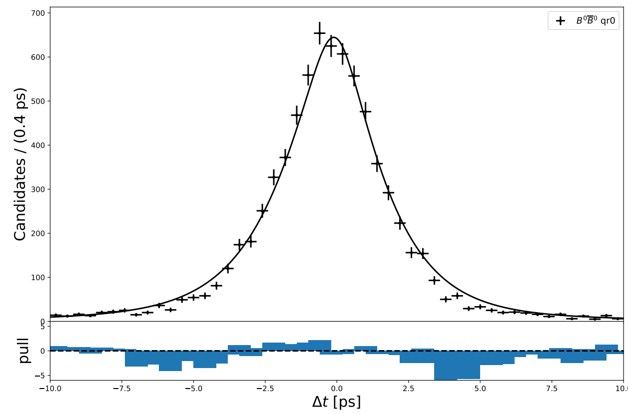
$B^0\overline{B}^0$ qr0
Candidates / (0.4 ps)
pull
Δt [ps]

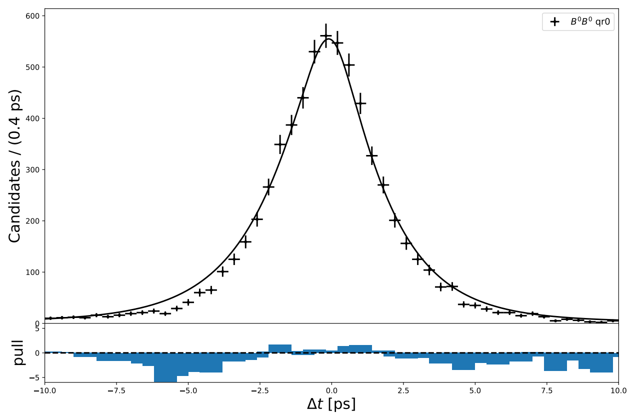
B^0B^0 qr0
Candidates / (0.4 ps)
pull
Δt [ps]

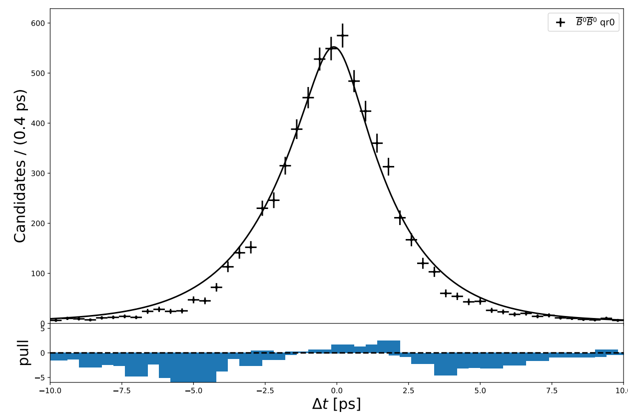
$\overline{B}^0\overline{B}^0$ qr0
Candidates / (0.4 ps)
pull
Δt [ps]

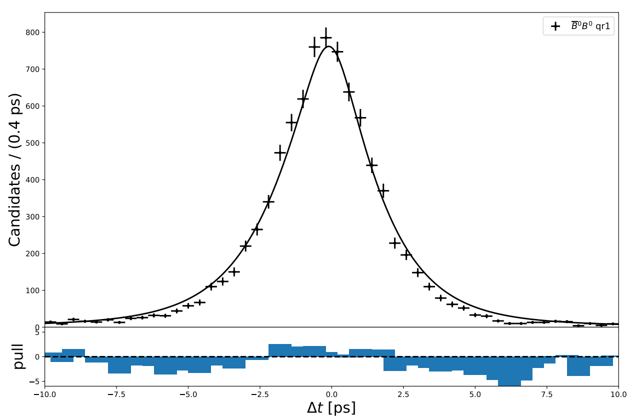
$\overline{B}^0B^0$ qr1
Candidates / (0.4 ps)
pull
Δt [ps]

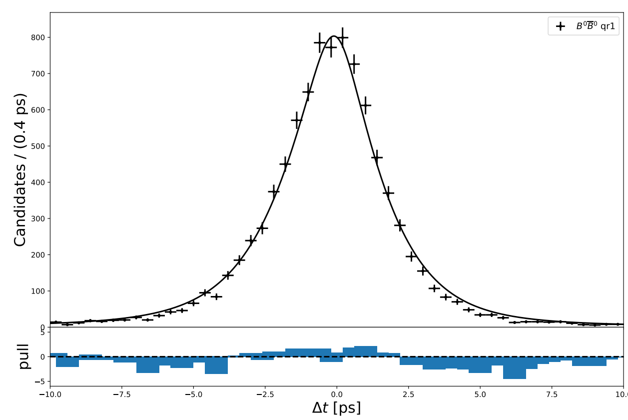
$B^0\overline{B}^0$ qr1
Candidates / (0.4 ps)
pull
Δt [ps]

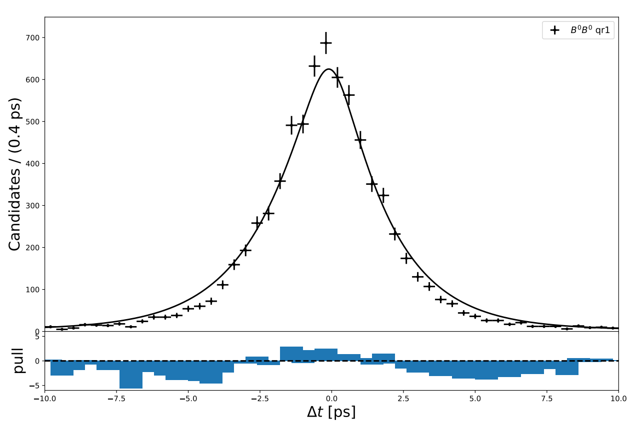
B^0B^0 qr1
Candidates / (0.4 ps)
pull
Δt [ps]

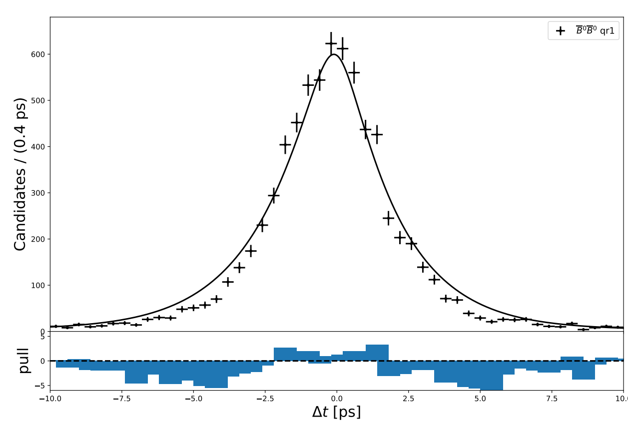
$\overline{B}^0\overline{B}^0$ qr1
Candidates / (0.4 ps)
pull
Δt [ps]

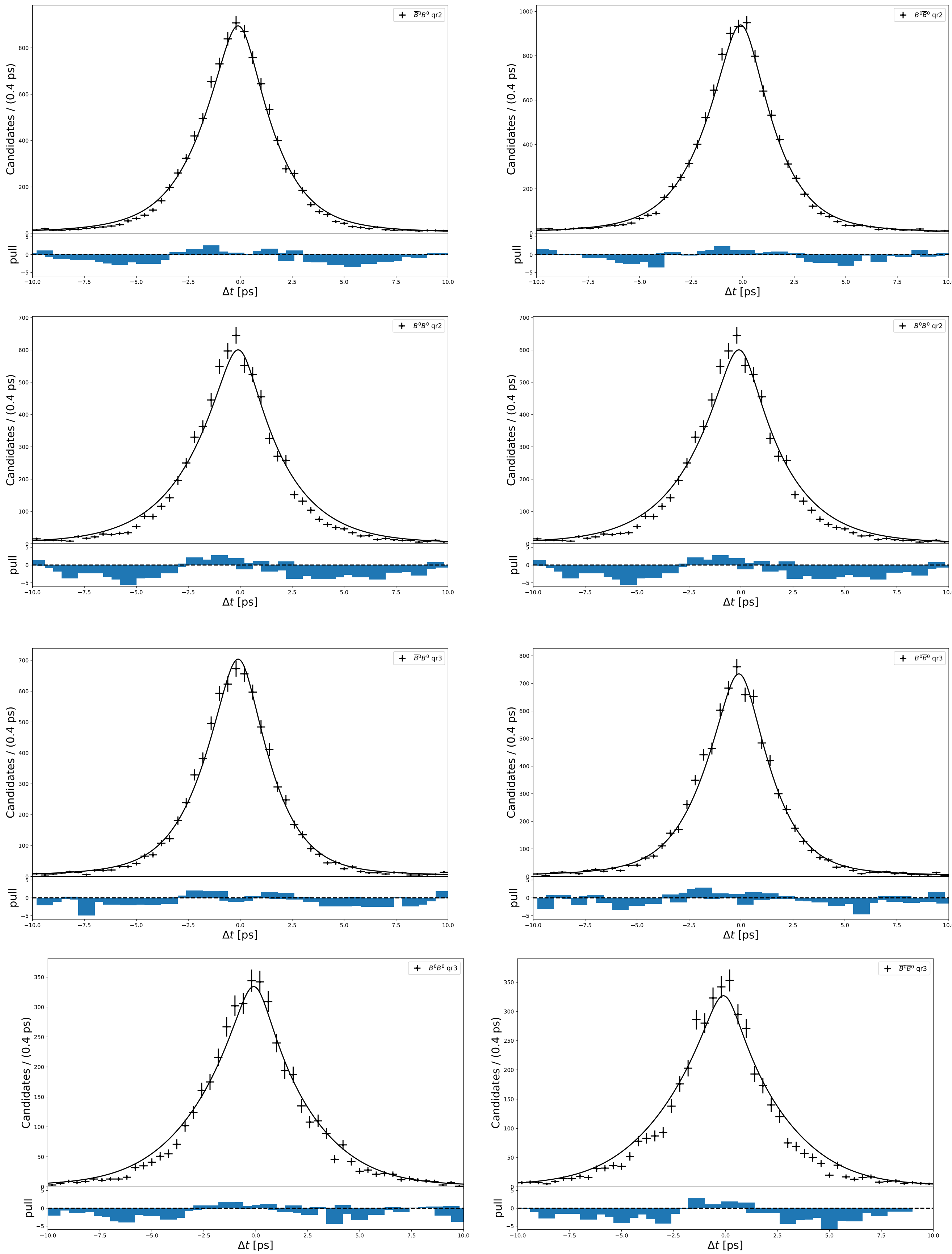
Candidates / (0.4 ps)
pull
Δt [ps]
$\overline{B}^0B^0$ qr2
$B^0\overline{B}^0$ qr2
B^0B^0 qr2
B^0B^0 qr2
$\overline{B}^0B^0$ qr3
$B^0\overline{B}^0$ qr3
B^0B^0 qr3
$\overline{B}^0\overline{B}^0$ qr3

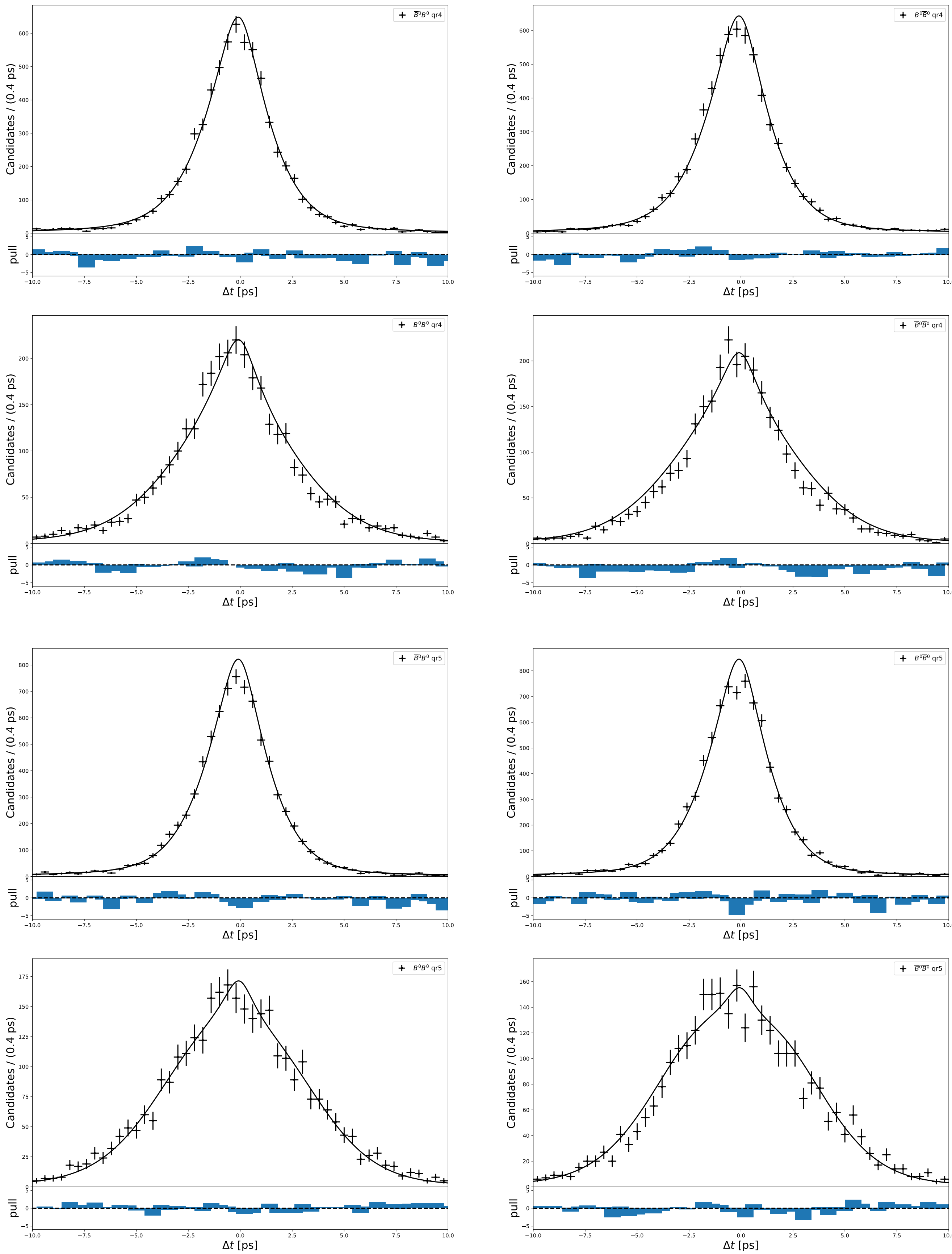
Candidates / (0.4 ps)
pull
Δt [ps]

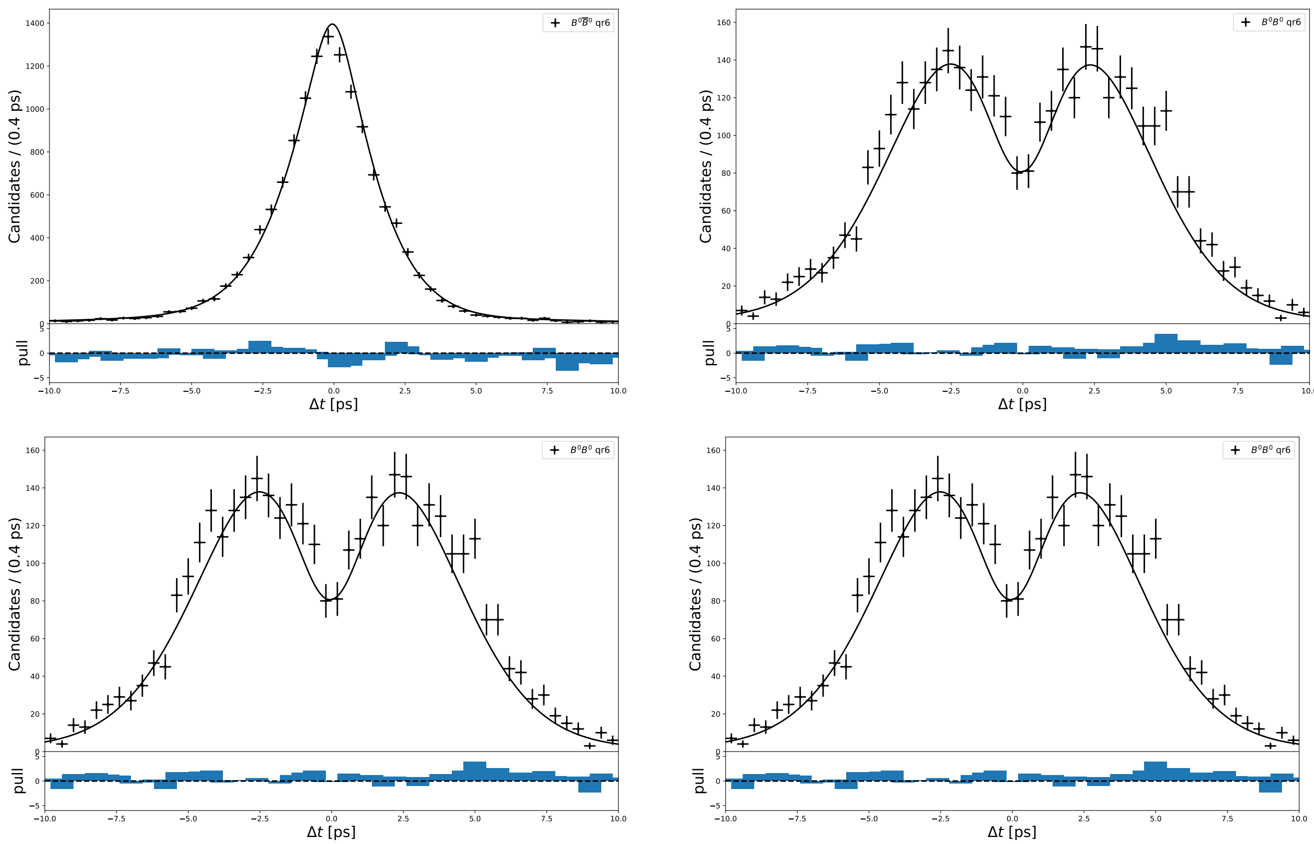

Figure A.5: Δt-distribution fitted to $B^{0*}\bar{B}^{0*}$ Signal MC data for all qr bins and four flavor combinations (left to right, top to bottom). Error bars show Signal MC data binned in qr bins and solid line shows the fit. The lower plot show the pulls.

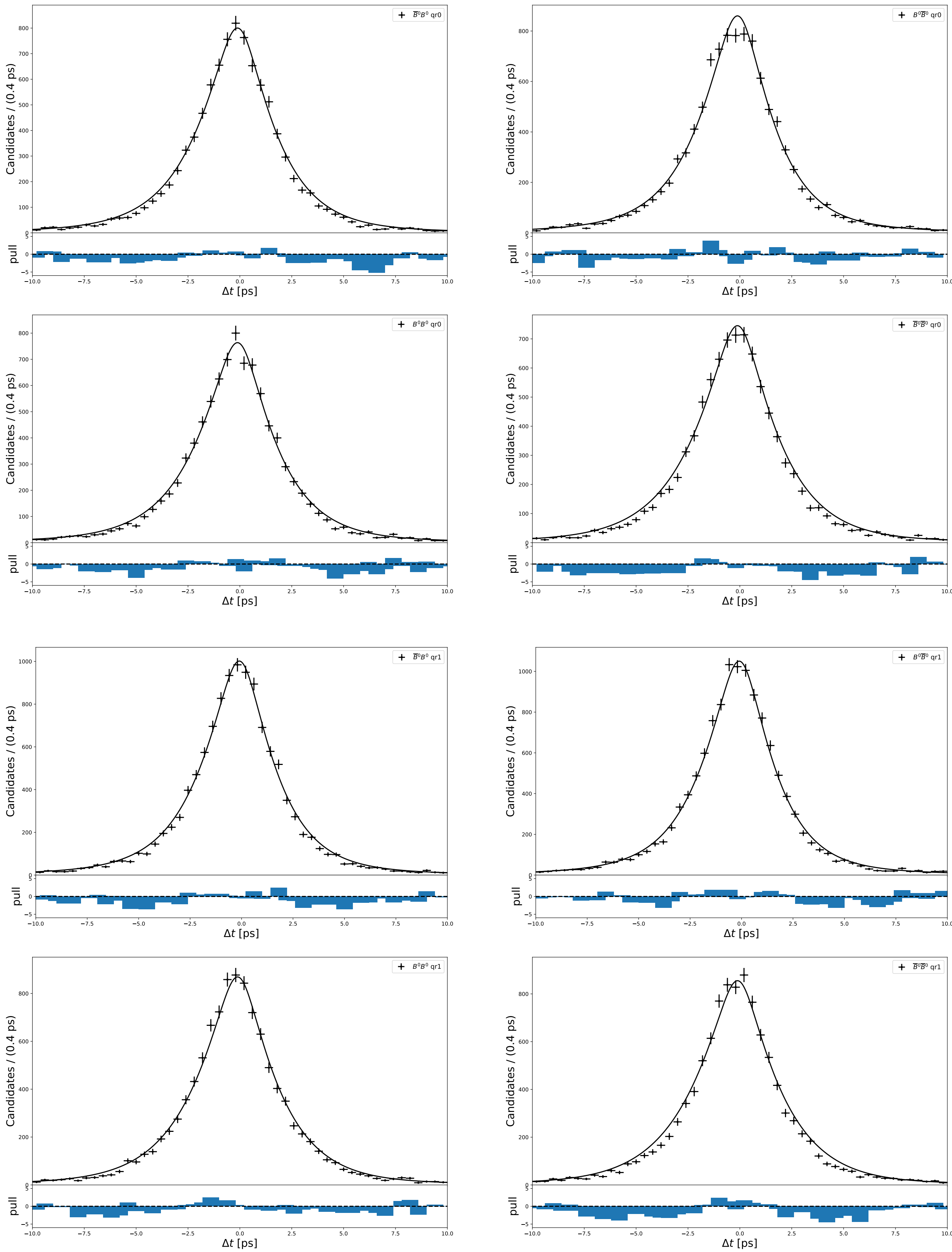
Candidates / (0.4 ps)
pull
Δt [ps]

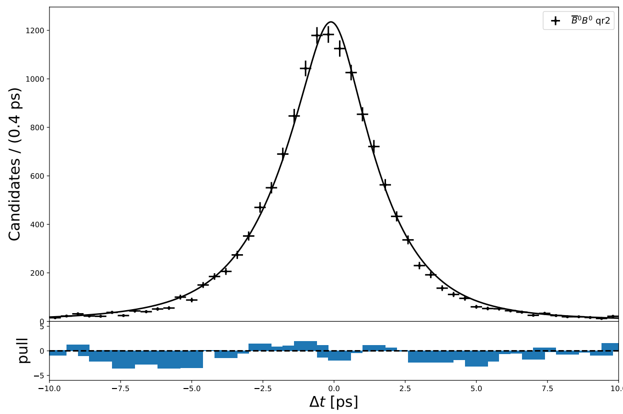
Candidates / (0.4 ps)
pull
Δt [ps]

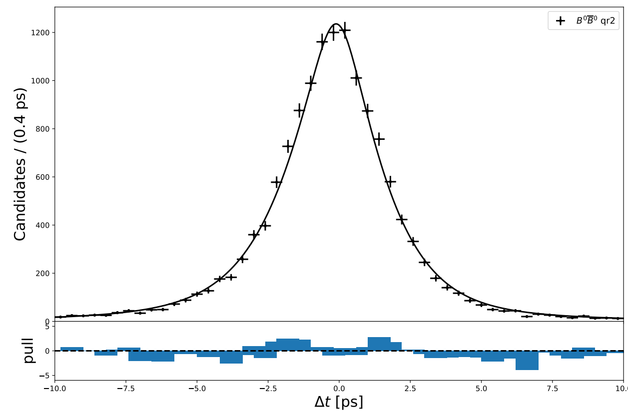
Candidates / (0.4 ps)
pull
Δt [ps]

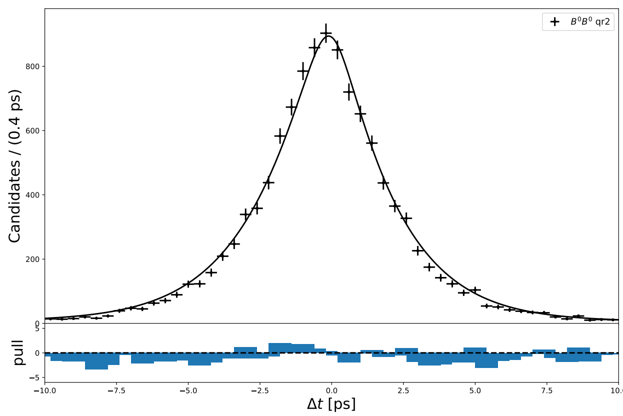
Candidates / (0.4 ps)
pull
Δt [ps]

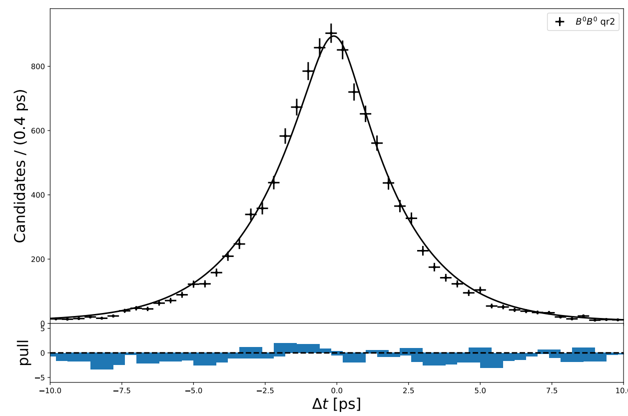
Candidates / (0.4 ps)
pull
Δt [ps]

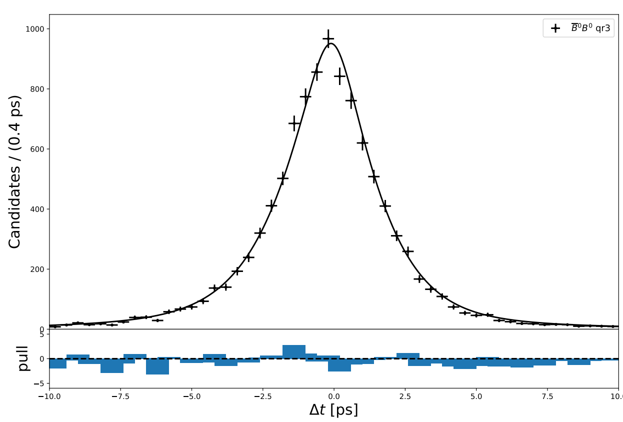
Candidates / (0.4 ps)
pull
Δt [ps]

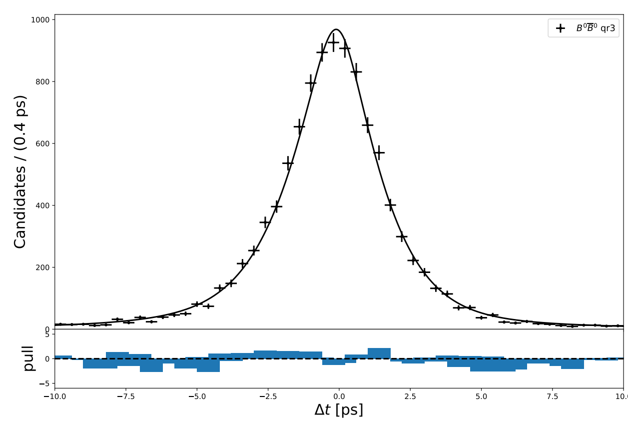
Candidates / (0.4 ps)
pull
Δt [ps]

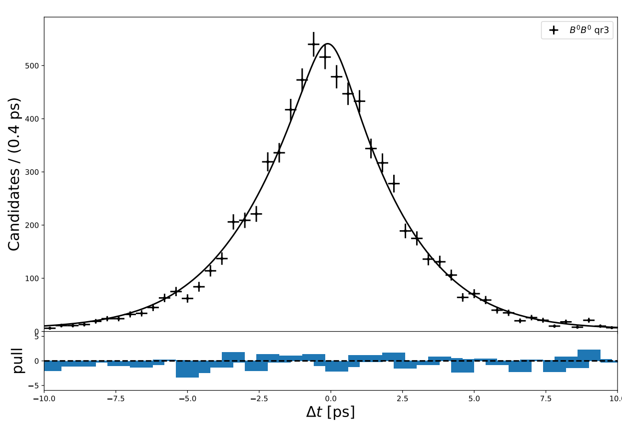
Candidates / (0.4 ps)
pull
Δt [ps]

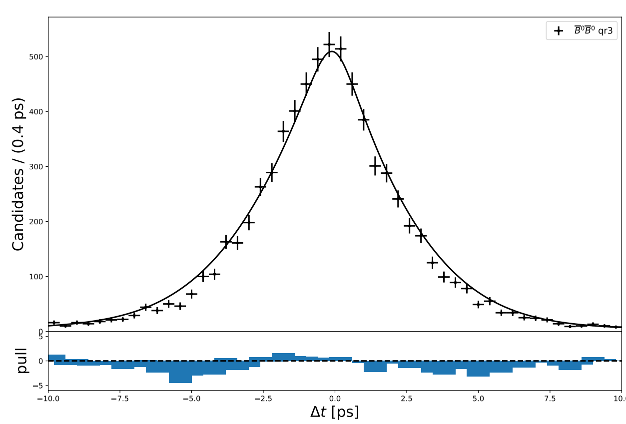
Candidates / (0.4 ps)
pull
Δt [ps]

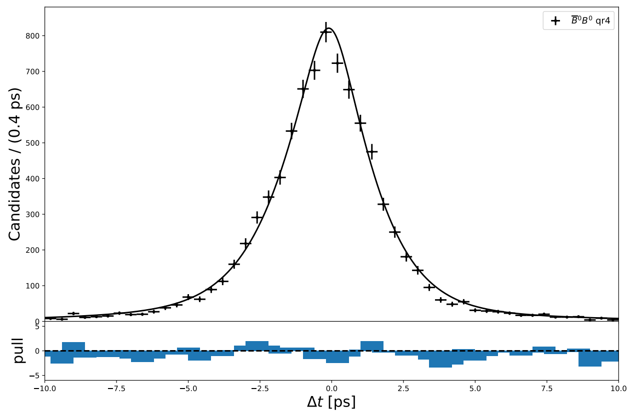
$\overline{B}^0B^0$ qr4
Candidates / (0.4 ps)
pull
Δt [ps]

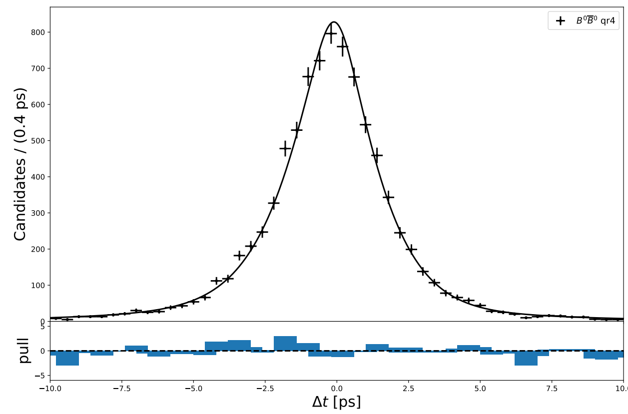
$B^0\overline{B}^0$ qr4
Candidates / (0.4 ps)
pull
Δt [ps]

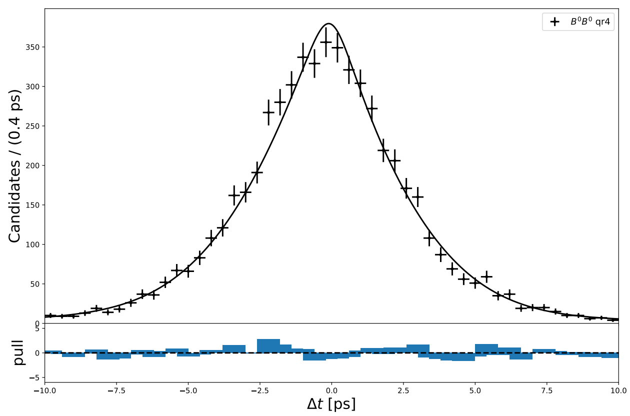
B^0B^0 qr4
Candidates / (0.4 ps)
pull
Δt [ps]

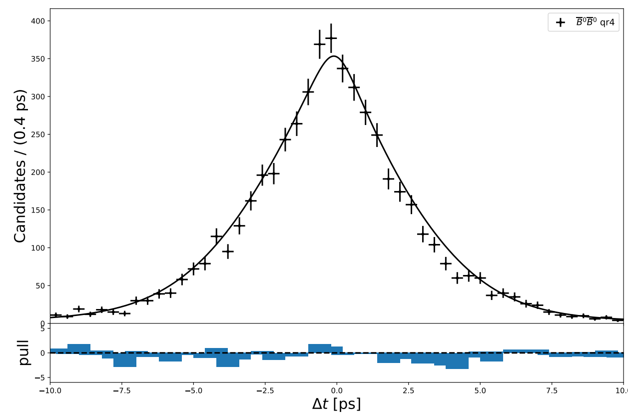
$\overline{B}^0\overline{B}^0$ qr4
Candidates / (0.4 ps)
pull
Δt [ps]

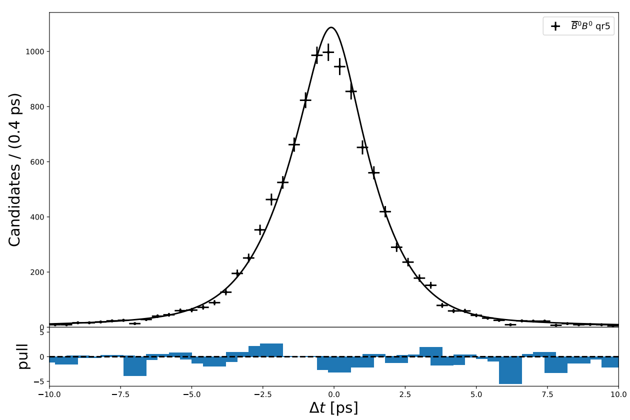
$\overline{B}^0B^0$ qr5
Candidates / (0.4 ps)
pull
Δt [ps]

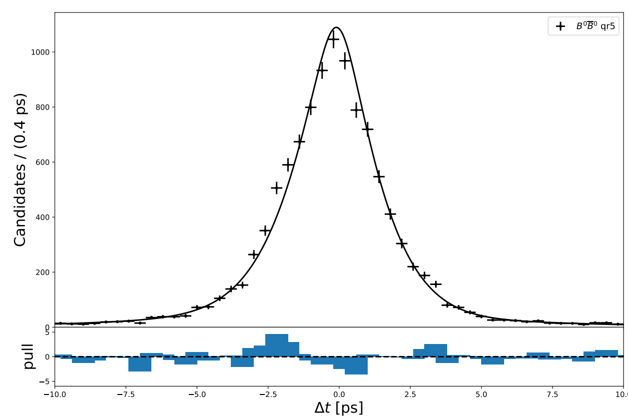
$B^0\overline{B}^0$ qr5
Candidates / (0.4 ps)
pull
Δt [ps]

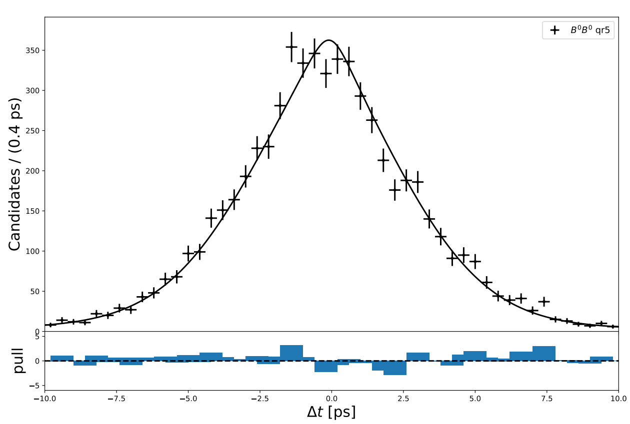
B^0B^0 qr5
Candidates / (0.4 ps)
pull
Δt [ps]

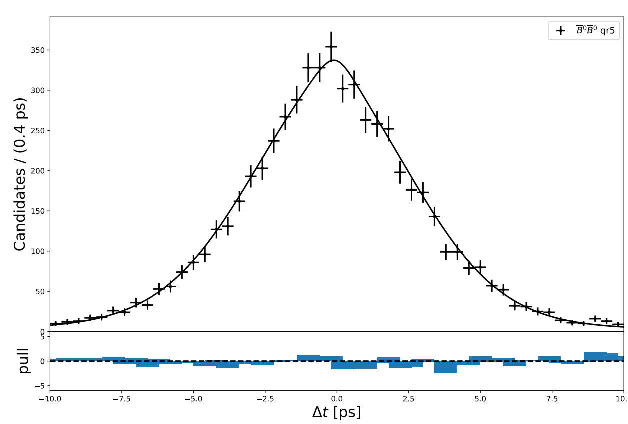
$\overline{B}^0\overline{B}^0$ qr5
Candidates / (0.4 ps)
pull
Δt [ps]

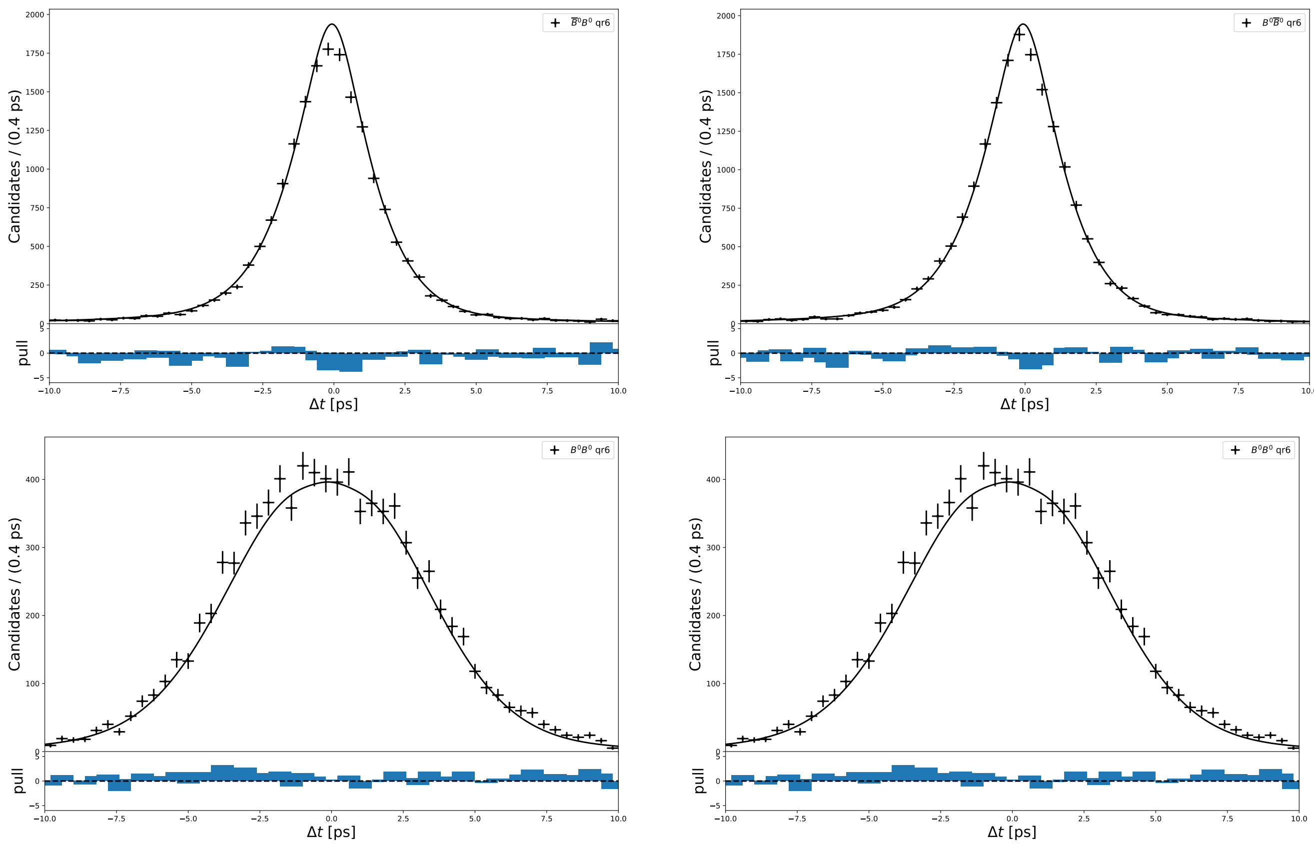

Figure A.6: Δt-distribution fitted to the Signal MC data of the equally mixture of $C = \pm 1$ states case for all qr bins and four flavor combinations (left to right, top to bottom). Error bars show Signal MC data binned in qr bins and solid line shows the fit. The lower plot show the pulls.

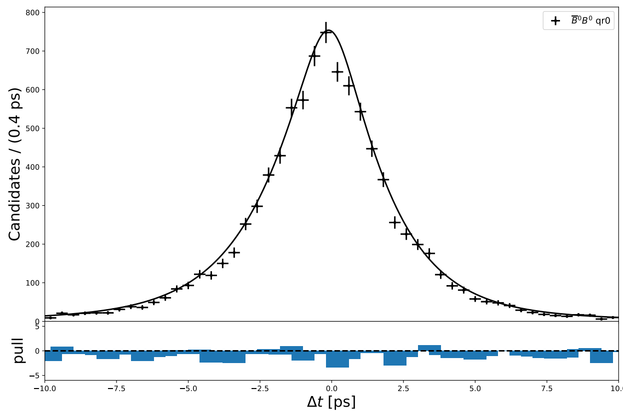
$\overline{B}^0B^0$ qr0
Candidates / (0.4 ps)
pull
Δt [ps]

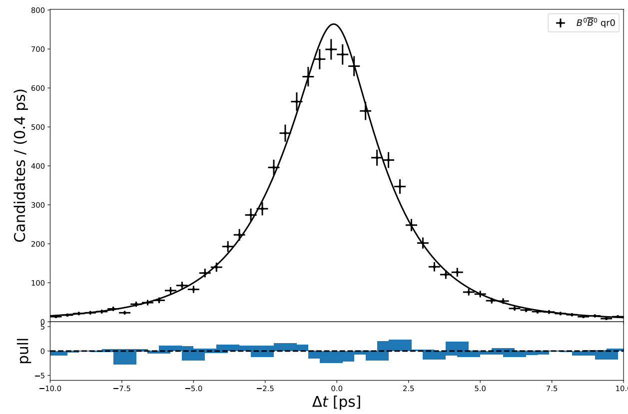
$B^0\overline{B}^0$ qr0
Candidates / (0.4 ps)
pull
Δt [ps]

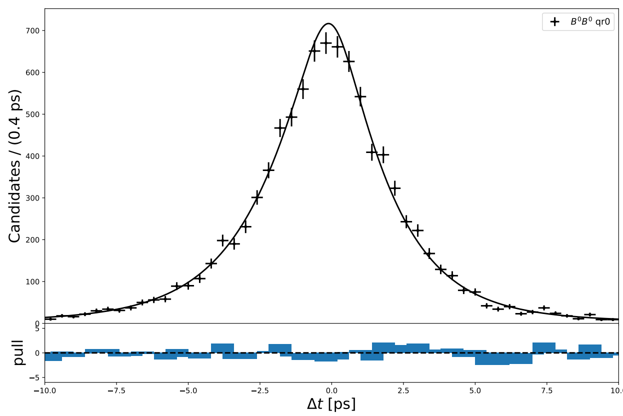
B^0B^0 qr0
Candidates / (0.4 ps)
pull
Δt [ps]

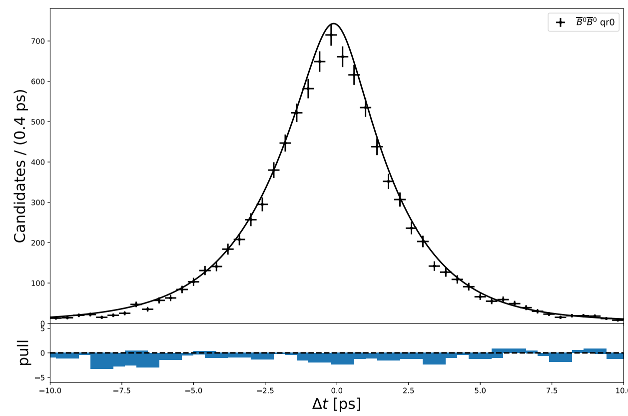
$\overline{B}^0\overline{B}^0$ qr0
Candidates / (0.4 ps)
pull
Δt [ps]

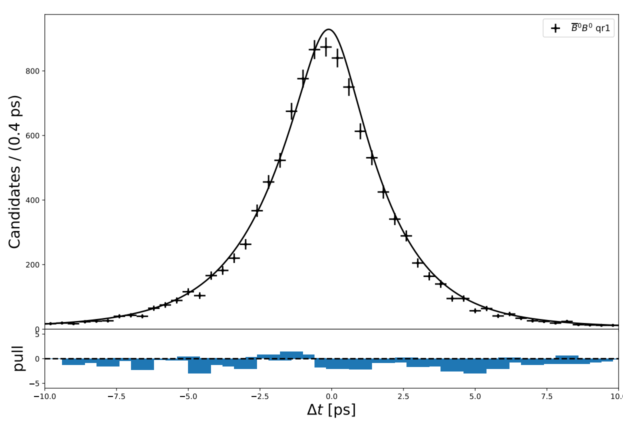
$\overline{B}^0B^0$ qr1
Candidates / (0.4 ps)
pull
Δt [ps]

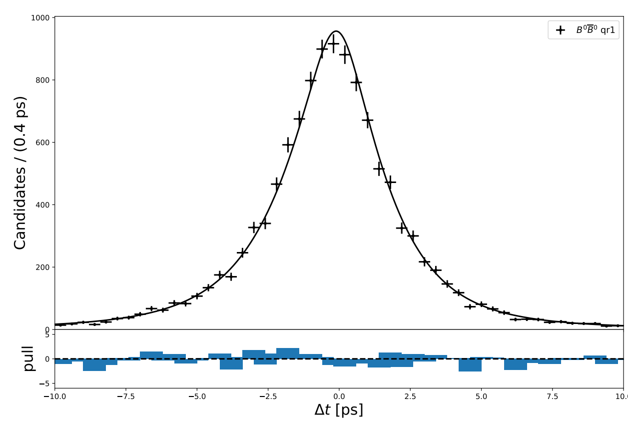
$B^0\overline{B}^0$ qr1
Candidates / (0.4 ps)
pull
Δt [ps]

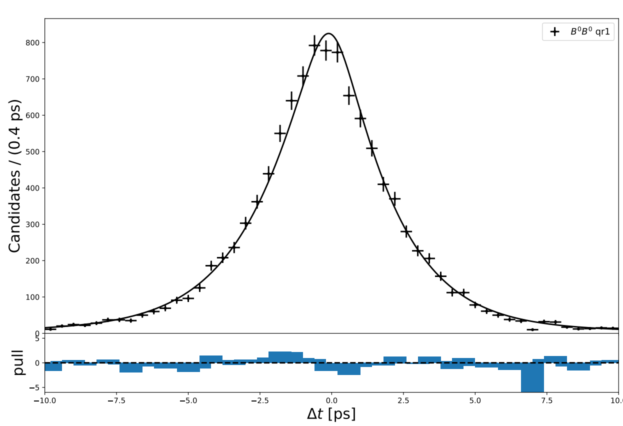
B^0B^0 qr1
Candidates / (0.4 ps)
pull
Δt [ps]

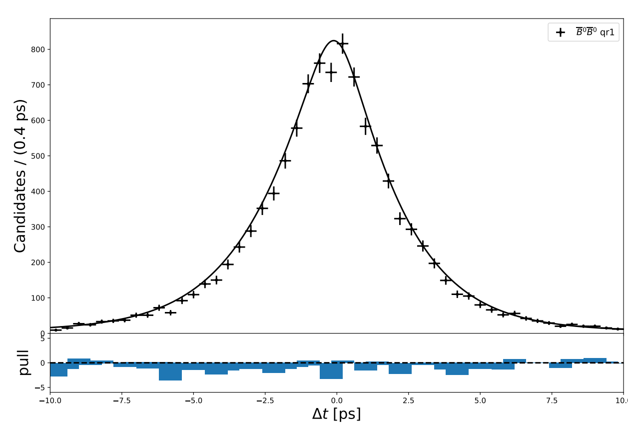
$\overline{B}^0\overline{B}^0$ qr1
Candidates / (0.4 ps)
pull
Δt [ps]

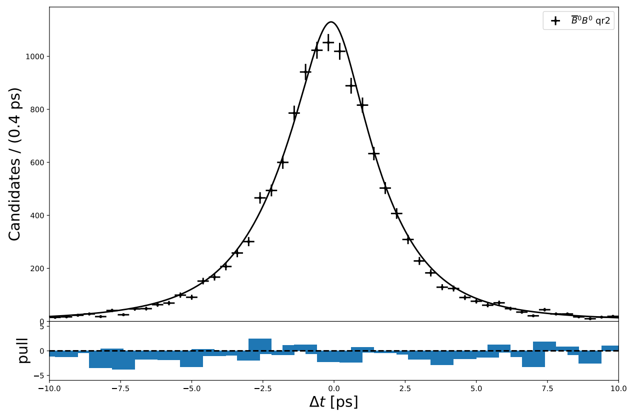
$\overline{B}^0B^0$ qr2
Candidates / (0.4 ps)
pull
Δt [ps]

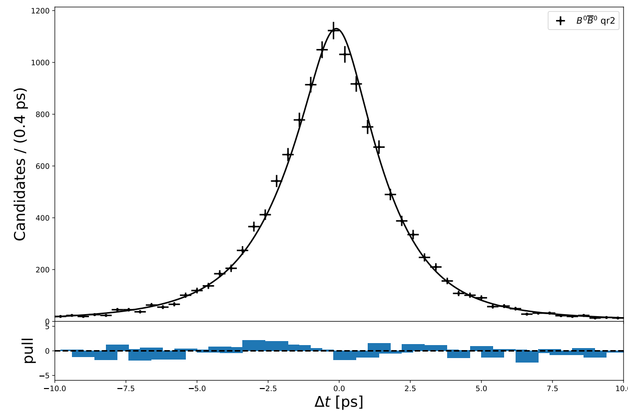
$B^0\overline{B}^0$ qr2
Candidates / (0.4 ps)
pull
Δt [ps]

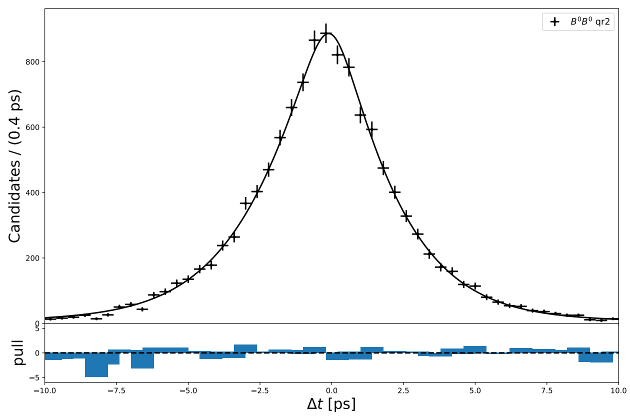
B^0B^0 qr2
Candidates / (0.4 ps)
pull
Δt [ps]

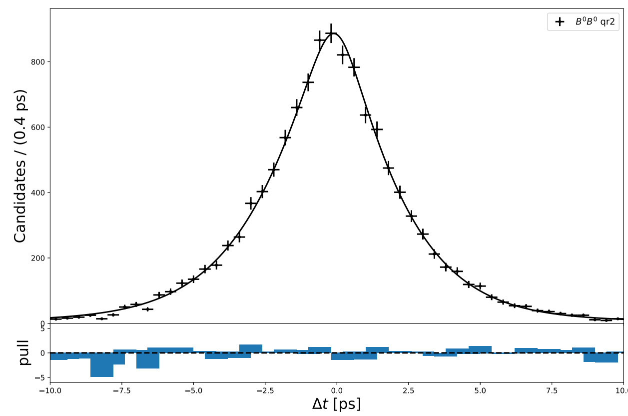
B^0B^0 qr2
Candidates / (0.4 ps)
pull
Δt [ps]

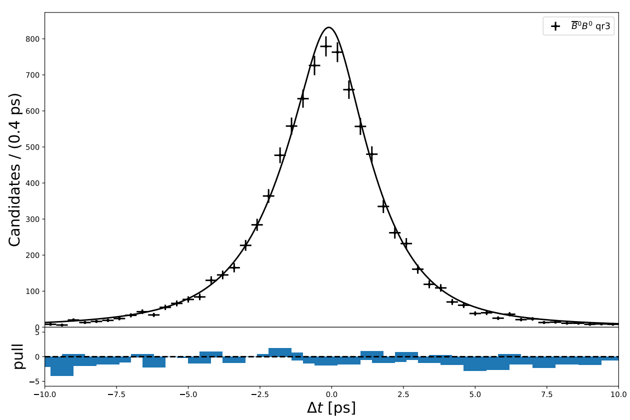
$\overline{B}^0B^0$ qr3
Candidates / (0.4 ps)
pull
Δt [ps]

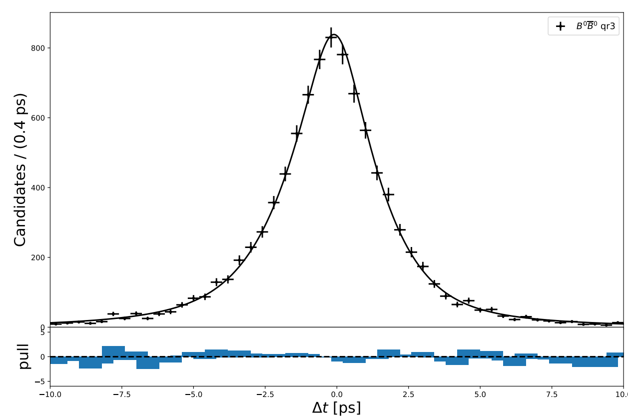
$B^0\overline{B}^0$ qr3
Candidates / (0.4 ps)
pull
Δt [ps]

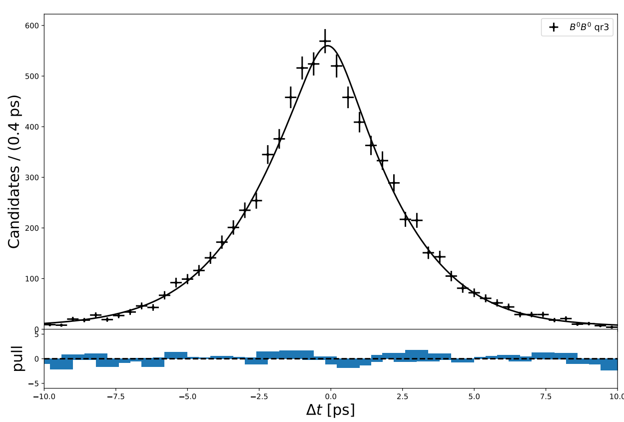
B^0B^0 qr3
Candidates / (0.4 ps)
pull
Δt [ps]

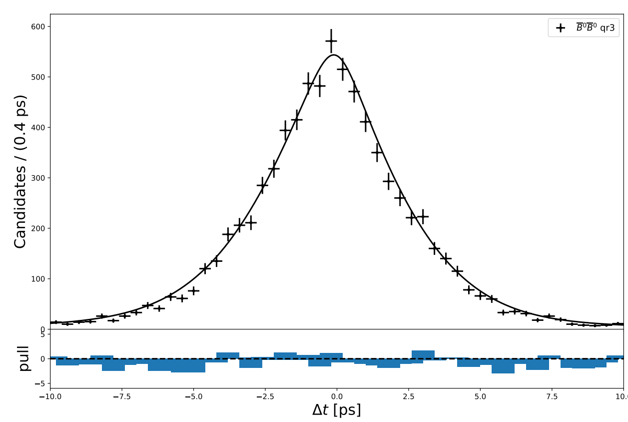
$\overline{B}^0\overline{B}^0$ qr3
Candidates / (0.4 ps)
pull
Δt [ps]

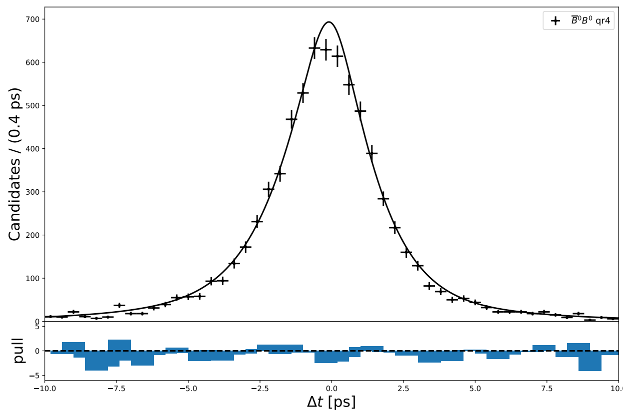
$\overline{B}^0B^0$ qr4
Candidates / (0.4 ps)
pull
Δt [ps]

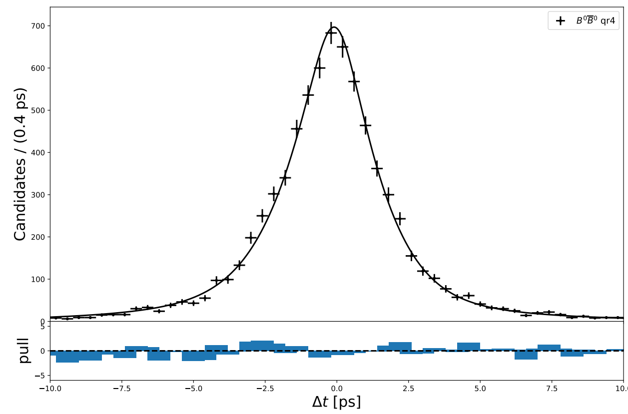
$B^0\overline{B}^0$ qr4
Candidates / (0.4 ps)
pull
Δt [ps]

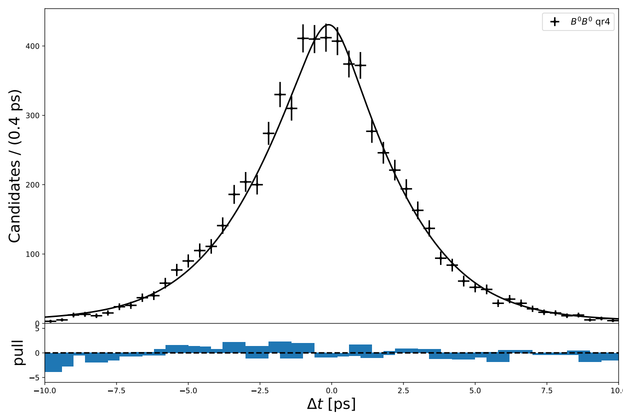
B^0B^0 qr4
Candidates / (0.4 ps)
pull
Δt [ps]

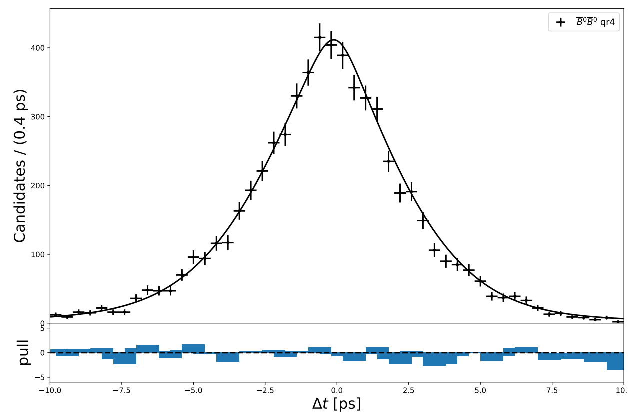
$\overline{B}^0\overline{B}^0$ qr4
Candidates / (0.4 ps)
pull
Δt [ps]

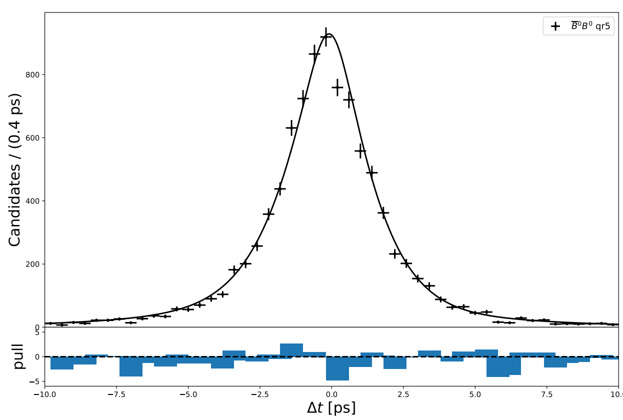
$\overline{B}^0B^0$ qr5
Candidates / (0.4 ps)
pull
Δt [ps]

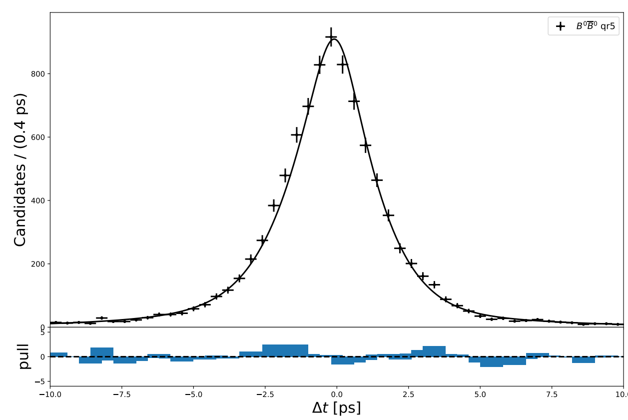
$B^0\overline{B}^0$ qr5
Candidates / (0.4 ps)
pull
Δt [ps]

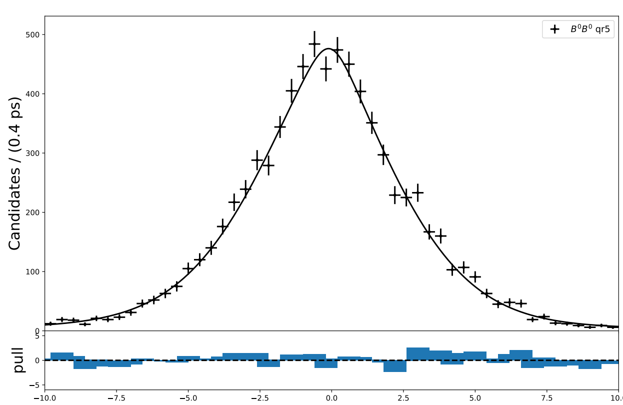
B^0B^0 qr5
Candidates / (0.4 ps)
pull
Δt [ps]

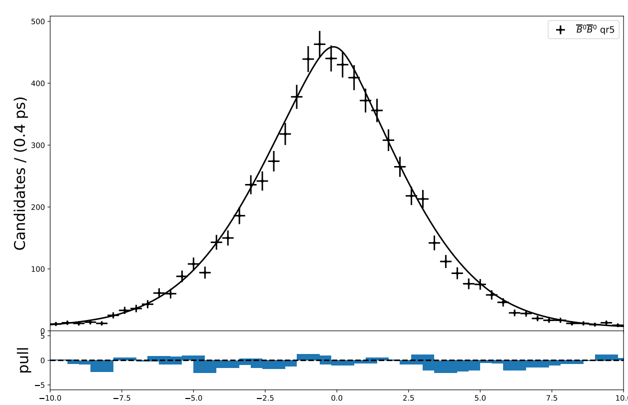
$\overline{B}^0\overline{B}^0$ qr5
Candidates / (0.4 ps)
pull
Δt [ps]

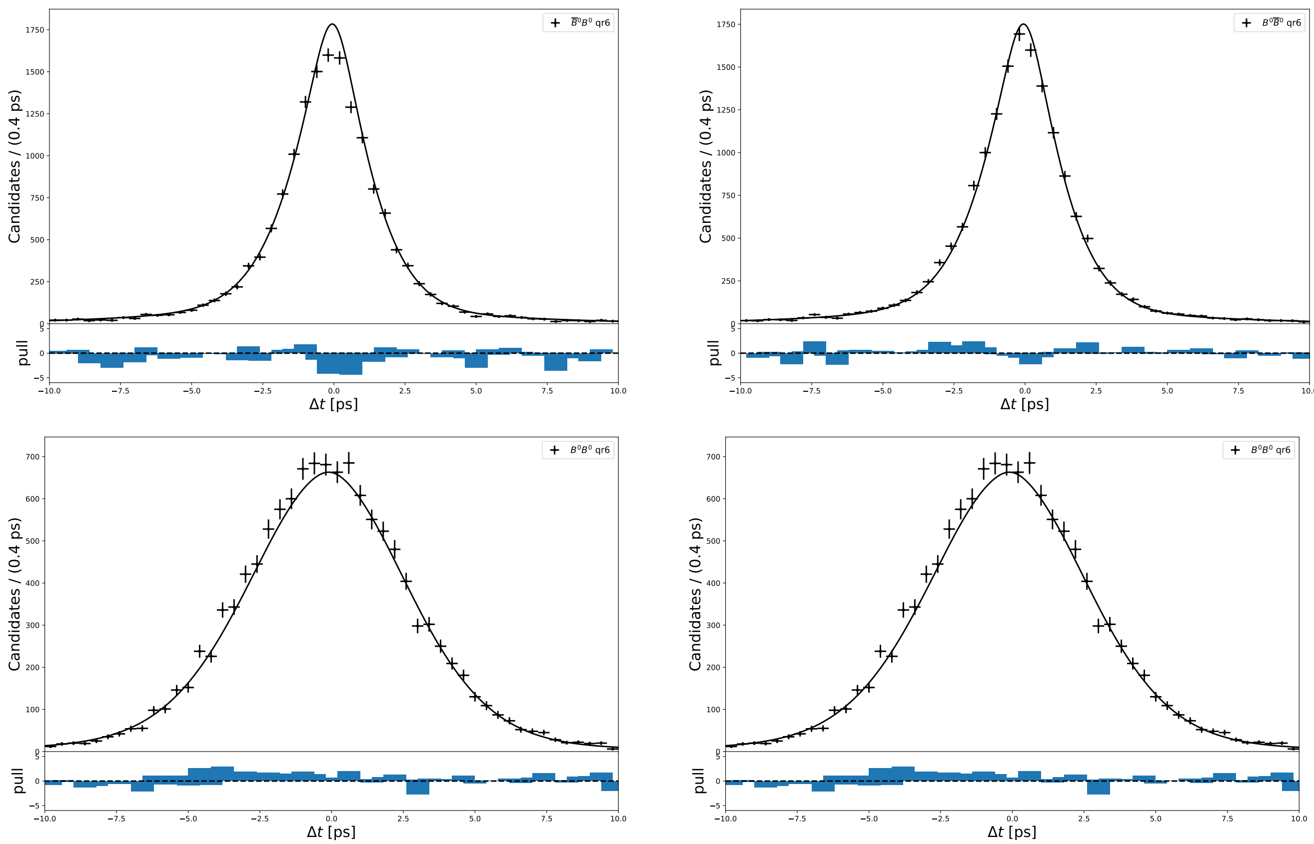

Figure A.7: Δt-distribution fitted to the $B^{0*}\bar{B}^0+$ c.c. Signal MC data for all qr bins and four flavor combinations (left to right, top to bottom). Error bars show Signal MC data binned in qr bins and solid line shows the fit. The lower plot show the pulls.

List of Figures

List of Tables

Bibliography

[1] A. J. Bevan et al. "The Physics of the B Factories". In: *The European Physical Journal C* 74.11 (Nov. 2014). ISSN: 1434-6052. DOI: 10.1140/epjc/s10052-014-3026-9. URL: http://dx.doi.org/10.1140/epjc/s10052-014-3026-9.

[2] Vladimir Chekelian et al. "Measurement of the B^0 lifetime and mixing frequency using hadronic decays with the Moriond 2022 dataset". In: *Belle II Internal Note* (2022).

[3] S. Navas et al. "Review of particle physics". In: *Phys. Rev. D* 110.3 (2024), p. 030001. DOI: 10.1103/PhysRevD.110.030001.

[4] David Schmid, Yìlè Yīng, and Matthew Leifer. *Copenhagenish interpretations of quantum mechanics*. 2025. arXiv: 2506.00112 [quant-ph]. URL: https://arxiv.org/abs/2506.00112.

[5] A. Einstein, B. Podolsky, and N. Rosen. "Can Quantum-Mechanical Description of Physical Reality Be Considered Complete?" In: *Phys. Rev.* 47 (10 May 1935), pp. 777–780. DOI: 10.1103/PhysRev.47.777. URL: https://link.aps.org/doi/10.1103/PhysRev.47.777.

[6] Wikipedia contributors. *Quantenverschränkung— Wikipedia, The Free Encyclopedia*. [Online; accessed 11/15/2025]. 2025. URL: https://de.wikipedia.org/wiki/Quantenverschr%C3%A4nkung.

[7] Wikipedia contributors. *Einstein-Podolsky-Rosen-Paradoxon— Wikipedia, The Free Encyclopedia*. [Online; accessed 11/15/2025]. 2025. URL: https://de.wikipedia.org/wiki/Einstein-Podolsky-Rosen-Paradoxon.

[8] Ryszard Horodecki et al. "Quantum entanglement". In: *Reviews of Modern Physics* 81.2 (June 2009), pp. 865–942. ISSN: 1539-0756. DOI: 10.1103/revmodphys.81.865. URL: http://dx.doi.org/10.1103/RevModPhys.81.865.

[9] J. S. Bell. "On the Einstein Podolsky Rosen paradox". In: *Physics Physique Fizika* 1 (3 Nov. 1964), pp. 195–200. DOI: 10.1103/PhysicsPhysiqueFizika.1.195. URL: https://link.aps.org/doi/10.1103/PhysicsPhysiqueFizika.1.195.

[10] Stuart J. Freedman and John F. Clauser. "Experimental Test of Local Hidden-Variable Theories". In: *Phys. Rev. Lett.* 28 (14 Apr. 1972), pp. 938–941. DOI: 10.1103/PhysRevLett.28.938. URL: https://link.aps.org/doi/10.1103/PhysRevLett.28.938.

[11] Nicolas J. Cerf and Chris Adami. "Information theory of quantum entanglement and measurement". In: *Physica D: Nonlinear Phenomena* 120.1–2 (Sept. 1998), pp. 62–81. ISSN: 0167-2789. DOI: 10.1016/s0167-2789(98)00045-1. URL: http://dx.doi.org/10.1016/S0167-2789(98)00045-1.

[12] Michael A. Nielsen and Isaac L. Chuang. *Quantum Computation and Quantum Information: 10th Anniversary Edition*. Cambridge University Press, 2010.

[13] Mark M. Wilde. *Quantum Information Theory*. Cambridge University Press, 2013.

[14] Scott Hill and William K. Wootters. "Entanglement of a Pair of Quantum Bits". In: *Physical Review Letters* 78.26 (June 1997), pp. 5022–5025. ISSN: 1079-7114. DOI: 10.1103/physrevlett.78.5022. URL: http://dx.doi.org/10.1103/PhysRevLett.78.5022.

[15] M. Gell-Mann and A. Pais. "Behavior of Neutral Particles under Charge Conjugation". In: *Phys. Rev.* 97 (5 Mar. 1955), pp. 1387–1389. DOI: 10.1103/PhysRev.97.1387. URL: https://link.aps.org/doi/10.1103/PhysRev.97.1387.

[16] Y. Amhis et al. "Averages of b-hadron, c-hadron, and τ-lepton properties as of 2021". In: *Phys. Rev. D* 107 (5 Mar. 2023), p. 052008. DOI: 10.1103/PhysRevD.107.052008. URL: https://link.aps.org/doi/10.1103/PhysRevD.107.052008.

[17] Lindblad G. "On the generators of quantum dynamical semigroups". In: *Commun.Math. Phys. 48, 119–130* (1976). DOI: https://doi.org/10.1007/BF01608499.

[18] Reinhold A. Bertlmann, Walter Grimus, and Beatrix C. Hiesmayr. "Open-quantum-system formulation of particle decay". In: *Physical Review A* 73.5 (May 2006). ISSN: 1094-1622. DOI: 10.1103/physreva.73.054101. URL: http://dx.doi.org/10.1103/PhysRevA.73.054101.

[19] A. Pompili and F. Selleri. In: *Eur. Phy. J. C 14, 469 (2000); Drascati Physics Series Vol.XXVI* 329 (2001).

[20] M. Dorigo et al. "Unlocking time-dependent CP violation without signal vertexing at B factories". In: *Phys. Rev. D* 112 (3 Aug. 2025), p. 032011. DOI: 10.1103/rzr8-l6l8. URL: https://link.aps.org/doi/10.1103/rzr8-l6l8.

[21] Adrian Liese. "Quantum Entanglement and Decoherence at the $\Upsilon(5S)$ Decay". Bachelor's Thesis. 2025.

[22] S. Navas et al. "Review of Particle Physics". In: *Phys. Rev. D* 110 (3 Aug. 2024), p. 030001. DOI: 10.1103/PhysRevD.110.030001. URL: https://link.aps.org/doi/10.1103/PhysRevD.110.030001.

[23] D Décamp et al. "A study of Bose-Einstein correlations in e+e- annihilation at 91 GeV". In: *Z. Phys. C* 54 (1992), pp. 75–86. DOI: 10.1007/BF01881709. URL: https://cds.cern.ch/record/226991.

[24] A. Go et al. "Measurement of EPR-type flavour entanglement in $\Upsilon(4S) \to B^0\overline{B}^0$ decays". In: *Physical Review Letters* 99.13 (Sept. 2007). ISSN: 1079-7114. DOI: 10.1103/physrevlett.99.131802. URL: http://dx.doi.org/10.1103/PhysRevLett.99.131802.

[25] H. Kakuno et al. "Neutral B Flavor Tagging for the Measurement of Mixing-induced CP Violation at Belle". In: *Nuclear Instruments and Methods in Physics Research Section A: Accelerators, Spectrometers, Detectors and Associated Equipment* 533.3 (Nov. 2004), pp. 516–531. ISSN: 0168-9002. DOI: 10.1016/j.nima.2004.06.159. URL: http://dx.doi.org/10.1016/j.nima.2004.06.159.

[26] Makoto Kobayashi and Toshihide Maskawa. "CP-Violation in the Renormalizable Theory of Weak Interaction". In: *Progress of Theoretical Physics* 49.2 (Feb. 1973), pp. 652–657. ISSN: 0033-068X. DOI: 10.1143/PTP.49.652. eprint: https://academic.oup.com/ptp/article-pdf/49/2/652/5257692/49-2-652.pdf. URL: https://doi.org/10.1143/PTP.49.652.

[27] Jolanta Brodzicka et al. *Physics Achievements from the Belle Experiment*. 2012. arXiv: 1212.5342 [hep-ex]. URL: https://arxiv.org/abs/1212.5342.

[28] S. Kurokawa and E. Kikutani. "Overview of the KEKB accelerators". In: *Nuclear Instruments and Methods in Physics Research Section A: Accelerators, Spectrometers, Detectors and Associated Equipment* 499.1 (2003). KEK-B: The KEK B-factory, pp. 1–7. ISSN: 0168-9002. DOI: https://doi.org/10.1016/S0168-9002(02)01771-0. URL: https://www.sciencedirect.com/science/article/pii/S0168900202017710.

[29] I Abe et al. "The KEKB injector linac". In: *Nuclear Instruments and Methods in Physics Research Section A: Accelerators, Spectrometers, Detectors and Associated Equipment* 499.1 (2003). KEK-B: The KEK B-factory, pp. 167–190. ISSN: 0168-9002. DOI: https://doi.org/10.1016/S0168-9002(02)01787-4. URL: https://www.sciencedirect.com/science/article/pii/S0168900202017874.

[30] A. Abashian et al. "The Belle detector". In: *Nuclear Instruments and Methods in Physics Research Section A: Accelerators, Spectrometers, Detectors and Associated Equipment* 479.1 (2002). Detectors for Asymmetric B-factories, pp. 117–232. ISSN: 0168-9002. DOI: https://doi.org/10.1016/S0168-9002(01)02013-7. URL: https://www.sciencedirect.com/science/article/pii/S0168900201020137.

[31] Kilian Brueckner. "Separation ot the different $B_0^*/\bar{B}_0^*$ Quantum States of the $\Upsilon(5S)$". Bachelor's Thesis. 2025.

[32] F. Jackl. “Disentanglement Theory”. In: *Bachelor Thesis* (2025).

[33] Belle Collaboration. *Upsilon(5S) group Home page*. 2022. URL: `https://belle.kek.jp/secured/wiki/doku.php?id=physics:ups5s:start.`.

[34] Belle Collaboration. *The Belle internal website*. 2025. URL: `https://belle.kek.jp/` (visited on 11/15/2025).

[35] Belle II Collaboration. *basf2 Tutorial Website*. 2025. URL: `https://software.belle2.org/development/sphinx/b2bii/doc/index.html` (visited on 11/14/2025).

[36] E Kou et al. “The Belle II Physics Book”. In: *Progress of Theoretical and Experimental Physics* 2019.12 (Dec. 2019). DOI: `10.1093/ptep/ptz106`. URL: `https://doi.org/10.1093%2Fptep%2Fptz106`.

[37] Anders Ryd et al. *EvtGen - A Monte Carlo Generator for B-Physics*. CERN, 2004. URL: `https://evtgen.hepforge.org/doc/EvtGenGuide.pdf`.

[38] Fernando Abudinén. “Development of a B^0 flavor tagger and performance study of a novel time-dependent CP analysis of the decay $B^0 \to \pi^0\pi^0$ at Belle II”. Oct. 2018. URL: `http://nbn-resolving.de/urn:nbn:de:bvb:19-230032`.

[39] F. Abudinén et al. “Measurement of the <mml:math xmlns:mml="http://www.w3.org/1998/Math/Mat
display="inline"><mml:msup><mml:mi>B</mml:mi><mml:mn>0</mml:mn></mml:msup></m
lifetime and flavor-oscillation frequency using hadronic decays reconstructed in 2019–2021 Belle II data”. In: *Physical Review D* 107.9 (May 2023). ISSN: 2470-0029. DOI: `10.1103/physrevd.107.l091102`. URL: `http://dx.doi.org/10.1103/PhysRevD.107.L091102`.

[40] A. Drutskoy et al. “Measurement of Υ(5S) decays to B^0 and B^+ mesons”. In: *Phys. Rev. D* 81 (11 June 2010), p. 112003. DOI: `10.1103/PhysRevD.81.112003`. URL: `https://link.aps.org/doi/10.1103/PhysRevD.81.112003`.

[41] Paolo Rocca, Giacomo Oliveri, and Andrea Massa. “Differential Evolution as Applied to Electromagnetics”. In: *IEEE Antennas and Propagation Magazine* 53 (2011), pp. 38–49. URL: `https://api.semanticscholar.org/CorpusID:27555808`.

[42] Maximilian Kei Hattenbach. “Studies of Quantum Entanglement in the $\Upsilon(4S) \to B^0\bar{B}^0$ system at BelleII using $B^0 \to D^{(*)-}\pi^+$ decays”. Master’s Thesis. 2025.

[43] Simeon Hamurcu. “Study of Quantum Entanglement and Coherence at Belle II”. Bachelor’s Thesis. 2024.

[44] Jonas Eschle et al. “zfit: Scalable pythonic fitting”. In: *SoftwareX* 11 (Jan. 2020), p. 100508. ISSN: 2352-7110. DOI: `10.1016/j.softx.2020.100508`. URL: `http://dx.doi.org/10.1016/j.softx.2020.100508`.

[45] Martín Abadi et al. *TensorFlow: Large-Scale Machine Learning on Heterogeneous Systems*. Software available from tensorflow.org. 2015. URL: https://www.tensorflow.org/.

[46] F. James and M. Roos. “Minuit - a system for function minimization and analysis of the parameter errors and correlations”. In: *Computer Physics Communications* 10.6 (1975), pp. 343–367. ISSN: 0010-4655. DOI: https://doi.org/10.1016/0010-4655(75)90039-9. URL: https://www.sciencedirect.com/science/article/pii/0010465575900399.

[47] Remi Louvot. “Simulation & Measurment of Same- and Opposite-sign Dileptons at the $\Upsilon(5S)$”. In: *Belle II Internal Note* (2011).

[48] R Brun et al. *GEANT 3*. Geneva: CERN, 1987. URL: https://cds.cern.ch/record/1119728.

[49] I. Adachi et al. “New graph-neural-network flavor tagger for Belle II and measurement of $\sin 2\phi_1$ in $B^0 \to J/\psi K^0_S$ decays”. In: *Physical Review D* 110.1 (July 2024). ISSN: 2470-0029. DOI: 10.1103/physrevd.110.012001. URL: http://dx.doi.org/10.1103/PhysRevD.110.012001.

[50] Particle Data Group et al. “Review of Particle Physics”. In: *Progress of Theoretical and Experimental Physics* 2020.8 (Aug. 2020), p. 083C01. ISSN: 2050-3911. DOI: 10.1093/ptep/ptaa104. eprint: https://academic.oup.com/ptep/article-pdf/2020/8/083C01/34673722/ptaa104.pdf. URL: https://doi.org/10.1093/ptep/ptaa104.

[51] Mirco Dorigo, Sebastiano Raiz, and Diego Tonelli. “An updated measurement of the properties of $B^0 \to \pi^0\pi^0$ decays reconstructed in 2019–2022 data”. In: *Belle II Internal Note* (2024).

[52] Jan-Åke Larsson. “Loopholes in Bell inequality tests of local realism”. In: *Journal of Physics A: Mathematical and Theoretical* 47.42 (Oct. 2014), p. 424003. ISSN: 1751-8121. DOI: 10.1088/1751-8113/47/42/424003. URL: http://dx.doi.org/10.1088/1751-8113/47/42/424003.

[53] Hans-Günther Moser. *Personal communication*.

[54] Kun Cheng et al. *Quantum Tomography in Neutral Meson and Antimeson Systems*. 2025. arXiv: 2507.12513 [hep-ph]. URL: https://arxiv.org/abs/2507.12513.

Acknowledgments

First of all, I would like to sincerely thank Prof. Dr. Christopher van Eldik for agreeing to supervise this Master's thesis and for taking the time during our regular updates to address the challenges and difficulties that arose during this work.
I would also like to extend special thanks to Dr. Hans Günther Moser, who came up with the idea for this project and consistently brought forward new and interesting suggestions for investigation. Next, I want to thank the entire Belle II group at MPP. You were always willing to help and made me feel very welcome. My thanks also go to Stefan Wallner, who I could always turn to with technical questions and who always provided excellent advice and solutions.
A special thanks goes to Max Hattenbach—thank you for helping me with all my $\Upsilon(5S)$ issues and for motivating me to keep going. I am grateful to have gained you as a new friend, even though our friendship was forged through the challenges of Δt fits and, of course, the occasional evening out with Claudia, Oskar, and Cosmo. You all made working and visiting Mensa in Garching much more enjoyable. Thank you, Oskar, for always motivating me and helping me whenever I had problems. Thank you, Claudia, for making the time at the Max Planck Institute so fun and for always being there when I needed to vent about problems—even when entanglement was not your field. The highlight was, of course, experiencing B2GM together and the trip to Japan. Thanks also to Adrian and Kilian, my companions in all things $\Upsilon(5S)$ and Belle. Finally, a huge thank you to my friends and family, who have always been there for me and supported me throughout my entire physics degree.

Eigenständigkeitserklärung

Hiermit versichere ich, dass ich die vorliegende Arbeit

Entanglement studies with $\Upsilon(5S)$ Belle Monte Carlo data

selbstständig verfasst und nur die angegebenen Quellen und Hilfsmittel benutzt habe. Wörtlich oder dem Sinn nach aus anderen Werken entnommene Stellen habe ich unter Angabe der Quellen kenntlich gemacht. Die Arbeit hat in gleicher oder ähnlicher Form noch keiner Prüfungsbehörde vorgelegen.

Ort, Datum

Unterschrift